

**Physiological Chemistry and Physics
and Medical NMR
Volume 36, Number 1, 2004**

Addresses of Chief Editor and Editorial College

Chief Editor

Gilbert N. Ling
P.O. Box 1452
Melville, New York 11747

Editorial College

O. D. Bonner
Department of Chemistry
University of South Carolina
Columbia, South Carolina 29208

Harris Busch
Department of Pharmacology
Baylor College of Medicine
Houston, Texas 77030

Ivan L. Cameron
Department of Anatomy
University of Texas Health Science Center
San Antonio, Texas 78284

Doriano Cavallini
Institute of Biological Chemistry
University of Rome
00185 Rome, Italy

James S. Clegg
Bodega Marine Laboratory
University of California
Bodega Bay, California 94923

George H. Czerlinski
Leibnitz Foundation Institute
P.O. Box 28521
Bellingham, Washington 98228

W. Drost-Hansen
Laboratorium Drost
Williamsburg, Virginia 23188-9415

Ludwig Edelmann
Anatomie und Zellbiologie
Universitdt des Saarlandes
D-66421 Homburg (Saar), Germany

Carlton F. Hazlewood
Research Consultants International
P.O. Box 130282
The Woodlands, Texas 77393

Ferdinand Heinmets
Technology Incorporated
P.O. Box 790644
San Antonio, Texas 78279-0644

S.R. Kasturi
Tata Institute of Fundamental Research
Mumbai 400 005, India

Miklós Kellermayer
Department of Clinical Chemistry
University Medical School
Pécs, 7624 Hungary

Janos Ladik
Institute of Physics and Theoretical Chemistry
University of Erlangen-Nurnberg
D-8520 Erlangen
Germany

Donald J. L. McIver
Department of Pharmacology
University of Western Ontario
London, N6A, 5C1, Canada

George M. Mrevlishvili
Department of Physics
Tbilisi State University
380028 Tbilisi
Republic of Georgia

Toshihiko Ubuka
Department of Clinical Nutrition
Kawasaki University of Medical Welfare
Kurashiki, Okayama, 701-0193, Japan

Vasile Vasilescu
Department of Biophysics
Faculty of Medicine
Bucharest 76241, Romania

Denys Wheatley
Department of Pathology
University of Aberdeen
Aberdeen AB9 2ZD, Scotland

EDITORIAL AND BUSINESS OFFICE

Physiological Chemistry and Physics
and Medical NMR

P.O. Box 1452
Melville, New York 11747

Editor In Chief, Dr. Gilbert N. Ling
Managing Editor, Margaret M. Ochsenfeld

SCOPE: PCP provides a forum for the review and publication of reports of original research in a broad range of subjects in biophysics, biochemistry and cellular physiology. Reports of direct applications of basic knowledge to human studies are invited; examples would include the measurements of relaxation times as part of NMR imaging. Single experiments, conclusions based on inadequate statistics, purely speculative papers, and clinical case reports are not accepted.

POLICY: The pages of PCP are accessible to competing viewpoints, interpretations, theories and opinions. Debate is invited via Editorial Comments and Letters to the Editor. Criteria for evaluating submissions include soundness of the study and clarity of presentation, and papers are not rejected on the basis of interpretation or theory, however controversial. PCP believes that scientific issues should be settled by investigation and open debate, not by an appeal to anonymous authority.

PCP attempts to achieve a balance between freedom of expression and constructive peer review. All papers are refereed by reviewers who may remain anonymous, but the Chief Editors make all final decisions, and will handle appeals from authors who feel their papers are unfairly reviewed.

The Editors endeavor to make decisions regarding acceptance or rejection of manuscripts quickly, and have set self-imposed deadlines for doing so. Referees also are given deadlines.

TYPES OF PAPERS: *Regular papers* may be experimental or theoretical. *Short notes*, *Priority notes* and *Letters* in response to published papers are invited. *Reviews* are desired, but authors are urged to contact an Editor before sending a finished review manuscript. *Symposia* may be published as regular or supplemental issues.

SUBSCRIPTIONS: Price is US\$80.00 per volume in the United States and US\$87.00 outside the United States. *Physiological Chemistry and Physics and Medical NMR* is published biannually, 2 issues per year, the volume numbered yearly. New subscriptions will start with the first issue of the volume in progress, unless the subscriber directs otherwise. Most back issues are available

Contributions appearing herein do not necessarily reflect views of the publisher, staff or Editorial College.

Instructions to Authors

SUBMISSIONS: An original and two copies of all material are requested. The original must be typewritten on one side only, but the copies may be double-sided to reduce cost of mailing. Papers should be sent to Dr. Gilbert N. Ling, Editor, P.O. Box 1452, Melville, New York 11747 U.S.A. Authors, especially those outside of North America, may send their papers to a member of the Editorial College in the same or a nearby country; the member of the college may elect to review the manuscript and/or obtain a second review before forwarding it to the Chief Editors. Manuscripts should be submitted only to this journal and not have been published in part or whole in another publication, except as short preliminary notes, abstracts, or as unpublished work in reviews or symposia. Be sure to keep a copy of your manuscript.

NOTE: Referees will be instructed to destroy their copies of the manuscript after reviewing them. We will return only the original manuscript to you for revision or if rejected.

MANUSCRIPTS: All material should be typed double-spaced with margins at least one inch wide and pages numbered beginning with the title page. In addition to a paper copy, you may send an IBM-compatible file on a floppy disk in Word, Wordperfect, ASCII or text. *Title Page* should include title (of at most 100 characters and spaces), full names of authors as you wish them to be published, names and cities of institutional affiliation(s) of authors and of institution(s) where the studies were performed, and name, full address and telephone number of the person to whom correspondence, proofs, and reprint requests are to be sent. Three or four *key words* should be listed on the title page.

Abstract should be concise and no longer than 225 words. *Body* may or may not be divided into Introduction, Materials and Methods, Results and Discussion, depending on the length and nature of the paper. Introductory remarks should indicate clearly the significance of the work presented. *References* may be indicated in the text and listed in the reference list in whatever style the author prefers, but we prefer that titles of articles be omitted.

TABLES: Tables should be typewritten on separate sheets and identified by roman numerals (eg. Table I) and titles. Table notes should be keyed by superscript italic lower-case letters (eg. ^aControl). The approximate locations of *tables* and *figures* should be indicated in the margins of the manuscript.

EQUATIONS should be broken in a manner estimated to fit into a column 5 inches wide when published. Solidus fraction (a/c) should be used instead of built-up ones ($\frac{a}{c}$) wherever possible.

ILLUSTRATIONS: Original artwork or glossy photostatic prints, together with two photocopies (like Xerox copies) should be provided. Each illustration should be numbered on the back in pencil, along with the authors' names. It is preferred that line drawings be made on paper that is not larger than 8½ by 13 inches, and that the drawing be its intended size in the printed paper. Most figures will occupy ½ to full column, that is 5 inches wide. Lines and lettering should be thick enough to allow reduction. A drawing of overall dimension of 8 by 10 inches that will be reduced to ¼ of its original size should be lettered with 18-point (capitals 6 mm high, lower-case 4 mm high) or larger lettering. Graphs and line drawings must be drawn and labeled in black India ink. Glossy photostatic prints are acceptable, and should be attached firmly to a sheet of paper the same size as the manuscript.

PHOTOGRAPHS: High-quality black and white glossy prints should be provided in triplicate, and may be provided as one print plus two photocopies if the photocopies are sufficiently clear to portray the original to referees. Photographs should be attached firmly to a sheet of paper the same size as the manuscript.

REFEREES: Two anonymous referees will be sought for each paper. Authors are encouraged to suggest names and addresses of suitable referees. Referees will be given deadlines for mailing manuscripts back or phoning reviews in, and will be invited to provide editorial statements or Letters that deal with issues raised by submitted papers.

REPRINTS: An order form is enclosed with proofs sent to authors.

PAGE CHARGES: Page charge is \$20.00 per published page. It may be waived in the case of severe international exchange difficulties. An additional charge of \$10.00 will be levied for photographs that require screening (eg., E.M's, chromatograms, scans).

What Determines the Normal Water Content of a Living Cell?

Gilbert Ling

*Damadian Foundation for Basic and Cancer Research
Tim and Kim Ling Foundation for Basic and Cancer Research
c/o Fonar Corporation, 110 Marcus Drive, Melville, NY 11747
E-mail: gilbertling@dobar.org*

Abstract: Most living cells contain a large amount of water. To improve our understanding of this fundamental phenomenon of cell physiology, five theories are critically examined in the light of three sets of relevant experimental findings. These findings are: (1) the diversity and specificity of the percentage water content to tissue type; (2) the limitation imposed by the Law of the Conservation of Energy on postulating membrane pumps and (3) the non-extractability of cell water from the open ends of muscle cells whose membrane covering has been surgically removed. Two of the five theories examined are called respectively the accidental theory (Theory I) and the direct water pump-leak theory (Theory III); both are introduced for the first time here as working hypotheses. Three others theories examined were published; they comprise the Donnan membrane equilibrium theory (Theory II), the indirect pump-leak (Theory IV) and the polarized-oriented multilayer (PM) theory of cell water (Theory V). The PM (Theory V) alone is in harmony with, and supported by all three sets of the experimental findings. The remaining theories are shown to be non-applicable to cell water by at least two of the findings

THIS COMMUNICATION begins with a brief description of five hypotheses or theories (designated Theory I to V respectively) on the basic physico-chemical mechanism by which living cells maintain their normal water content. Of the five theories considered, three were published. The remaining two are, to the best of my knowledge, published for the first time here (as working hypotheses) — even though it is very likely that these ideas have occurred to others.

An examination of each of these theories follows in the light of three sets of relevant experimental findings to be described.

I. Five theories on the underlying mechanism of the (high) water content of living cells

(1) **Theory I** (The Accidental Theory) **High water content of living cell as an accident**

According to this, the simplest of the five theories, water is found in large amount in the living cell because the cell lives in water — be it water in an ocean, water in a pond

or water in tissue fluid. Thus, in this theory, living cells are chockfull of water for the same reason that an old beer-can fished out of a river is chockfull of water.

(2) Theory II. (Donnan's Theory of Membrane Equilibrium — Donnan 1924) High water content of living cells due to osmotic activity of entrapped impermeant and permeant ions in cells

In the version introduced by Boyle and Conway (1941), muscle cell membrane is postulated to be impermeable to certain intracellular organic anions. These impermeant anions, a matching concentration of (permeant) K^+ cation as well as other permeant intracellular ions of both signs, draw water into the cell and maintains it at a high steady level.

(3) Theory III. (The Direct Water Pump-Leak Theory) High water content in living cells as a result of an incessant inward pumping of water molecules balanced by its outward leakage

In the membrane pump theory, each living cell is surrounded by a cell membrane so thin that if one stacks 10,000 of them in a pile, the pile would have a thickness of this piece of paper at which you are looking (Jain 1972, Table 4.4, p. 110.) For the most part, this membrane is postulated to exist in the form of a phospholipid bilayer, which has a permeability for water (Jain 1972 p. 117), for alkali metal ions (Miyamoto and Thompson 1967) and for D-glucose (Wood *et al.* 1968) orders of magnitude lower than real-life living cell membrane (for water, see Ling 1987, 2001 p. 127; for alkali metal ions, see Ling 1997 pp. 150–152; for D-glucose, see Ling 2001, p. 252.) As such, the substance of the postulated phospholipid bilayer membrane would act as a virtually impenetrable barrier to the intra-, extra-cellular traffic of water and substances dissolved in water. It is an assortment of specific channels (e.g., “potassium channels”, “sodium channels”, “water channels”) as well as membrane-straddling devices called membrane pumps that have been postulated to permit the traffic of water and solutes to proceed. By their ceaseless activities 24 hours a day and 7 days a week, the membrane pumps maintain unchanging the chemical makeup of each type of living cell.

A by-no-means comprehensive survey made in 1968 shows that 18 membrane pumps had already been formally introduced by that time (Ling *et al.* 1973.) Some of these are not single pumps but categories of pumps like the sugar pumps or free amino acid pumps, each comprising a multitude of individual pumps.

In the context of this membrane pump philosophy, the large amount of water found in living cells can also be explained by a (direct) water pump, which I postulate here as a working hypothesis. That is, water accumulates inside living cells in large amount because water pumps located in the phospholipid bilayer membrane ceaselessly pump water into the cells against its constant outward diffusion or “leakage.” Like all the other pumps already postulated, the energy needed to operate the water pump must also come from the cell's energy metabolism.

(4) Theory IV. (The Indirect Pump-Leak Theory) High water content of living cells as an indirect consequence of the ceaseless activities of the sodium-potassium pump

This indirect water pump model is an extension of the (non-water) membrane pump theories already formally postulated. Thus, the accumulation of a large and unchanging amount of water in living cells is seen as the indirect consequence of the net result of K^+ ion being pumped into the cell and Na^+ ion being pumped out of the cell by the sodium

pump (*alias* the sodium-potassium pump) (Dean 1941; Skou 1965.) The resultant rising osmotic activity inside the cell draws water into the cell and maintains it at the high level against a steady leak of water from the cell (Dowben 1969, Gutknecht *et al.* 1978.)

(5) Theory V: (The Polarized-Oriented Multilayer (PM) theory of cell water) High water content of living cells in consequence of the polarization-orientation of multilayers of water molecules by cell proteins

In 1965 I presented in the Symposium on *Forms of Water in Biological Systems* held in New York, the polarized multilayer (PM) theory of cell water as an integral part of the larger unifying theory of the living cell called the **association-induction hypothesis** (Ling 1962.) Recently the name has been amended to **polarized-oriented multilayer theory of cell water**, although the short name, PM theory, remains unchanged (Ling 2003.)

In this PM theory, “*all or nearly all water molecules in a living cell exist as polarized multilayers oriented on the surface of cell proteins*” (Ling 1965, p. 407.) Figure 1 is a reproduction of the original figure (Figure 5) used at that time to illustrate the theory. It emphasizes the graded motional restriction of (layers of) water molecules in consequence of direct or indirect interaction with cell proteins.

(For the benefit of conscientious science historians of the future, I would like to point out that this was the first time that a member of the human race formally suggested that

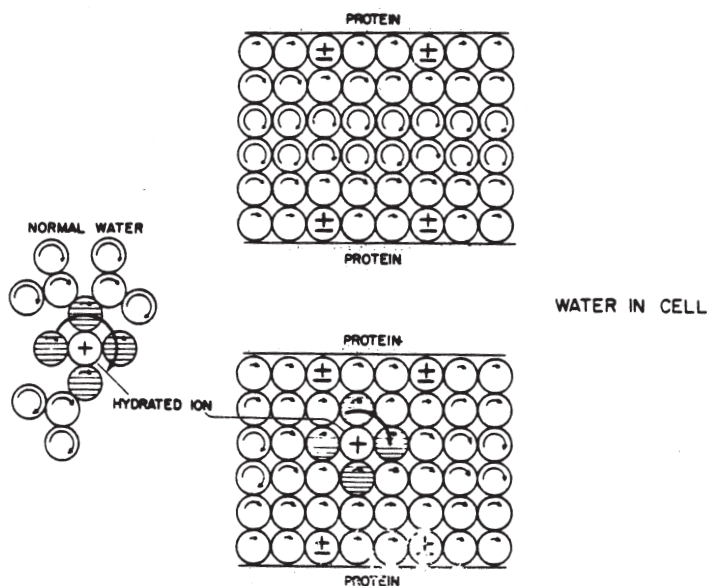


FIGURE 1. The diagrammatic illustration that launched the first polarized multilayer theory of cell water content as well as the first theory of solute exclusion in consequence of the dynamic structuring of cell water. The left figure shows a hypothetical diagram of a hydrated (e.g., sodium) ion in normal liquid water. The length of the arrows in the water molecules and elsewhere was intended to roughly illustrate the degree of rotational freedom of the molecule involved (from Ling 1965, by permission of the New York Academy of Sciences, USA., copyright 1965.)

the large amount of water making up a human being and his/her non-human cousins is not normal liquid water.)

This PM theory presented in 1965 offers an explanation why a large amount of water exists in all living cells, clear and simple. However, the immediate aim of that presentation was to describe a new molecular mechanism for the maintained low level of Na^+ and other solutes found in living cells — *in lieu* of the postulated sodium pump (see below, for evidence of its excessive energy need.) As an equilibrium state, the unequal intra-, extra-cellular distribution of Na^+ and other solutes in this new theory does not demand continual energy expenditure.

II. Three sets of relevant experimental facts and what they tell us about the five theories listed above

(1) **Finding I. The similarity of the water contents of cells serving the same physiological function and divergence of the water content of cells serving different physiological functions.**

The water contents of living cells are, roughly speaking, specific and to varying degree predictable. As the data presented in Tables I and II demonstrate, the cell water content tends to be similar in tissues or cells serving the same physiological function even among widely different kind of living species (Table I.) In contrast, the water content tends to be different among tissues or cells serving different physiological functions even in the same species (Table II.)

Rough as it is, the specificity of water content shown in Tables I and II could not be accidental. So the accidental theory of cell water is out from these facts alone.

Nor can the Donnan theory (Theory II), the direct water pump-leak theory (Theory III), the indirect water pump-leak theory (Theory IV) predict the specificity of cell water content.

In contrast, the **PM theory** (Theory V) can explain readily the specificity of water content: a specific amount of water accumulates in a specific kind of cell because the free energy of water adsorption on the **specific proteins** in that type of cells is most favorable. In the PM theory, the quantity and kinds of proteins determine the total amount of water in each type of living cells. Accordingly, the PM theory anticipates that cells serving the same physiological function have similar assortments of proteins — even among different living organisms. On the other hand, cells serving different physiological functions even in the same organism would have different profiles of the kind and amount of proteins. In fact, Ling, Reid and Murphy (1986) have already confirmed this anticipation 18 years ago. Their figures are reproduced here as Figures. 2, 3 and 4..

Figure 2 shows the SDS-PAGE profiles of (all) the proteins of each of the three kinds of tissues (liver, lung and spleen) from four different strains of mice (A: Balb/c; B: C₃D₂-F₁/J; C:57BL; D: DBA/2.) The protein profiles of the same tissues in all four strains of mice are highly similar; the protein profiles of different tissues in the same or different strains of mice are consistently different. Figure 3 shows the SDS-PAGE runs of (all) the proteins in tissues of representative species of five classes of animals: A. Fish (gold fish); B. Amphibian (frog); C. Reptile (skink); D. Bird (chicken); E. Mammal (mouse.) Again, the total protein profiles are similar for the same tissue from representatives of all five

TABLE I. Water contents of red blood cells from different animals (from Ponder 1948.)

Man	63.9 to 66.1 ± 1.4*
Rabbit	63.3 to 66.8 ± 1.1*
Ox	58.6 to 71.2 ± 1.4*
Sheep	60.5 to 70.9 ± 1.1*
Pig	62.6
Horse	61.3
Dog	64.4
Cat	62.4
Goat	60.9

TABLE II. Water contents of eight types of living cells of North American leopard frogs.

	Cell Water Content (%)	Extracellular Space (%)	Tissue Water Content (%)
Egg	49.4 ± 1.94		
Heart	80.3 ± 0.32	15.7 ± 0.72	83.4 ± 0.35
Kidney	77.0 ± 0.33	17.6 ± 1.44	81.0 ± 0.50
Liver	68.3 ± 0.36	15.9 ± 1.38	73.3 ± 0.46
Muscle	77.4 ± 0.52	8.20 ± 0.32	79.3 ± 0.49
Oviduct	75.8 ± 0.46	10.8 ± 1.44	78.4 ± 0.54
Spleen	75.1 ± 0.40	7.94 ± 1.60	77.1 ± 2.48
Testis	82.1 ± 1.10	18.5 ± 3.64	85.4 ± 1.14

Tissues were isolated and immediately put into cold Ringer phosphate medium (4° C) in what is known as Medium 731 that permits long term preservations of isolated frog muscle for up to 8 days at room temperature, much longer at 4° C. (Other details and composition of the 731 medium are described by Ling and Bohr, 1969.) The water contents of the cells were computed from the total tissue water contents after correcting for the water trapped in the extracellular space (column 3.) The volume percentages of the extracellular fluid were determined by the centrifugation technique of Ling and Walton (1975) described in the text and in the legend of Figure 7. All weights were determined on a torsion balance kept in a cold room. A standardized blotting procedure was used in all cases to remove adhering fluids. After the last weighing in the wet state, the tissues were air-dried in a warm room for 3 days before transferring to an oven maintained at 100° C and dried for another 24 hours before final weighing to determine the dry weight.

classes of animals. But the protein profiles are uniformly different from different tissues from the same or different classes of animals.

Of course, to perform different cell physiological functions *also* requires a specific assortment of proteins in each type of living cells. Why water, polarized and oriented to a different degree, may be a key component of the living mechanisms underlying physiological functions is a part of the central theme of the association-induction hypothesis, of which the PM theory is an integral part (Ling 1962, 1984, 1992, 2001.)

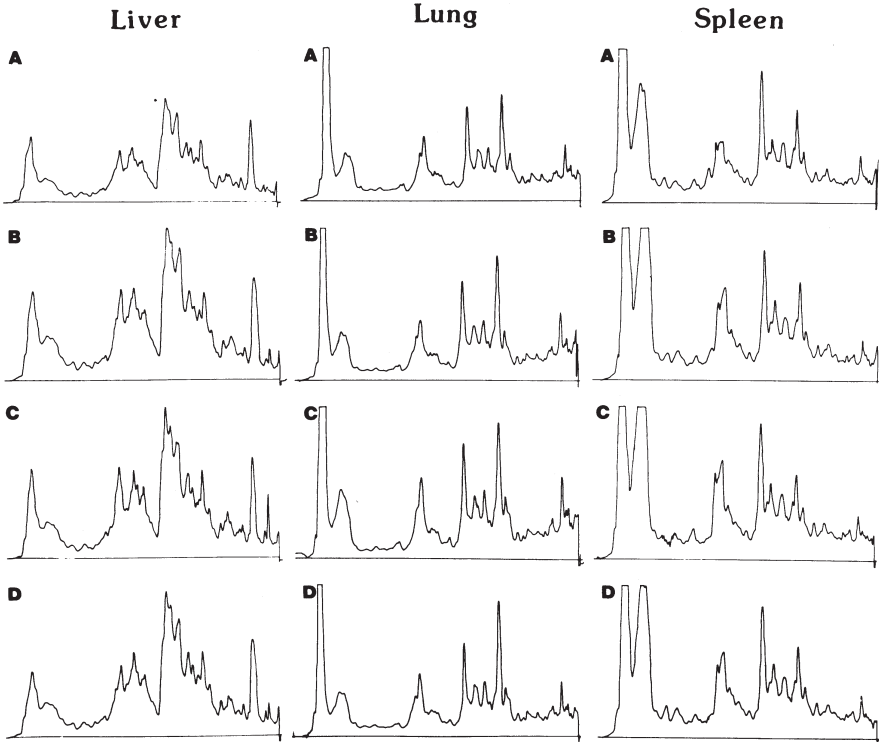


FIGURE 2. Densitometer tracing of SDS-PAGE runs of normal liver, lung and spleen tissues from four strains of mice: A, Balb/c; B, C₃D₂Fi/J; C, C57BL; D, DBA/2. 20–40 mg of normal tissues were frozen in liquid nitrogen and ground in cold stainless tube and grinder. 20 times tissue weight of 50% glycerin was added to the suspension and homogenized. To 0.05 ml of the homogeneous suspension was added 0.2 ml of sample buffer containing 4.0 part 10% SDS, 2.5 part of 0.5 M Tris-HCl at pH 6.8, 1.0 part mercaptoethanol, 1.6 part 0.025% Bromophenol Blue and 6.9 parts water. The mixture was heated in a boiling water bath for 2.5 min. 65 μ l of the cooled sample was placed in each well of the electrophoresis gel. For comparison, all samples and standards were run on the same gel and their densitometer tracing taken at a single setting (from Ling *et al.*, 1986.)

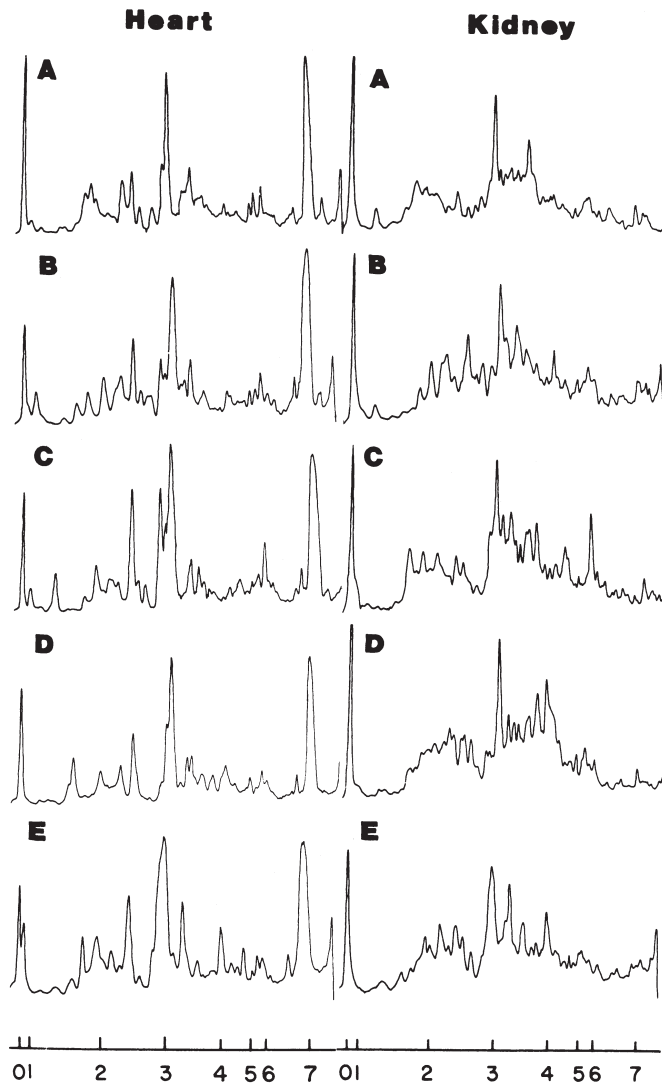


FIGURE 3. Densitometer tracings of SDS-PAGE runs of normal heart and kidney tissues from representative species of each of five classes of animals: gold fish, leopard frog, skink, chicken, mouse. Methods were same as described in legend of Figure 2. Numbered stubs on the abscissa correspond to positions of standards from Sigma Chemical Co., St. Louis, MO: 0, lysozyme (M.W. 14,400 daltons); 1, soybean trypsin inhibitor, 21,500; 2, carbonic anhydrase, 31,000; 3, ovalbumin, 45,000; 4, bovine serum albumin, 66,200; 5, phosphorylase B, 92,500; 6, β -galactosidase, 116,250; 7, myosin, 200,000. (from Ling *et al.*, 1986.)

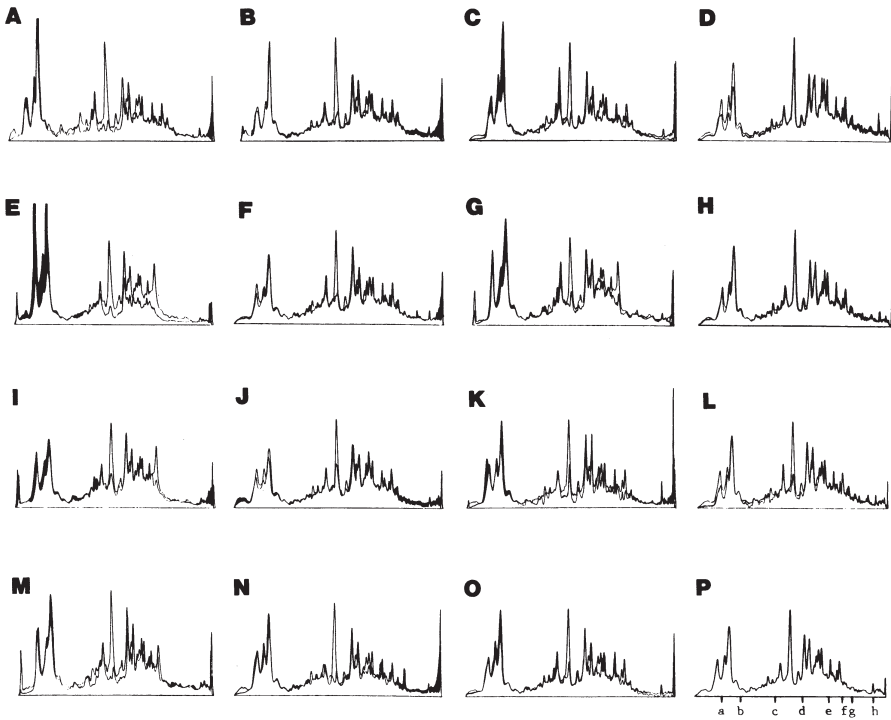


FIGURE 4. Densitometer tracings of the SDS-PAGE separated protein bands of mouse ascites cancers. On each tracing from one kind of cancer cell is superposed a similar tracing from Ehrlich ascites cancer cells, which serves as an internal standard to fine-tune the similarity (and differences) of the tracings. Darkened (shaded) areas represent lesser abundance of the protein of that molecular weight in the Ehrlich tracing. Unshaded areas represent greater abundance of the protein of the molecular weight in the Ehrlich standard tracing. Downward stubs on abscissa on the abscissa of P shows positions of molecular weight standards: a, lysozyme (M.W., 14.4 kilodaltons or kd); b, soybean trypsin inhibitor (21.5 kd) c, carbonic anhydrase, (31.0 kd); d, ovalbumin (45.0 kd); e, bovine serum albumin, (66.2 kd) f, phosphorylase B (92.5 kd); g, galactosidase, (116.3 kd) h, myosin (200.0 kd.) (from Ling *et al.*, 1986.)

Finally, Figure 4 shows highly similar protein profiles from 15 kinds of mouse (ascites) cancer cells — even though the tissues from which the cancer cells were derived are widely different. This similarity of protein profiles among cancer cells of different tissue origins is in harmony with the fact that cancer cells as a class tend to have high water contents (Ling and Tucker 1980, Table 2; Beall *et al.* 1984, Tables 5-8, 5-9 and 9-10.) And it also supports the idea expressed many years ago by Greenstein, Knox and others (Greenstein 1947; Knox 1967) that cancer cells represent a reversion to a common, embryonic form of cells.

In summary, the specificity of the water content to the type of living cells cannot be explained by the accident theory; the Donnan membrane equilibrium theory, the direct pump-leak theory nor the indirect pump- theory. On the other hand, the water-content specificity is in full accord with the PM theory, according to which it is the kind and

amount of different proteins in a cell that determine its total water content. The experimental demonstration that the protein profiles indeed reflect the physiological function of the cell adds more weight to the PM theory.

(2) Finding 2. Limitation of the postulation of membrane pumps set by the Law of Conservation of Energy

One of the most fundamental laws of physics in our Universe is the law of the conservation of energy — also known as the First Law of Thermodynamics. In the simplest of terms, it says that without energy, work cannot be done.

In 1952 I presented in the Symposium on Phosphorus Metabolism held at the Johns Hopkins University in Baltimore, results of my early study of the energy need of the hypothetical sodium pump. Based on the rather limited data then on hand, I reached the tentative conclusion that if the muscle cells spend all their energy in pumping sodium, the minimum energy need of the sodium pump would still require 400% of the maximally available energy (Ling 1952, p.767.)

In the succeeding years I continued to improve the methods used in the earlier study and the accuracy in this line of investigations. Eventually, I counted a total of 78 sets of complete and incomplete experiments. Their results uniformly point in the same general direction my 1952 report showed, namely, frog muscle under rigorously controlled conditions, does not have enough energy to operate the postulated sodium pump.

The last three sets of completed studies carried out in 1956, considered to be the most accurate of all my studies, are graphically represented in Figure 5. They show that the minimum energy need to operate just one of the postulated pumps, the sodium pump (*alias* the sodium-potassium pump) is from 15 to 30 times the maximum available energy (Ling 1962 Chapter 8; data reproduced and expanded in Ling 1997.) These energy balance studies have left no doubt that both Theory III, the (direct) water pump-leak theory and Theory IV, the indirect pump-leak theory are also not tenable.

Theory V, the PM theory, is once again in accord with the results of the energy balance study. As multilayer adsorption, the accumulation of a large amount of water in living cells is an expression of an equilibrium phenomenon. As such, it does not entail a steady expenditure of energy.

(3) Finding 3. High speed centrifugation, which quantitatively removes all water in the extracellular space of a frog sartorius muscle fails to extract any detectable amount of water from the cut ends of muscle cells after their covering cell membrane has been surgically removed.

According to the membrane theory or its variant, the membrane-pump theory, cell water is essentially normal liquid water (for history, see Ling 2001, Chapt. 5.) The Donnan membrane equilibrium theory (Theory II), the direct water pump-leak theory (Theory III) and the indirect pump-leak theory (Theory IV) are all extensions of the membrane (pump) theory. As such, these three theories as well as the accidental theory (Theory I) all see water in living cells as normal liquid water. Theory V, the PM theory, differs.

A familiar property of normal liquid water is its propensity to flow from a high place to a low place. This kind of water flow is caused by the force (or weight, w) acting on an object of mass m , by the gravitational acceleration g of the Earth, where the force or weight is equal to the product of the mass and the gravitational acceleration, g . A man-

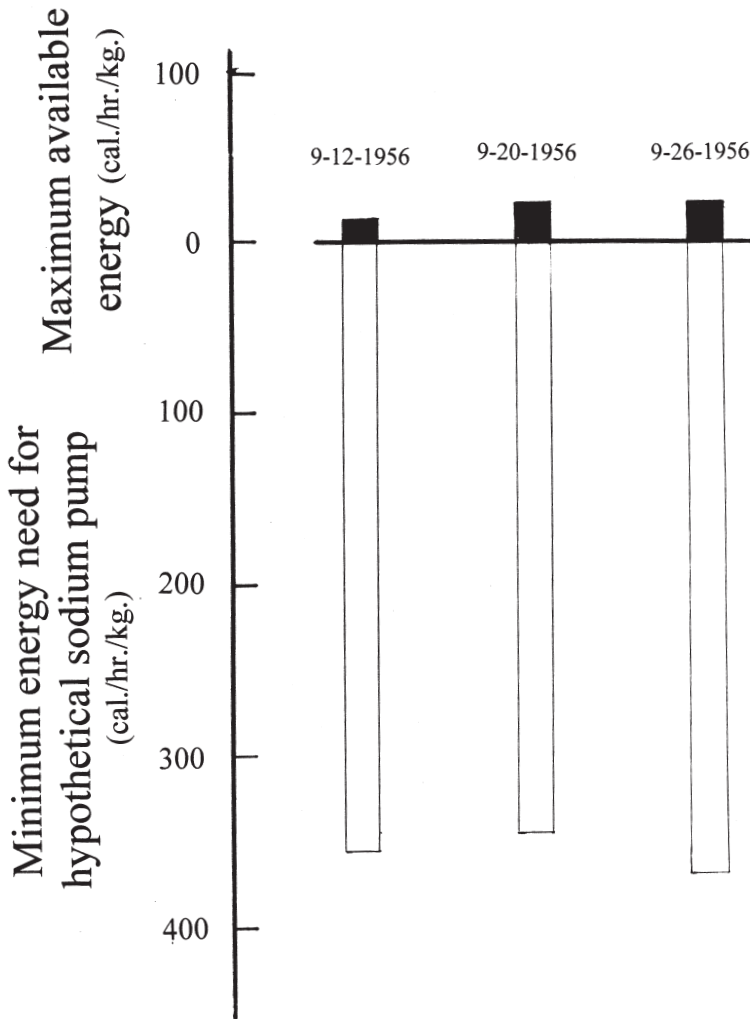


FIGURE 5. A comparison of the maximally available energy of (poisoned) frog sartorius muscle cells at 0°C (upward black bars) and the minimum energy need to pump Na^+ against both (measured) electric potential gradient and a concentration gradient. Duration of the experimental observation for experiment 9-12-1956 lasted 10 hrs.; Experiment 9-20-1956, 4 hrs.; Experiment 9-26-1956, 4.5 hrs. Active oxidative metabolism was suppressed by exposure to pure nitrogen (99.99%, in addition to 0.001 M NaCN); glycolytic metabolism, by sodium iodoacetate and doubly insured by actual lactate analysis before and after the experiment. Other detailed studies reported in 1952 (Ling 1952, Table 5 on page 765) and in 1962 (Ling 1962, Table 8.4) showed respectively that under similar conditions of 0° C temperature and virtually complete inhibition of active energy metabolism, the K^+ and Na^+ concentrations in frog muscle, nerves and other tissues remained essentially unchanged for as long as the experiments lasted (5 hrs. for the 1952 reported experiment, and 7 hrs. 45 min. in the 1962 reported findings.) (For additional details, see Ling 1962, Chapter 8 and Ling 1997.) Since the book referred to here as Ling 1962 has been out of print, its entire Chapter 8 has been reproduced as an Appendix in the article, Ling 1997 bearing the title: "Debunking the Alleged Resurrection of the Sodium Pump Hypothesis". In all the computations, it was assumed that the frog muscle cell does not use its metabolic energy for any other purpose(s) than pumping sodium ion and that all energy transformation and utilization are 100% efficient.

made centrifuge, by spinning an object at high speed, can exert a much stronger pulling force than gravitation.

Thus, in theory at least, spinning a broken living cell in a centrifuge may produce a decisive experiment that could tell us if water in living cells is indeed mostly normal liquid water (as predicted in Theory I, II, III and IV) or polarized-oriented — and thus less free to flow — as predicted in Theory V, the PM theory (Ling 1965, 2003.) However, to achieve that goal, we must first establish that such centrifugation at high speed can indeed extract all or virtually all authentic normal liquid water found in a cell preparation. That in turn requires a population of highly similar living cells that can be handled easily as a unit.

It turned out that Nature has provided us with just what we need in the form of a frog sartorius muscle. As illustrated in the top picture of Figure 6, this is a thin sheet of a muscle on the ventral side of a frog's thighs, about 3-cm long, a third to half of a centimeter wide. It also comes with a predictable amount of indisputably normal liquid water in the extracellular space of each sartorius muscle — that past studies have established quantitatively. This gives us, so to speak, a built-in marker that would tell us if the centrifugation technique to be described immediately below can indeed remove all the free water in a muscle and nothing beyond that.

A freshly isolated frog sartorius muscle is blotted dry on moist filter paper to remove adhering fluid by a standardized procedure described by Ling, Neville *et al.* (1969, pp. 87–88) and weighed on a torsion balance kept in a humidity-controlled glove box. The

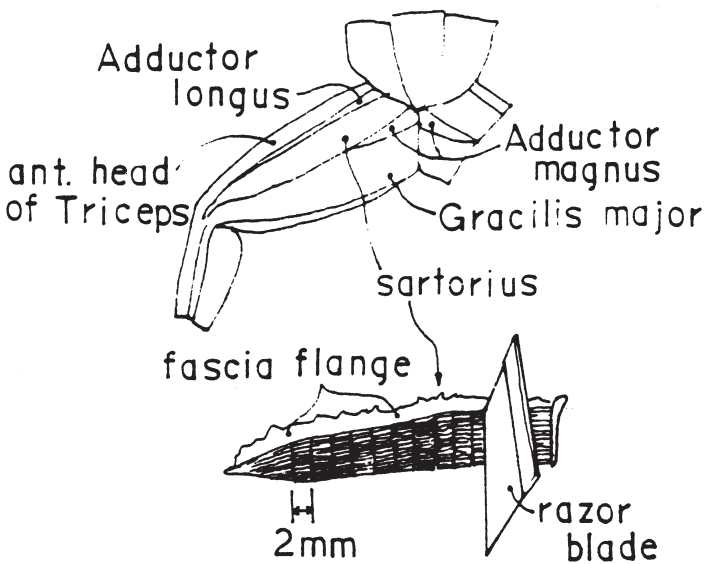


FIGURE 6. The top figure shows the ventral surface of the skinned thigh of a leopard frog, demonstrating the location and shape of the sartorius muscle. The bottom figure illustrates how razor blade cuts can make frog muscle cell segments with open ends. But since the illustration was from a different project, the product is not the accordion-like assembly of 2 mm- and 4mm-wide segments but fully isolated assemblies of segments containing uniformly 2 mm wide muscle cell segments. (From Ling and Ochsenfeld 1991.)

muscle is then placed upon a stack of properly-wetted filter paper (for details, see Materials and Methods of Ling and Walton 1975) and the assembly of muscle and moist filter paper wrapped in a sheet of paraffin film (Parafilm) to form a hermetically-sealed packet. Each packet is then placed at the bottom of an empty 250-ml centrifuge-tube-shield in a refrigerated centrifuge and spun at from 50 to 2000 g for varying duration. Following that, the muscle is removed from the packet and weighed again to obtain the amount of liquid water lost to the muscle as a result of the centrifugation.

As shown in Figures 7 and 8, the weight loss of the muscle is constant at a centrifugal force between 400 g and 1400 g (all for 4 minutes) and averages 9.3%. At 1000 g, spinning from 2 to 16 minutes extracted on the average 9.4% of the weight of the muscle..

Statistically speaking, these values of 9.3% to 9.4% are not different from the average weight percentage of water, $9.1\% \pm 0.76$ (S.D.), found in the extracellular space of the sartorius muscle earlier with the aid of four new and different independent methods: the low-inulin probe method, 10.3%; poly-L-glutamate method, 8.9%; single muscle fiber sucrose space method (9%); ^{86}Br method, 8.2%. (For sources of publications, see Ling and Walton 1975, p. 217.) The good accord of the centrifugation extractable weight and the weight percentage of water in the extracellular space established that centrifugation for 4 minutes at 1000 g quantitatively removes all the normal liquid water from the extracellular space of a frog sartorius muscle but leaves water and other materials inside the cell unchanged.

Our next chore was to find a way of destroying the membrane barrier to the free flow of water in and out of the cell; that is, if cell water truly exists as (free-flowing) normal liquid water as prescribed by Theory I, II, III and IV. Again the anatomical makeup of the sartorius muscle makes this task easy to achieve and to achieve effectively.

As indicated above, the sartorius muscle contains some 1000 highly similar hair-like muscle fibers or cells, each running all the way from its distal tibial end to its proximal pelvic end without interruption (Ling 1973, p.299.). Nor is there any internal barriers across the width of the muscle cell that would prevent the water molecules from moving smoothly from the inside of one end of the cell to the other end (see Ling and Ochsenfeld 1973, Figure 1, A,B,C for evidence of unhindered (radioactively-labeled) water diffusion in the longitudinal direction along the length of the sartorius muscle cells.)

Accordingly, a simple razor blade cut across the muscle (at a point a few millimeters proximal to the tapering tibial end of the muscle) would destroy at once the intactness of the membrane of all the 1000-some muscle cells in the sartorius. The next task is to prove that the cut end of the muscle cell thus laid bare does not regenerate a new covering cell membrane. In fact, that too has been established from two different approaches, one with the aid of electron-microscopy; the other using chemical probes.

Figure 9 reproduced from Cameron (1988), shows that the exposed ends of the cut muscle cells do not regenerate new cell membranes. Table III from Ling (1973) shows that the strongly enhanced permeability of the cut end of muscle cells to radioactively labeled sodium ion and sucrose remained unchanged 24 hours later, again indicating no membrane regeneration.

Having found that spinning 4 minutes at 1000 g provides us with the means of removing exclusively all the normal liquid water from a frog sartorius muscle and that a razor blade cut destroys lastingly the integrity of the cell membrane as a diffusion barrier, we were in a position to perform the incisive experiment aimed at determining if the the bulk-

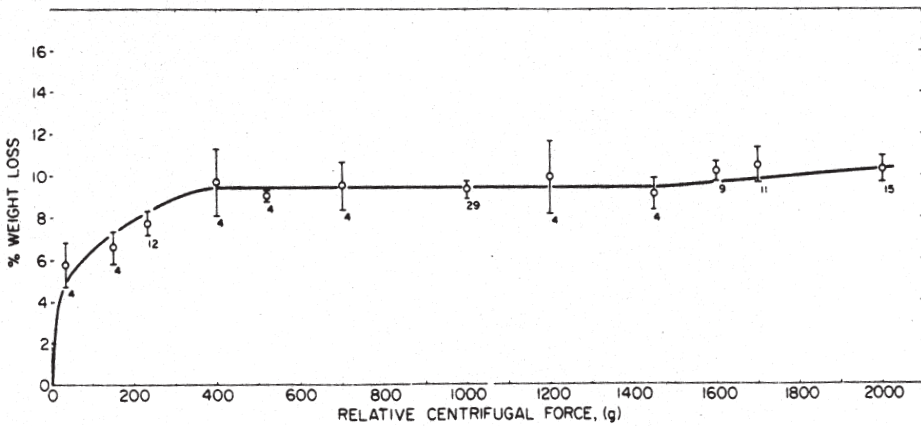


FIGURE 7. Weight loss as a percentage of initial weight (ordinate) following spinning in a hermetically sealed packet at different relative centrifugal force. Centrifugal force represented as multiples of g. Time of spinning was uniformly 4 minutes. Number under each experimental data point indicates number of independent experiments performed. The distance between the horizontal bars represents twice the standard errors (from Ling and Walton 1975.)

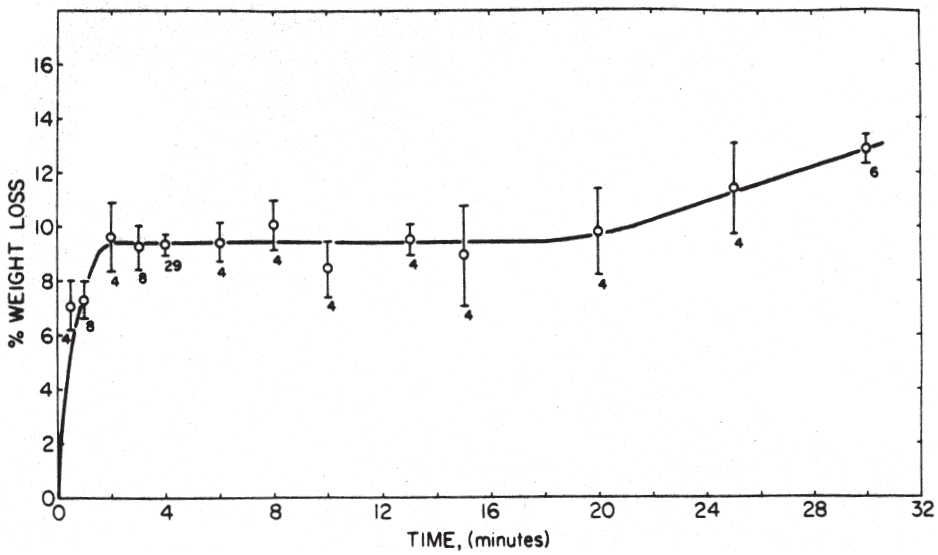


FIGURE 8. Percentage weight loss of frog sartorius muscle after centrifugation at 1000 g for varying lengths of time. Symbols have same meaning as described under Figure 7 (from Ling and Walton, 1975.)

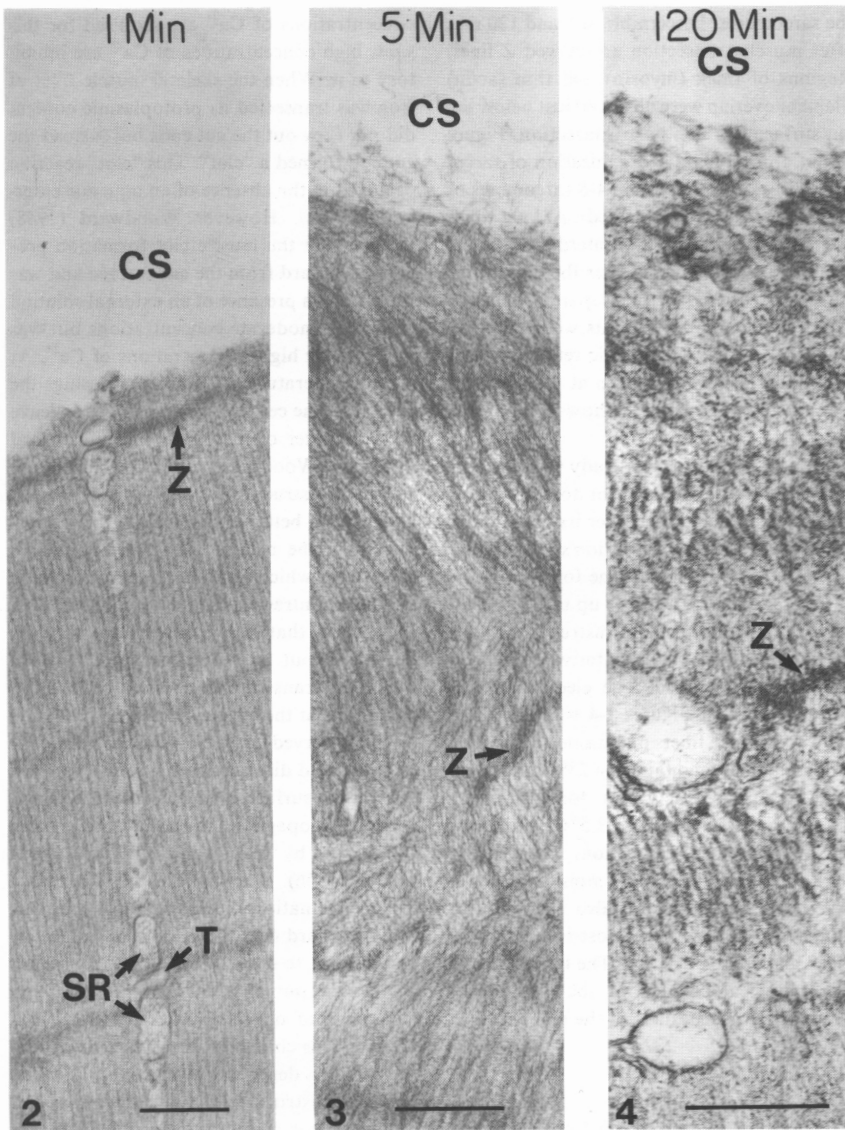


FIGURE 9. Electron-micrographs of the cut ends of 1 mm-long frog muscle fiber (cell) fixed at 1 minute (Plate 2), 5 minutes (Plate 3) and 120 minutes (Plate 4) after trans-section of the muscle fibers. Plate 2 shows contraction of the sarcomere immediately next to the cut surface (CS). Plate 3 and 4 show progressive disorganization of the surface sarcomere and failure of the surface to regenerate a new plasma membrane. A one micron marker bar is at the bottom of each Plate. Z, T and SR represent respectively the Z-line, T-tubule and sarcoplasmic reticulum. (from Cameron 1988.)

Table III. Chemical evidence that the exposed surface of frog muscle cells after a (razor-blade) cut does not regenerate a new cell membrane.

	Rate before Cutting ($\mu\text{moles/g}$)	Rate After Cutting ($\mu\text{moles/g}$)	
		immediately after cutting	incubated after cutting
sucrose	0.073 ± 0.013	0.174 ± 0.031	0.168 ± 0.016 (24 hrs)
Na^+		22.7 ± 2.5	22.3 ± 5.1 (51 hrs)

A frog sartorius muscle was cut crosswise (once) with a razor blade at a location proximal to the tapering tibial end of the muscle (to ensure the exposure of the inside of all the 1000-some muscle fibers to the labeled probes.) The cut muscle was then mounted in what is known as *Effectively Membrane-pump-less Open-ended Cell* (EMOC) preparation, which holds the bulk of the sartorius muscle in moistened air and exposes only the open end of the muscle to the Ringer's solution containing radioactively-labeled Na^+ and radioactively-labeled sucrose. Last column gives duration of exposure in hours to sucrose and labelled Na^+ , respectively. Illustrations of the EMOC setup can be found in Ling 2001 p. 53 (from Ling 1973 reproduced in Ling 2001.)

phase water in frog muscle cells is truly normal liquid water. And here are the additional details on how the incisive experiment was actually carried out.

By making razor blade cut half way across the muscle on alternate sides, one or more accordion-like preparation(s) of muscle cell fragments can be made from a single sartorius muscle. (For more complete razor blade sectioning, see bottom illustration of Figure 6.) Each of these individual preparations contains a population of some 1000 muscle cell fragments, either 2 mm or 4 mm long and with both ends open. This accordion-like assembly of open-ended muscle was then carefully blotted on moist filter paper by the standard procedure mentioned above. Freed of extra surface-adhering fluid, the preparation was weighed, wrapped in Parafilm and spun for 4 minutes at 1000 g, before weighing again on the torsion balance in the humidity chamber — in exactly the same way as described for extracting normal liquid water from intact sartorius muscles. In 1976, Ling and Walton published their centrifugation study in Volume 191 of the *Science* magazine under the title, "What Retains Water in Living Cells?"

In Figure 10 reproduced from that 1976 publication, the bar-graphs, $a_1 a_2$, $b_1 b_2$, $c_1 c_2$ show that cutting frog sartorius muscle or rat diaphragm muscle into 2- and 4-mm wide segments with two open ends did not significantly increase the percentage of *centrifugation extractable fluid* (CEF) shown in the top figures. The same percentages of CEF were obtained from the cut muscle segments as from their paired muscle that were kept intact. In other words, no outflow of (normal) liquid water from cells with open ends occurred. Since the same treatment (4 minutes of spinning at 1000 g) does remove quantitatively all the normal liquid water found in between the muscle fibers, this set of findings has clearly shown that there is no detectable amount of normal liquid water within frog sartorius muscle cells.

Furthermore, intact sartorius muscles or cut muscle segments, when leached exhaustively in large volumes of pure distilled water loses virtually all its K^+ and other intracellular solutes (for details, see Endnote 1 located at the end of this article.) Nonetheless, these leached muscles retained the same percentages of water content as their normal counterparts after centrifugation for 4 minutes at 1000 g. Indeed, the only major components left in these leached and centrifuged muscles segments are water and proteins.

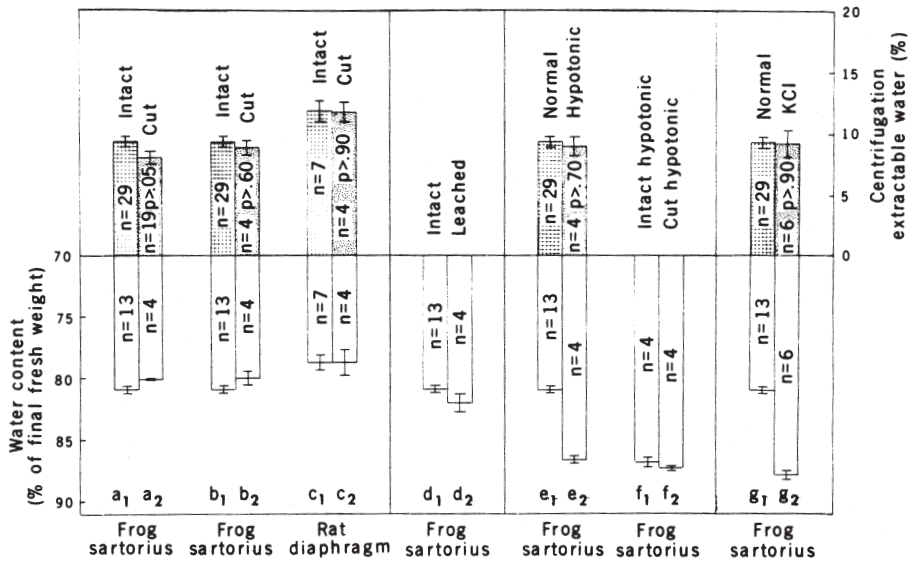


FIGURE 10. Data show that cutting frog muscle cells into 2 mm- and 4 mm-segments with both ends open, does not significantly increase the centrifugation-extractable water ($a_1 a_2$, $b_1 b_2$, $c_1 c_2$.) Nor does leaching (intact muscle cells) in large volumes of distilled water, which removes most of the solutes in the cells (see Endnote 1 for detailed data) significantly reduce the percentage of water retained in the leached muscle after centrifugation for 4 min. at 1000 g. (d_1 , d_2 .) Upper bars represent CEF; lower ones, water content at conclusion of the described treatments (from Ling and Walton 1976, by permission of Science.)

In summary, the centrifugation experiment has produced three sets of facts of far-reaching significance. (1) there is no free normal liquid water in frog muscle cells; (2) the retention of a normal amount of water in living cells does not depend on the presence of an intact, enclosing cell membrane and (3) nor does the retention of the cell water depend on the presence of a high concentration of intracellular ions like K^+ .

III. Conclusions

It is not difficult to see that each of the three iconoclastic findings from the centrifugation experiment (no free water in cell; intact enclosing cell membrane unnecessary; high concentration in intracellular ions unnecessary) is enough to disprove four of the five theories of cell water considered. They are the accidental theory (Theory I), the Donnan equilibrium theory (Theory II), the direct water pump-leak theory (Theory III) and the indirect pump-leak theory (Theory IV.)

That the sodium pump demands far more energy than available has disproved yet another time the direct, and indirect pump-leak theories (Theory III, IV.).

The demonstration of function specificity of cell water content has disproved the accidental theory (Theory I) yet another time. Nor do the Donnan membrane equilibrium

theory (Theory II), the direct- and indirect pump-leak theories (Theory III and IV) predict the functional specificity of cell water content.

One theory alone, the polarized-oriented multilayer theory of cell water (Theory V) survived all three sets of experimental findings. In fact, like hand and glove, they are in full harmony with and eloquently support the theory.

Having said that, I must point out that it is important to recognize that the resistance to centrifugal extraction of intracellular water can only be expected from cells like the frog muscle, in which as a stiff gel, the intracellular proteins (and associated water-ion assemblies) are immobilized.

In contrast, even gravitational force alone (at 1 g) is able to cause the outpouring of normal liquid water from the large central vacuoles of mature plant cells,—which in the case of giant algal cells can be substantial in quantity. Furthermore, the protoplasm surrounding the central vacuole of these giant algal cells are also fluid in nature and can flow out of the cut end of the giant cell as shown in Figure 11, taken from Kuroda (1964.) Indeed, it was this type of fluid protoplasm emerging from broken protozoan cells that had led to the discovery of what was later named protoplasm by Felix DuJardin more than a century and half ago (Ling 2001, p.6.) However, what flows out of the cut end of the

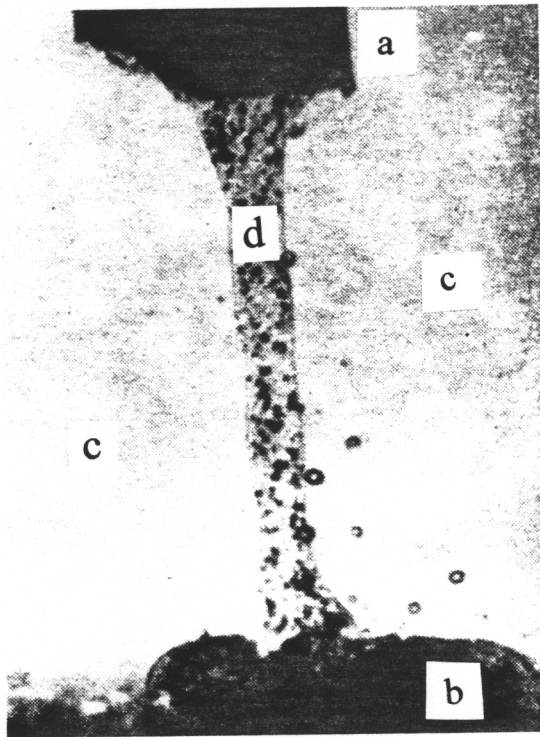


FIGURE 11. Outflow of protoplasm (endoplasm) (d) from the cut end of a *Nitella* cell (a) into a culture medium (c) The protoplasm collected as a flattened round drop (b) on the bottom of the cuvette. Note air bubbles in the culture medium. The picture was taken 5 minutes after the cut was made (from Kuroda, 1964 reprinted with permission of the Academic Press.)

Nitella cell is not normal liquid water but a fluid form of living protoplasm, of which water is an integral and indispensable part. Indeed, in a balanced salt solution, the isolated protoplasm could be kept alive for 3 days after its isolation (Kamiya and Kuroda 1957 ; Kuroda 1964, pp.32–33.)

I thank Dr. Raymond Damadian and his Fonar Corporation, Inc. for their continued support, Margaret Ochsenfeld and Dr. Zhen-dong Chen for their dedicated and skillful help and valuable scientific contributions.

Endnotes

1. The concentrations of several cations found in frog sartorius muscles after extensive leaching in repeated changes of large volume of cold distilled water at 4° C: K^+ , $0.242 \pm 0.242 \mu\text{moles/gram}$ fresh weight (in normal muscle, 85.8 $\mu\text{moles/gram}$); Na^+ , 1.34 ± 0.68 (normal 24.9); Mg^{++} , 1.90 ± 0.30 (normal, 10.8); Ca^{++} , 0.225 ± 0.093 (normal, 4.08.). Assuming that all the (remaining) ions estimated above are free and that an equivalent amount of anions (in the form of monovalent Cl^-) also exists in the leached muscle cells, the maximum osmolarity would be about 9.5 milli-osmolar. This is to be compared with the total osmolarity of 125.6 milli-osmolar from the above-mentioned intracellular cations alone in normal frog muscle. That is, if one assumes that these cations are all free as according to the membrane pump theory but not as according to the AI Hypothesis and its extensive supporting evidence as summarized in 2001 (Ling 2001, Chapter 10.)

References

- Beall, P.T., Amtey, S.R. and Kasturi, S.R. (1984) *NMR Data Handbook for Biomedical Applications*, Pergamon Press, New York .
- Boyle, P.J. and Conway, E.J. (1941) *J. Physiol.* 100: 1.
- Cameron, I.L. (1988) *Physiol. Chem. Phys. & Med. NMR* 20: 221.
- Dean, R. (1941) *Biol. Symp.* 3: 331.
- Donnan, F. (1924) *Chem. Rev.* 1: 73.
- Dowben, R.M. (1969) *General Physiology; A Molecular Approach*, Harper and Rowe, New York.
- Greenstein, J.P. (1947) *Biochemistry of Cancer*, Academic Press, New York, 1st ed., p. 267.
- Gutknecht, J., Hastings, D.F. and Bisson, M.A. (1978) In *Transport Across Multi-membrane Systems* (G. Giebisch, ed.) Springer Verlag, Berlin p. 125.
- Jain, M.K. (1972) *The Bimolecular Lipid Membrane: A System*, van Nostrand-Reinhold Co., New York.
- Knox, W.E. (1967) *Adv. Cancer Res.* 10: 117.
- Kamiya, N. and Kuroda, K. (1957) *Proc. Japan Acad.* 33: 149
- Kuroda, K. (1964) In *Primitive Motile Systems in Cell Biology* (R.D. Allen and N. Kamiya, eds.) Academic Press, New York p. 31.
- Ling, G.N. (1952) In: *Phosphorus Metabolism* (Vol. II) (W.D. McElroy and B. Glass, eds.) The Johns Hopkins Univ. Press, Baltimore, p. 748.
- Ling, G.N. (1962) *A Physical Theory of the Living State: The Association-Induction Hypothesis*, Blasidell Publishing Co., Waltham, Mass.
- Ling, G.N. (1965) *Ann. New York Acad. Sci.* 125: 401.
- Ling, G.N. (1973) *Physiol. Chem. Phys.* 5: 295.
- Ling, G.N. (1984) *In Search of the Physical Basis of Life*, Plenum Publish. Co., New York.

- Ling, G.N. (1987) *Physiol. Chem. Phys. & Med. NMR* 19: 199.
- Ling, G.N. (1992) *A Revolution in the Physiology of the Living Cell*, Krieger Publish, Co., Malabar, FL.
- Ling, G.N. (1997) *Physiol. Chem. Phys. & Med. NMR* 29: 123.
- Ling, G.N. (2001) *Life at the Cell and Below-Cell Level: the Hidden History of a Fundamental Revolution in Biology*, Pacific Press, New York.
- Ling, G.N. (2003) *Physiol. Chem. Phys. & Med. NMR* 35: 91.
- Ling, G.N. and Bohr, G. (1969) *Physiol. Chem. Phys.* 1: 591.
- Ling, G.N. and Ochsenfeld, M.M. (1973) *Science* 181: 78.
- Ling, G.N. and Ochsenfeld, M.M. (1991) *Physiol. Chem, Phys. & Med. NMR* 23: 133.
- Ling, G.N. and Tucker, M. (1980) *J. Nat. Cancer Inst.* 64: 1199.
- Ling, G.N. and Walton, C.L. (1975) *Physiol. Chem. Phys.* 7: 215.
- Ling, G.N. and Walton, C.L. (1976) *Science* 191: 295.
- Ling, G.N., Neville, M.C., Will, S. and Shannon, P. (1969) *Physiol. Chem. Phys.* 1: 85.
- Ling, G.N., Miller, C. and Ochsenfeld, M.M. (1973) *Ann. N.Y. Acad. Sci.* 204: 6.
- Ling, G.N., Reid, C. and Murphy, R.C. (1986) *Physiol. Chem. Phys. & Med. NMR* 18: 147.
- Miyamoto, V.K. and Thompson, T.E. (1967) *J. Colloid Interf. Sci.* 25: 16.
- Ponder, E. (1948) *Hemolysis and Related Phenomena*, Grune and Stratton, New York.
- Skou, S.J. (1965) *Physiol. Rev.* 45: 596.
- Wood, R.E., Wirth, F.P. and Morgan, H.E. (1968) *Biochem. Biophys. Acta* 163: 171.

Received August 17, 2004;
accepted September 10, 2004.

17 β -Estradiol Suppresses ROS-induced Apoptosis of CHO Cells through Inhibition of Lipid Peroxidation-coupled Membrane Permeability Transition

Chosei Miyaguchi^{1,2}, Shikibu Muranaka^{2,3*}, Tomoko Kanno³, Hirofumi Fujita^{2,3}, Jitsuo Akiyama², Tamotsu Yoshioka³ and Tatsuji Yasuda¹

¹Department of Cell Chemistry, Okayama University Graduate School of Medicine and Dentistry, Okayama 700-8558, Japan, ²Doonan Institute of Medical Science, Ishikawa-cho, Hakodate 041-8502, Japan, ³Institute of Medical Science, Kurashiki Medical Center, Kurashiki 710-8522, Japan

*Author for correspondence

Abstract: Oxidative stress-induced apoptotic cell death has been implicated to play a critical role in the mechanism of corpus luteum regression and follicular atresia. Recent studies suggests that reactive oxygen species (ROS) might play important roles in the regulation of luteal function. The present work describes the inhibitory effect of 17 β -estradiol (E2) on ROS-induced mitochondrial membrane permeability transition (MPT) and apoptosis of Chinese hamster ovary (CHO) cells. ROS generated by Fe²⁺ and H₂O₂ induced mitochondrial lipid peroxidation, depolarization, activation of caspase-3 and DNA fragmentation in CHO cells by some E2-inhibitable mechanism. E2 suppressed the Fe²⁺/H₂O₂-induced lipid peroxidation and MPT of isolated mitochondria that was characterized by cyclosporin A-inhibitable swelling, depolarization and cytochrome c release. Furthermore, E2 scavenged the xanthine oxidase generated ROS. These results suggests that Fe²⁺/H₂O₂ induced MPT and apoptosis of CHO cells by a mechanism that could be suppressed by antioxidant properties of E2.

OXIDATIVE STRESS-INDUCED apoptosis has been implicated in the mechanisms for the regression of corpus luteum and follicular atresia (1). Recent studies revealed that

Abbreviations: AMC, 7-amino-4-methyl-coumarin; CHO, Chinese hamster ovary; Ac-DCFH-DA, 2', 7-dichlorofluorescein diacetate; DEVD-MCA, acetyl-Asp-Glu-Val-Asp-MCA; E2, 17 β -estradiol; MPT, membrane permeability transition; ·OH, hydroxyl radical; JC-1, 5,5',6,6'-tetrachloro-1,1',3,3'-tetraethylbenzimidazol carbocyanine iodide; RNase, ribonuclease; ROS, reactive oxygen species; TBARS, thiobarbituric acid reactive substance.

reactive oxygen species (ROS) play important roles in the regulation of luteal function (2). The aim of the present work is to clarify the mechanism of suppression of Chinese hamster ovary (CHO) cell apoptosis by 17 β -estradiol (E2).

It has been known that E2 and its oxidized products inhibit lipid peroxidation (3). E2 donates hydrogen atoms from its phenolic hydroxyl groups to lipid peroxyradicals and terminates the chain reactions of membranous phospholipid oxidation leading to cell death. Apoptosis induced by oxidative stress has been postulated to underlie the mechanism of corpus luteum regression and follicular atresia (1). Since estradiol exhibits antioxidant activity and inhibits apoptosis in luteal and follicular tissues exposed to hydrogen peroxide, this hormone seems to function as a scavenger for ROS in the ovary during the pregnancy-mediated luteal rescue and folliculogenesis (4–7). Suppression of estradiol production in proestrous state by an aromatase inhibitor was associated with lipid peroxidation and testosterone accumulation in the follicles, and apoptosis of granulosa cells. E2 stimulated nuclear antigen in proliferating granulosa cells and protected cells from ROS-induced apoptosis (8). Thus, it appears that cytoprotective action of estradiol operates in preovulatory follicles. Cytoprotective effect of estradiol was also observed with apoptosis of other types of cells induced by ROS (9). However, the molecular mechanism of antiapoptotic action of E2 has not been fully elucidated.

Several lines of evidence indicate that changes in mitochondrial functions underlie the mechanism of apoptosis (10). Apoptosis-related proteins released from mitochondria through membrane permeability transition (MPT) stimulate caspase cascade, thereby inducing apoptosis of various cells (11). To get further insight into the mechanism of cell death and its inhibition by E2, we investigated the effect of E2 on the $\text{Fe}^{2+}/\text{H}_2\text{O}_2$ -induced MPT and apoptosis of CHO cells. We also demonstrated that E2 inhibited the apoptosis of CHO cells by suppressing directly inhibiting cellular accumulation of lipid peroxides and hydroxyl radical ($\cdot\text{OH}$). The protective effect of E2 appeared independently from the presence or activation of E2 receptors. These results suggest that ROS underlie the mechanism for cell death in ovarian tissues and that E2 plays important roles in the regulation of apoptosis through modulating mitochondrial MPT.

Materials and Methods

Chemicals

E2, ferricytochrome c (Cyt. c), 5,5',6,6'-tetrachloro-1,1',3,3'-tetraethylbenzimidazolyl-carbocyanine iodide (JC-1), ribonuclease (RNase) A and proteinase K were obtained from Sigma Chemical Co. (USA). Dichlorofluorescein-diacetate (DCFH-DA) was purchased from Molecular Probes, Inc. (USA). Monoclonal antibody against cytochrome c was purchased from PharMingen (USA). Fluorogenic substrates for caspase-3, such as Ac-DEVD-MCA, were obtained from the Peptide Institute (Japan). All other chemicals were of analytical grade and obtained from Nacalai Tesque (Japan).

Cell Line

Chinese hamster ovary cells were maintained in MEM supplemented with 10% heat-inactivated fetal bovine serum (SIGMA), 100 U/ml penicillin and 100 $\mu\text{g}/\text{ml}$ streptomycin.

Cells were grown in a humidified incubator at 37°C under 5% CO₂ and 95% air and used for assays during their exponential phase of growth. Cells were routinely counted to maintain a low population density and their viability was assayed by the trypan blue exclusion method (12).

Treatment of cells with Fe²⁺/H₂O₂

CHO cells (1.7 x 10⁵ cells) were generally plated in 1.5 ml of MEM containing 10% fetal bovine serum and incubated for 16 h before treatment with various reagents. Before starting experiments, cells were preincubated with E2 at 37°C for 1 h. In the presence of Fe²⁺/H₂O₂, cells were incubated for various times in the presence or absence of various concentrations of E2.

Assay for generation of reactive oxygen species in CHO cells

Cellular levels of ROS were measured by using oxidation-sensitive fluorescent probe DCFH-DA as described previously (13). Before and after incubation with Fe²⁺/H₂O₂ in the presence or absence of E2, cells were incubated for 30 min with 20 μ M DCFH-DA in phosphate buffer saline (PBS). ROS was quantitated after washing cells with PBS by a FACScan flow cytometer (Becton Dickinson).

Isolation of rat liver mitochondria

Male Wistar rats weighing 200 g were used for experiments after overnight fasting. The liver was homogenized in 0.25 M sucrose containing 10 mM Tris-HCl buffer (pH 7.4) and 0.1 mM EDTA at 4°C. Mitochondria were isolated by the method of Hogeboom as described in a previous paper (14).

Assay for reactive oxygen species and thiobarbituric acid reactive substances

Because mitochondria contain a large amount of Mn-SOD, a highly sensitive chemiluminescence (CHL) probe, L-012, was used for the analysis of mitochondrial ROS (15). Isolated mitochondria (0.1 mg protein/ml) were incubated in 10 mM Tris-HCl buffer (pH 7.4) containing 150 mM KCl, 3 mM succinate and 1 mM phosphate (Pi) buffer (pH 7.4) in the presence of 50 μ M L-120 at 25°C. After incubation of mitochondria for 1 min at 25°C, reaction was started by adding 50 μ M CaCl₂. During the incubation, CHL intensity was recorded continuously for ~ 20 min using Intercellular Ion Analyzer (Jasco CAF-110) (CHL mode, Jasco PL-03). ROS was also generated by 2 mU/ml xanthine oxidase in PBS containing 40 μ M hypoxanthine and 50 μ M L-120 at 37°C. Thiobarbituric acid-reactive substances (TBARS) in CHO cells and isolated mitochondria were assayed by the method of Ohkawa *et al.* (16).

Analysis for DNA fragmentation

The extent of DNA fragmentation was determined spectrophotometrically by the di-phenylamine method (17). Briefly, after incubation with Fe²⁺/H₂O₂ and E2, cells were lysed in 200 μ l of lysis buffer [10 mM Tris-HCl buffer (pH 7.4), 10 mM EDTA and 0.5% Triton X-100] at 4°C for 30 min. The lysate was centrifuged at 13,000 x g and 4°C for 20 min to separate intact and fragmented chromatin. Both pellet and supernatant were

precipitated by 6% perchloric acid at 4°C for 30 min. The precipitates were sedimented at 13,000 x g and 4°C for 20 min. The DNA specimens were heated at 70°C for 20 min in 50 µl of 6% perchloric acid, and mixed with 100 µl of 1.5% diphenylamine solution containing 1.5% sulfuric acid and 0.01% acetaldehyde in acetic acid. After overnight incubation at 30°C in the dark, they were measured spectrophotometrically at 600 nm, and the percentage of DNA fragmentation was calculated.

DNA ladder formation was observed with agarose gel electrophoresis (12, 17). The lysate was treated with 400 µg/ml RNase A at 37°C for 1 h and subsequently with 400 µg/ml proteinase K at 37°C for 1 h. DNA samples were precipitated with an equal volume of isopropanol and then electrophoresed at 50 V through a 2% agarose gel in TBE buffer [90 mM Tris-borate buffer (pH 8.3), containing 2 mM EDTA]. DNA bands were visualized under ultraviolet illumination and photographed on a Polaroid 667 film.

Assay for caspase-3 activity

Caspase activity was determined as described previously (18) in 20 mM HEPES buffer (pH 7.5) containing 0.1 M NaCl and 5 mM dithiothreitol at 37°C using 10 µM of Ac-DEVD-MCA. One unit of the enzyme was defined as the amount of enzyme required for the liberation of 1 µmole of substrate during 1 h.

Assay for mitochondrial membrane potential in CHO cells

After incubation with Fe²⁺/H₂O₂ for 72 h in the presence or absence of E2, cells were washed with PBS, stained with 5 µg/ml of JC-1 for 30 min at 37°C. Then, cells were re-suspended in PBS and analyzed using a FACScan flow cytometer (Becton Dickinson, San Jose, CA, USA) to determine mitochondrial membrane potential in CHO cells (19, 20). Protein concentrations were determined by the method of Bradford (21) using bovine serum albumin as a standard.

Assay for mitochondrial functions

Mitochondrial swelling and depolarization were assessed spectrophotometrically. Mitochondria (0.1 mg protein/ml) were incubated in 10 mM Tris-HCl (pH 7.4) containing 0.15 M KCl at 25°C. The change in the absorbancy at 540 nm was recorded in a Shimadzu UV-3000 (22). Membrane potential of mitochondria was measured by fluorescence intensity at 670 nm during the excitation at 622 nm in a medium containing 0.15 µg/ml diS-C3-(5) (22). Release of Cyt.c from mitochondria was analyzed as described previously (23, 24). Mitochondria (0.1 mg protein/ml) suspended in a standard medium containing 2.5 mM succinate were incubated with 20 µM Fe²⁺ and 100 µM H₂O₂ at 25°C for 10 min in the presence or absence of 25 µM E2. After centrifugation at 7,000 x g for 10 min, the supernatants were added to 0.5 volume of SDS-sample buffer containing 125 mM Tris-HCl (pH 6.8), 4% SDS, 10% β-mercaptoethanol, 20% glycerol and 0.002% bromophenol blue. After incubation at 100°C for 5 min, the samples were subjected to SDS-polyacrylamide gel electrophoresis followed by Western blotting analysis using specific antibodies and ECL kit (Amersham). Uptake and release of Ca²⁺ was analyzed by monitoring the fluorescence intensity of antipyrilazo III at 720–790 nm (25). Uptake and release of Ca²⁺ by mitochondria were analyzed by adding 0.1 µM FCCP at the end of each experiment.

Results

Suppression of ROS generation, lipid peroxidation and membrane depolarization of CHO cells by E2

Although the presence of either Fe^{2+} or H_2O_2 had no appreciable effect on CHO cells, the presence of both Fe^{2+} and H_2O_2 induced DNA fragmentation (Figure 1).

When cells were exposed to hydroxyl radical, they started to generate large amounts of ROS in the cells. In fact, $\text{Fe}^{2+}/\text{H}_2\text{O}_2$ stimulated the cellular generation of ROS as detected by DCFH-DA. The oxidized DCFH in cytoplasm increased with time concomitant increase in TBARS. E2 suppressed the generation of ROS and TBARS (Figure 2).

Since mitochondria have been postulated to play important roles in the mechanism of apoptosis, we examined the effect of $\text{Fe}^{2+}/\text{H}_2\text{O}_2$ on membrane potential of CHO cells. Treatment of CHO cells with $\text{Fe}^{2+}/\text{H}_2\text{O}_2$ induced the depolarization of mitochondrial membranes by a mechanism that was suppressed by the presence of either E2 or cyclosporin A, a specific inhibitor of MPT (Figure 3). The result suggests that mitochondrial MPT also play an important role in the process of apoptosis induced by $\text{Fe}^{2+}/\text{H}_2\text{O}_2$.

Suppression of ROS-induced apoptosis by E2

Release of cytochrome c from mitochondria might activate caspase-3 in cytosol. The effect of $\text{Fe}^{2+}/\text{H}_2\text{O}_2$ on the caspase-3-like activity in CHO cells is seen in Figure 4. When exposed to $\text{Fe}^{2+}/\text{H}_2\text{O}_2$, caspase-3 activity in the cells increased. Thus, activation of caspase cascade seems to underlie the mechanism of apoptosis induced by $\text{Fe}^{2+}/\text{H}_2\text{O}_2$.

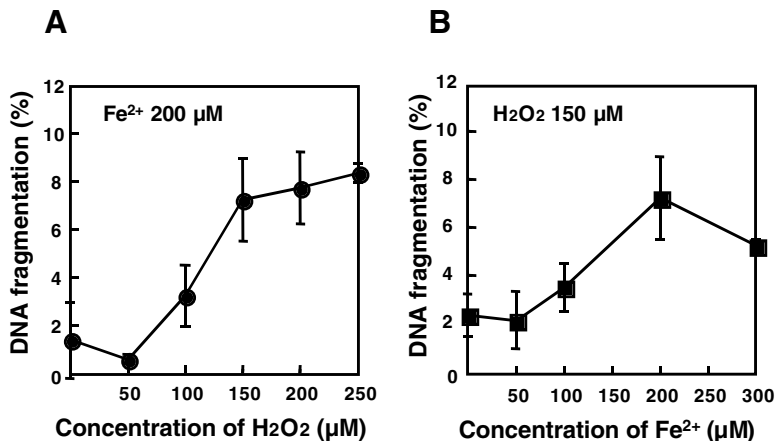


FIGURE 1. $\text{Fe}^{2+}/\text{H}_2\text{O}_2$ -induced concentration dependent DNA-fragmentation of CHO cells. The cell were treated with $\text{Fe}^{2+}/\text{H}_2\text{O}_2$ and the percentage of fragmented DNA was determined by the diphenylamine method. (A) H_2O_2 dependent curve of DNA-fragmentation in the presence of 200 μM Fe^{2+} at 72h. (B) Fe^{2+} dependent curve of DNA-fragmentation in the presence of 150 μM H_2O_2 at 72h. Data are means \pm SD from three independent experiments.

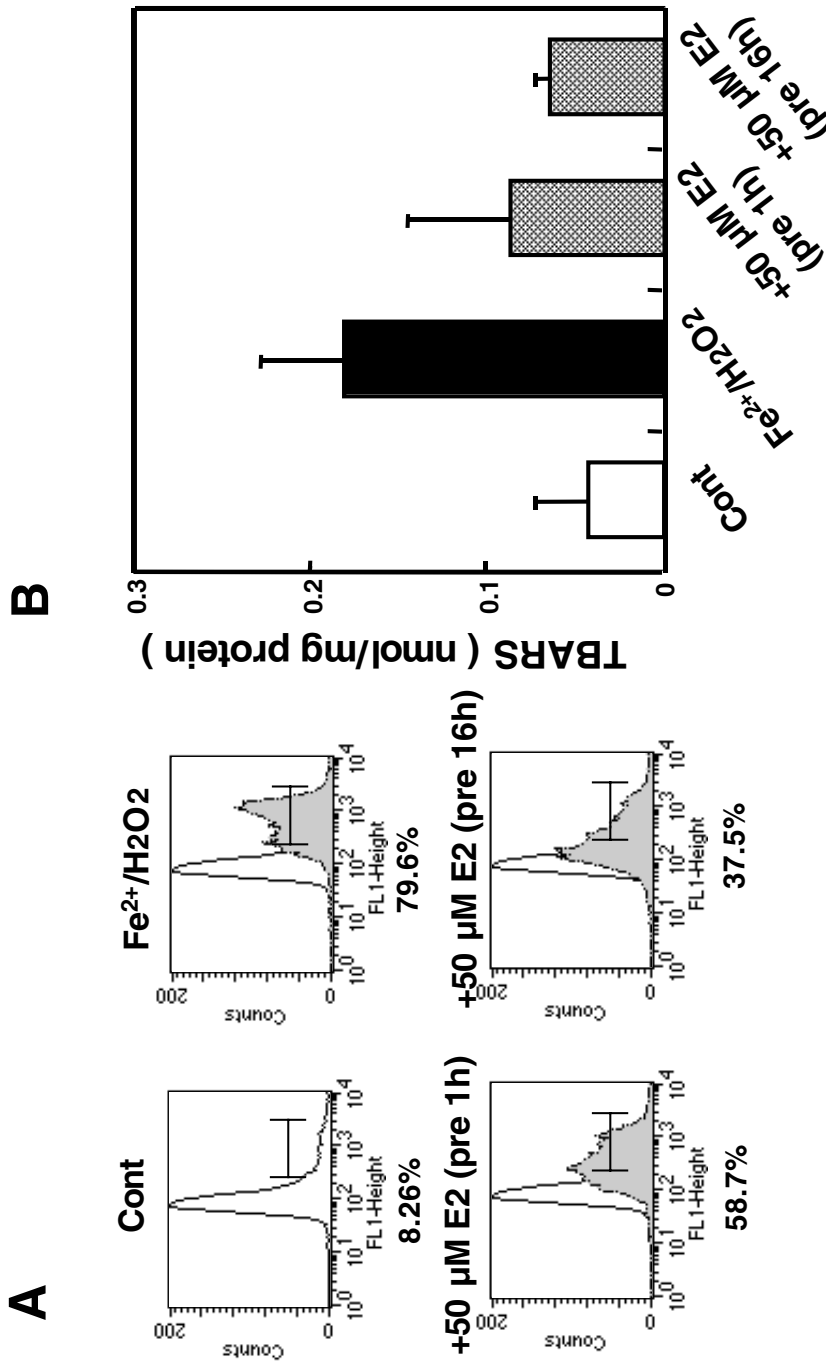


FIGURE 2. Suppression of Fe²⁺/H₂O₂-induced ROS generation and lipid peroxidation in CHO cells by E₂. Experimental conditions were as described in Figure 1. Cells were preincubated 1 ~ 16 h with 50 μM E₂. (A) The cells were stained with DCFH-DA after incubation for 3 h with 200 μM Fe²⁺/150 μM H₂O₂ in PBS and generated ROS was quantitated by a FACScan flow cytometer. Similar results were obtained in three separate experiments. (B) Effect of E₂ on the Fe²⁺/H₂O₂-induced lipid peroxidation of CHO cells. Lipid per-oxidation was induced by 3 h incubation with 200 μM Fe²⁺/150 μM H₂O₂ in PBS and expressed by the value as TBARS (16). Data are means ± SD from three independent experiments.

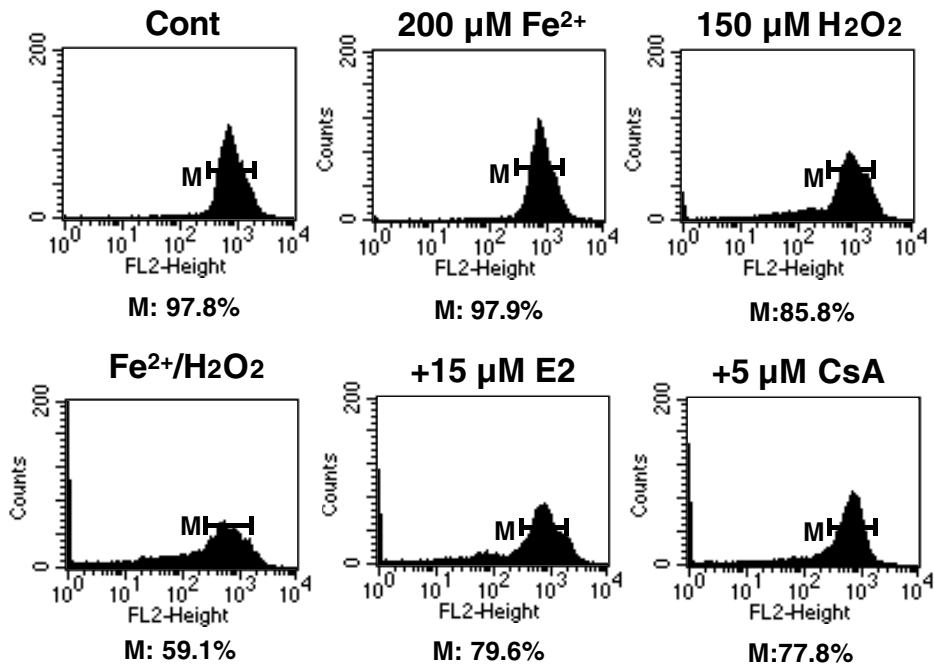


FIGURE 3. Suppression of Fe²⁺/H₂O₂-induced membrane depolarization of CHO cells by E2. CHO cells were preincubated 1 h with 15 μ M E2 or 5 μ M cyclosporin A and incubated for 72h in the presence or absence of 200 μ M Fe²⁺/150 μ M H₂O₂. After incubation, cells were stained with JC-1, and membrane potential was measured by flow cytometry. M shows the percent of polarized cells. Similar results were obtained in three separate experiments.

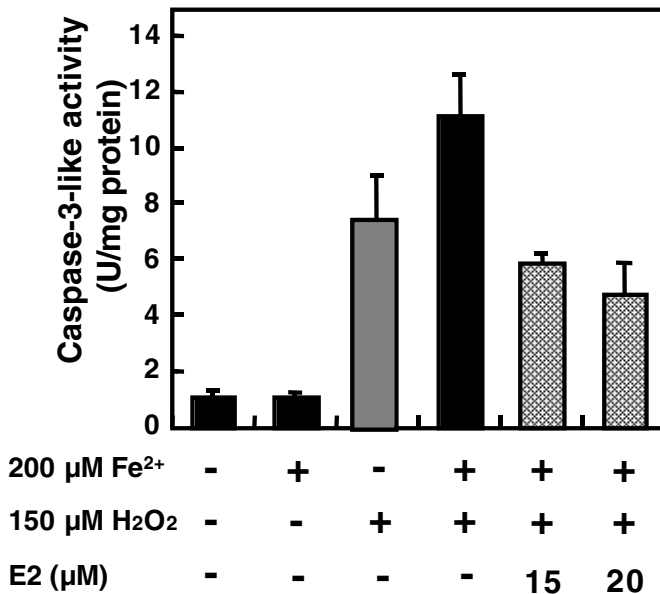


FIGURE 4. Suppression of Fe²⁺/H₂O₂-induced caspase-3 activation in CHO cells by E2. Cells were preincubated with 15 ~ 20 μ M E2 for 1h and incubated with 200 μ M Fe²⁺/150 μ M H₂O₂ for 72h. The cytosol of the cells (50 μ l) was incubated with 10 μ M fluorogenic peptide, DEVD, for caspase-3 (-like). Data are the means \pm SD from three independent experiments.

Figure 5 shows DNA fragmentation in CHO cells induced by $\text{Fe}^{2+}/\text{H}_2\text{O}_2$. DNA fragmentation was suppressed by E2 in a concentration-dependent manner. The DNA fragmentation and its sensitivity to E2 were further confirmed by observing ladder formation of cellular DNA.

To analyze the inhibitory mechanism of E2 against ROS-induced apoptosis, its effect on the functions of $\text{Fe}^{2+}/\text{H}_2\text{O}_2$ -treated mitochondria was examined. In the presence of respiratory substrates and Pi, mitochondria rapidly accumulated Ca^{2+} and then released it after being uncoupled by $\text{Fe}^{2+}/\text{H}_2\text{O}_2$ (Figure 6). The release of Ca^{2+} from mitochondria was suppressed by the presence of either E2 or α -tocopherol. These results suggest that E2 suppresses the release of Ca^{2+} by its antioxidant properties.

Since $\text{Fe}^{2+}/\text{H}_2\text{O}_2$ -induced membrane depolarization and caspase-3 activation were inhibited by E2, we examined the effect of E2 on mitochondrial swelling and cytochrome c release. The classic type of mitochondrial MPT is characterized by its Ca^{2+} - and energy-dependency, swelling, depolarization and cyclosporin A-sensitivity. E2 suppressed the $\text{Fe}^{2+}/\text{H}_2\text{O}_2$ -induced mitochondrial swelling, depolarization and cytochrome c release in a concentration-dependent manner (Figure 7). These events induced by $\text{Fe}^{2+}/\text{H}_2\text{O}_2$ were also suppressed by cyclosporin A (data not shown).

Suppression of mitochondrial lipid peroxidation by E2

$\text{Fe}^{2+}/\text{H}_2\text{O}_2$ induced mitochondrial MPT with concomitant induction of lipid peroxidation by an E2-inhibitable mechanism. $\text{Fe}^{2+}/\text{H}_2\text{O}_2$ -induced increase in TBARS was suppressed by E2 in a concentration dependent manner (Figure 8). We also analyzed the effect of E2 on ROS generated by Pi- and Ca^{2+} -treated mitochondria. As shown in Figure 9A, E2 suppressed the intensity of the CHL in a concentration dependent manner. E2 also suppressed the L-012 CHL developed by xanthine oxidase-induced ROS generation in a concentration dependent manner (Figure 9B). Kinetic analysis revealed that L-012 developed CHL predominantly by reacting with superoxide, hydroxyl radical and hypochlorite (15). The inhibitory effects of α -tocopherol and trifluoperazine, inhibitors of lipid peroxidation, were similar to those of E2 (data not shown). These results suggested that, E2 suppressed the generation of not only superoxide radical but also hydroxyl radical, thereby suppressing mitochondrial MPT leading to apoptosis.

Discussion

The present work clearly demonstrates that both E2 and cyclosporin A suppress the ROS-induced membrane depolarization, cytochrome c release, caspase-3 activation and DNA-fragmentation in CHO cells. E2 is synthesized in ovarian cells to regulate luteal functions and their gene expression (26). ROS have been postulated to play important roles in the regulation of luteal functions while E2 functions as a potent protector of cells through its antioxidant activity (1). ROS have been shown to play critical roles in the mechanism of apoptosis. ROS exhibit both luteolytic and luteotrophic actions (2). Oxidative stress-induced apoptosis has been postulated to play important roles in the mechanisms of corpus luteum regression and follicular atresia. However, high concentrations of estradiol are required for the inhibition (1). These results suggest that E2 inhibits the ROS-induced apoptosis of cells through a transcription-independent mechanism. It has

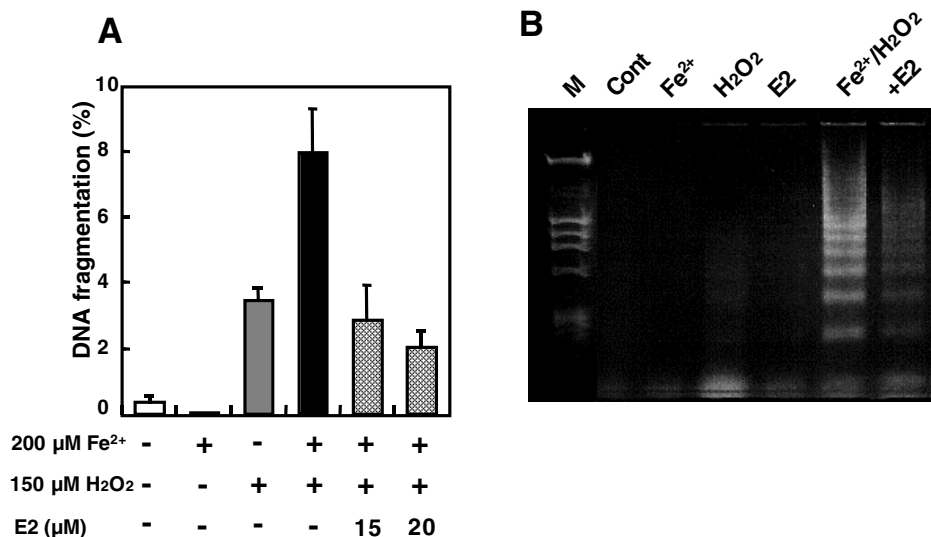


FIGURE 5. Suppression of $\text{Fe}^{2+}/\text{H}_2\text{O}_2$ -induced DNA fragmentation and ladder formation by E2. Experimental conditions were the same as described in Figure 4. (A) $\text{Fe}^{2+}/\text{H}_2\text{O}_2$ -induced DNA-fragmentation. Data are means \pm SD from three independent experiments. (B) $\text{Fe}^{2+}/\text{H}_2\text{O}_2$ -induced ladder formation of DNA. Experimental conditions were the same as described in Figure 4. Similar results were obtained in three separate experiments.

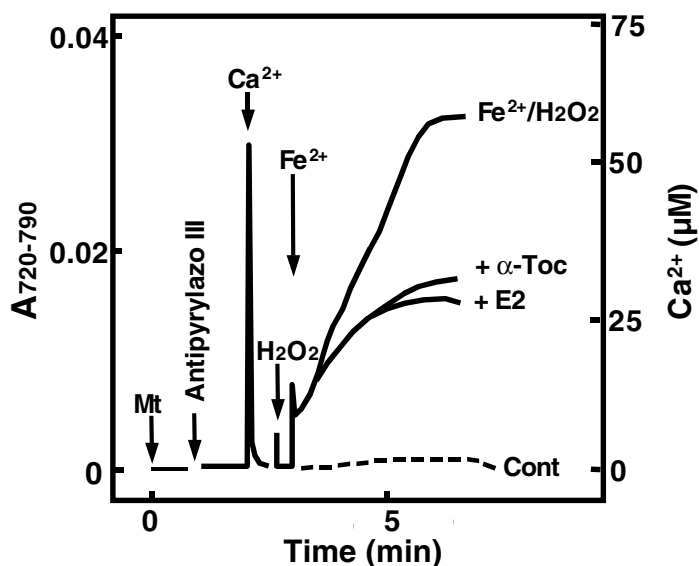


FIGURE 6. Suppression of $\text{Fe}^{2+}/\text{H}_2\text{O}_2$ -induced Ca^{2+} release from mitochondria by E2. Mitochondria (0.5 mg protein/ml) were incubated in 10 mM Tris-HCl buffer (pH 7.4) containing 150 mM KCl and antipyrylazo III at 25°C. Reaction was induced in the presence 2 mM Pi, 5 mM succinate and 5 μM Ca^{2+} and treated with 20 μM $\text{Fe}^{2+}/100$ μM H_2O_2 in the presence or absence of 50 μM E2 or 50 μM α -tocopherol. Similar results were obtained in three separate experiments.

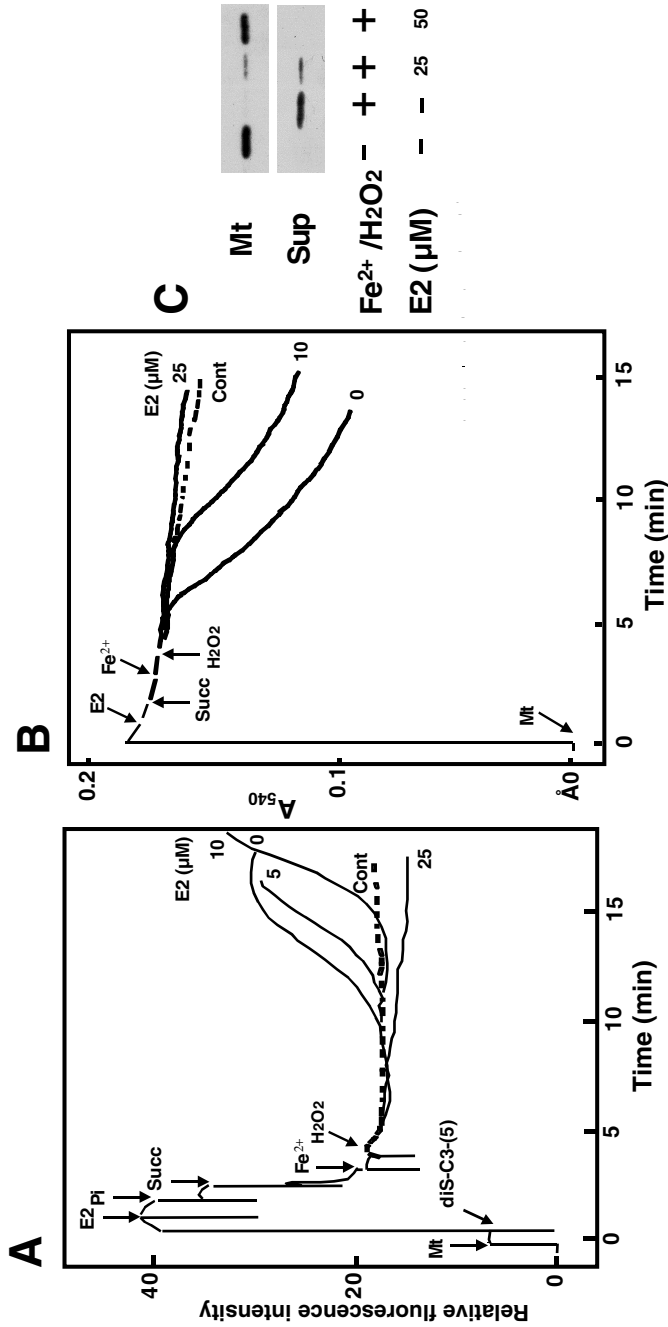


FIGURE 7. Suppression of Fe²⁺/H₂O₂-induced mitochondrial MPT and cytochrome c release by E2. Rat liver mitochondria (0.1 mg protein/ml) were incubated in 10 mM Tris-HCl (pH 7.4) containing 150 mM KCl at 25°C. Mitochondria were treated with 20 μM Fe²⁺/100 μM H₂O₂ in the presence or absence of various concentration of E2. (A) Membrane potential change; Upward deflection showed depolarization. (B) Swelling; Downward deflection showed swelling. (C) Cytochrome c release. Similar results were obtained in three separate experiments.

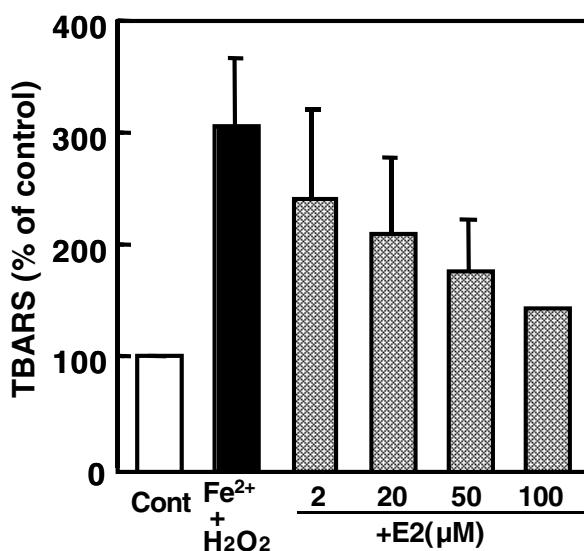


FIGURE 8. Effect of E2 on the lipid peroxidation of mitochondria induced by Fe²⁺/H₂O₂. Experimental conditions were the same as described in Figure 7. Mitochondria (0.5 mg protein) were incubated with 20 μM Fe²⁺/50 μM H₂O₂ in the presence or absence of various concentration of E2. After incubation for 10 min at 25°C, lipid peroxidation was assessed by the method of Okawa *et al.* (16) and expressed by the value as TBARS. Data are means ± SD from three independent experiments.

been shown that estrogen protects postmenopausal women against cardiovascular diseases, at least in part, through its antioxidant activity (27–29).

It has been reported that ovarian levels of Mn-superoxide dismutase (SOD), but not Cu/Zn-SOD, decreased markedly during the maturation of the rat while mRNA levels for Mn-SOD markedly increased during the ovulatory process induced by human chorionic gonadotropin (30). Furthermore, intravenous injection of a long-acting SOD inhibited the ovulation (31). ROS has been shown to play an important role in the apoptosis of germ cells (32). These observations suggested that superoxide and/or its metabolites might play critical roles in the mechanism ovulation (30–32). The present work shows the increased generation of in ROS and TBARS in CHO cells prior to the induction of DNA-fragmentation.

Mammalian cells have two major pathways leading to apoptosis; the one involves tumor necrosis factor- α (TNF- α) and related cytokines and their transmembranous death receptors (33–35) and the other involves mitochondrial depolarization, swelling and cytochrome c release to activates caspase-9 (36, 37). Both pathways finally activate caspase-3 and induce the fragmentation of nuclear DNA. Several lines of evidence indicate that the induction of mitochondrial MPT is the rate-limiting step of apoptosis (38, 39).

The present work demonstrates that Fe²⁺/H₂O₂ induced apoptosis of CHO cells through the induction of lipid peroxidation coupled with classic type of MPT and supports the hypothesis that ROS play important roles in the regulation of luteal function (2, 40–41). We detected the ROS generation in CHO cells 3 hour after adding Fe²⁺/H₂O₂. Since the Fe²⁺/H₂O₂-derived hydroxyl radical has been postulated to oxidize DCFH (42), genera-

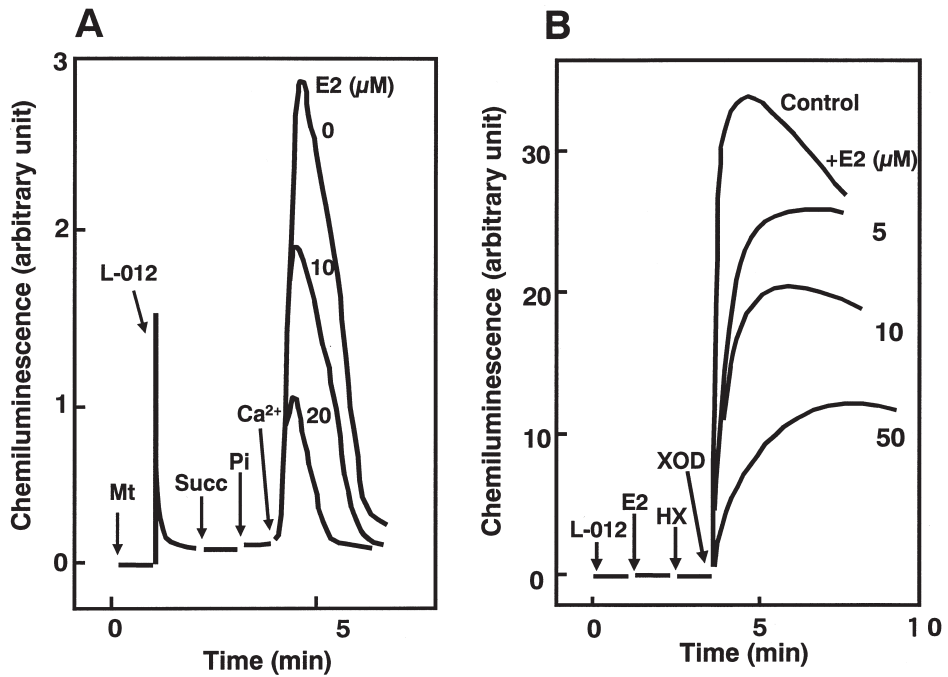


FIGURE 9. Effect of E2 on the generation of ROS by mitochondria and xanthine oxidase. (A) Suppression of ROS generation in mitochondria by E2. Isolated mitochondria were incubated in the presence of L-012, succinate and Pi at 25°C. ROS was generated by adding CaCl₂ in the presence or absence of E2. ROS was measured by CHL of L-012. (B) Suppression of ROS generation in xanthine/xanthine oxidase system by E2. CHL of L-012 was induced by xanthine oxidase in PBS containing hypoxanthine and L-012. Similar results were obtained in three separate experiments.

tion of ROS particularly hydroxyl radical might underlie the initial event to induce lipid peroxidation of mitochondrial membrane followed by apoptosis of cells. Lipid peroxidation has been shown to play important roles in the regulation of the liver by regulating the balance between apoptosis and proliferation of cells (43). Thus, the suppression of ROS-induced apoptosis of CHO cells by E2 might result from the inhibition of lipid peroxidation through its antioxidant activity. Recent studies revealed that lipid peroxidation product, 4-hydroxynonenal (4-HNE), directly reacts with adenine nucleotide translocator (ANT) to induce mitochondrial MPT and apoptosis (44). Thus, lipid peroxidation occurring around the cyclosporin A-sensitive sites in mitochondria might trigger the apoptosis of CHO cells.

Relatively high concentrations of E2 have been used for the suppression of apoptosis (45, 46). The minimum concentration of E2 used to suppress the apoptosis was 10-times higher than its physiological concentrations. However, the concentration of E2 in ovarian cells might be fairly high *in vivo*. Furthermore, a recent report showed that 0.1 μM E2 suppressed the Ca²⁺-induced cytochrome c release from mitochondria (47). These observations support the hypothesis that ROS and E2 play important roles in the differentiation of ovarian cells by modulating their apoptosis.

This work was supported, in part, by grants from the Japanese Ministry of Education, Science and Literature and the Japan Keirin Association. We thank Dr. Masayasu Inoue for his suggestion on this manuscript.

References

1. Murdoch, W.J. (1998) Inhibition by oestradiol of oxidative stress-induced apoptosis in pig ovarian tissues. *J. Reprod. Fertil.* 114: 127–130.
2. Kato, H., Sugino, N., Takiguchi, S., Kashida, S. and Nakamura, Y. (1997) Roles of reactive oxygen species in the regulation of luteal function. *Rev. Reprod.* 2: 81–83.
3. Subbiah, M.T. and Abplanalp, W. (2002) Evidence of increased formation of products retaining strong antioxidant activity from estradiol-17 β oxidation in the presence of human plasma lipoproteins. *J. Lab. Clin. Med.* 139: 357–363.
4. Bednarek-Tupikowska, G. (2002) Antioxidant properties of estrogens. *Ginekol. Pol.* 73: 61–67.
5. Murdoch, W.J. (1998) Inhibition by oestradiol of oxidative stress-induced apoptosis in pig ovarian tissues. *J. Reprod. Fertil.* 114: 127–130.
6. Ayres, S.A., Tang, M. and Subbiah, M.T.R. (1996) Estrdiol-17 β as an antioxidant: some distinct features when compared with common fat-soluble antioxidants. *J. Lab. Clin. Med.* 128: 367–375.
7. Tatemoto, H., Sakurai, N., and Muto, N. (2000) Protection of porcine oocytes against apoptotic cell death caused by oxidative stress during In vitro maturation: role of cumulus cells. *Biol. Reprod.* 63: 805–810.
8. Lund, S.A., Murdoch, J., Van Kirk, E.A. and Murdoch, W.J. (1999) Mitogenic and antioxidant mechanisms of estradiol action in preovulatory ovine follicles: relevance to luteal function. *Biol. Reprod.* 61: 388–392.
9. Jimenez, M., Del Rio and Velez-Pardo, C. (2002) 17 beta-estradiol protects lymphocytes against dopamine and iron-induced apoptosis by a genomic-independent mechanism. Implication in Parkinson's disease. *Gen. Pharmacol.* 35: 1–9.
10. Pollack, M. and Leeuwenburgh, C. (2001) Apoptosis and aging: role of the mitochondria. *J. Gerontol. A. Biol. Sci. Med. Sci.* 56: 475–82.
11. Crompton, M. (1999) The mitochondrial permeability transition pore and its role in cell death. *Biochem. J.* 341: 233–249.
12. Yabuki, M., Kariya, S., Ishisaka, R., Yasuda, T., Yoshioka, T., Horton, A.A. and Utsumi, K. (1999) Resistance to nitric oxide-mediated apoptosis in HL-60 variant cells is associated with increased activities of Cu/Zn-superoxide dismutase and catalase. *Free Rad. Biol. Med.* 26: 325–332.
13. Carter, W.O., Narayanan, P.K., and Robinson, J.P. (1994) Intracellular hydrogen peroxide and superoxide anion detection in endothelial cells. *J. Leukoc. Biology* 55: 253–258.
14. Hogeboom, G.H. (1955) Fractionation of cell components of animal tissues. *Method in Enzymol.* 1: 16–19.
15. Imada, I., Sato, E.F., Miyamoto, M., Ichimori, Y., Minamiyama, Y., Konaka, R. and Inoue, M. (1999) Analysis of reactive oxygen species generated by neutrophils using a chemiluminescence probe L-012. *Analy. Biochem.* 271: 53–58.
16. Ohkawa, H., Ohnishi, N. and Yagi, K. (1979) Assay for lipid peroxides in animal tissues by thiobarbituric acid reaction. *Anal. Biochem.* 95: 351–358.
17. Yamamoto, S., Tamai, H., Ishisaka, R., Kanno, T., Arita, K., Kobuchi, H. and Utsumi, K. (2000) Mechanism of α -tocopheryl succinate-induced apoptosis of promyelocytic leukemia cells. *Free Rad. Res.* 33: 407–418.
18. Arita, K., Utsumi, T., Kato, A., Kanno, T., Kobuchi, H., Inoue, B., Akiyama, J. and Utsumi, K. (2001) Mechanism of Dibucaine-Induced Apoptosis in Promyelocytic Leukemia Cells(HL-60). *Biochem. Pharmacol.* 60: 905–915..

19. Salvioi, S., Ardizzoni, A., Franceschi, C. and Cossarizza, A. (1997) JC-1, but not DiOC6(3) or rhodamine 123, is a reliable fluorescent probe to assess delta psi changes in intact cells: implications for studies on mitochondrial functionality during apoptosis. *FEBS Lett* 411: 77–82.
20. Yamada, K., Arita, K., Kobuchi, H., Yamamoto, S., Yoshioka, T., Tamai, H. and Utsumi, K. (2003) Cholesterol-succinate induced apoptosis of promyeroctytic leukemia HL-60 cells through membrane permeability transition mechanism. *Biochem. Pharmacol.* 63: 339–348.
21. Bradford, M.M. (1976) A rapid and sensitive method for the quantitation of microgram quantities of protein utilizing the principle of protein-dye binding. *Anal. Biochem.* 72: 248–254.
22. Furuno, T., Kanno, T., Arita, K., Asami, M., Utsumi, T., Doi, Y., Inoue, M. and Utsumi, K. (2001) Role of long chain fatty acids and carnitine in membrane permeability transition of mitochondria and apoptosis of HL-60 cells. *Biochem. Pharmacol.* 62: 1037–1046.
23. Ishisaka, R., Kanno, T., Akiyama, J., Yoshioka, T., Utsumi, K. and Utsumi, T. (2001) Activation of caspase-3 by lysosomal cysteine proteases and its role in 2,2'-azobis-(2-amidino-propane) dihydrochloride (AAPH)-induced apoptosis in HL-60 cells. *J. Biochem.* 129: 35–41.
24. Kanno, T., Sato, E.F., Muranaka, S., Fujita, F., Fujiwara, T., Utsumi, T., Inoue, M. and Utsumi, K. (2004) Oxidative stress underlies the mechanism for Ca²⁺-induced permeability transition of mitochondria. *Free Rad. Res.* 38: 27–35.
25. Kanno, T., Fujita, H., Muranaka, S., Yano, H., Kajitani, N., Yoshioka, T., Inoue, M. and Utsumi, K. (2002) Mitochondrial swelling and cytochrome c release: correlation to cyclosporin A-sensitivity and Ca²⁺-dependency. *Phys. Chem. & Phys. and Med NMR.* 34: 91–102.
26. Findlay, J.K., Britt, K., Kerr, J.B., O'Donnell, L., Jones, M.E., and Drummond, A.E., Simpson, E.R. (2001) The road to ovulation: the role of oestrogens. *Reprod. Fertil. Dev.* 13: 543–547.
27. Murdoch, W.J. (1998) Inhibition by oestradiol of oxidative stress-induced apoptosis in pig ovarian tissues. *J. Reprod. Fertil.* 114: 127–130.
28. Dharmarajan, A.M., Hisheh, S., Singh, B., Parkinson, S., Tilly, K.I. and Tilly, J.L. (1999) Antioxidants mimic the ability of chorionic gonadotropin to suppress apoptosis in the rabbit corpus luteum in vitro: a novel role for superoxide dismutase in regulating bax expression. *Endocrinol.* 140: 2555–2561.
29. Keaney, J.F. Jr., Shwaery, G.T., Xu, A., Nicolosi, R.J., Loscalzo, J., Foxall, T.L., and Vita, J.A. (1994) 17 beta-estradiol preserves endothelial vasodilator function and limits low-density lipoprotein oxidation in hypercholesterolemic swine. *Circulation.* 89: 2251–229.
30. Sato, E.F., Kobuchi, H., Edashige, K., Takahashi, M., Yoshioka, T., Utsumi, K. and Inoue M. (1992) Dynamic aspects of ovarian superoxide dismutase isozymes during the ovulatory process in the rat. *FEBS Lett.* 303: 121–125.
31. Inoue, M., Ebashi, I., Watanabe, N. and Morino, Y. (1989) Synthesis of a superoxide dismutase derivative that circulates bound to albumin and accumulates in tissues whose pH is decreased. *Biochemistry.* 28: 6619–6624.
32. Kasahara, E., Sato, E.F., Miyoshi, M., Konaka, R., Hiramoto, K., Sasaki, J., Tokuda, M., Nakano, Y. and Inoue, M. (2002) Role of oxidative stress in germ cell apoptosis induced by di(2-ethylhexyl)phthalate. *Biochem J.* 365: 849–856.
33. Wajant, H. (2002) The Fas signaling pathway: more than a paradigm. *Science* 296: 1635–1636.
34. Ashkenazi, A. and Dixit, V.M. (1999) Apoptosis control by death and decoy receptors. *Curr. Opin. Cell Biol.* 11: 255–260.
35. Salvesen, G.S. and Dixit, V.M. (1997) Caspases: intracellular signaling by proteolysis. *Cell* 91: 443–446.
36. Green, D.R. and Reed, J.C. (1998) Mitochondria and apoptosis. *Science* 281: 1309–1312.
37. Kuida, K. (2000) Caspase-9. *Int. J. Biochem. Cell Biol.* 32: 121–124.

38. Zoratti, M. and Szabo, I. (1995) The mitochondrial permeability transition. *Biochim. Biophys. Acta* 1241: 139–176.
39. Mancini, M., Nicholson, D. and Roy, S. Thornberry, N., Peterson, E., Casciola-Rosen, L. and Rosen, A. (1998) The caspase-3 precursor has a cytosolic and mitochondrial distribution: implications for apoptotic signaling. *J. Cell Biol.* 140: 1485–1495.
40. Ayres, S., Abplanalp, W., Liu, J.H. and Subbiah, M.T. (1998) Mechanisms involved in the protective effect of estradiol-17 β on lipid peroxidation and DNA damage. *Am. J. Physiol.* 274: E1002–1008.
41. Arteaga, E., Rojas, A., Villaseca, P., Bianchi, M. (2000) The effect of 17 β -estradiol and alpha-tocopherol on the oxidation of LDL cholesterol from postmenopausal women and the minor effect of gamma-tocopherol and melatonin. *Menopause.* 7: 112–116.
42. LeBel, C.P., Ischiropoulos, H., Bondy, S.C. (1992) Evaluation of the probe 2',7'- dichlorofluorescein as an indicator of reactive oxygen species formation and oxidative stress. *Chem Res Toxicol.* 5: 227–31.
43. Ronco, M.T., deAlvarez, M.L., Monti, J., Carrillo, M.C., Pisani, G., Lugano, M.C. and Carnovale, C.E. (2002) Modulation of balance between apoptosis and proliferation by lipid peroxidation (LPO) during rat liver regeneration. *Mol. Med.* 8: 808–817.
44. Vieira, H.L., Belzacq, A.S., Haouzi, D., Bernassola, F., Cohen, I., Jacotot, E., Ferri, K.F., El Hamel, C., Bartle, L.M., Melino, G., Brenner, C., Goldmacher, V. and Kroemer, G. (2001) The adenine nucleotide translocator: a target of nitric oxide, peroxynitrite, and 4-hydroxynonenal. *Oncogene.* 20: 4305–4316.
45. Gotz, M.E., Ahlbom, E., Zhivotovsky, B., Blum-Degen, D., Oettel, M., Romer, W., Riederer, P., Orrenius, S. and Ceccatelli, S. (1999) Radical scavenging compound J 811 inhibits hydrogen peroxide-induced death of cerebellar granule cells. *J. Neurosci. Res.* 56: 420–426.
46. Ronco, M.T., deAlvarez, M.L., Monti, J., Carrillo, M.C., Pisani, G., Lugano, M.C., and Carnovale, C.E. (2002) Modulation of balance between apoptosis and proliferation by lipid peroxidation (LPO) during rat liver regeneration. *Mol. Med.* 8: 808–817.
47. Morkuniene, R., Jekabsone, A. and Borutaite, V. (2002) Estrogens prevent calcium-induced release of cytochrome c from heart mitochondria. *FEBS Lett.* 521: 53–56.

*Received January 29, 2004;
accepted April 27, 2004.*

Evaluation of a Simple Carrier Molecule to Enhance Drug Penetration of Dermal Layers by Utilizing Multivariate Methods, Structure Property Correlations, and Continuous System Modeling

Ronald Bartzatt

*University of Nebraska, College of Arts & Sciences, Chemistry Department,
Omaha, Nebraska 68182 USA*

Abstract: Nicotinic acid is shown to be comparable to dihydropyridine in its capacity to facilitate penetration of an attached antibacterial drug through dermal layers. Antibacterial drugs examined with nicotinic acid or dihydropyridine carriers were β -lactam antibiotics: methicillin, oxacillin, benzylpenicillin, penicillin F, penicillin dihydro F, propicillin, carbenicillin, penicillin K, penicillin X, and ampicillin. An oxymethyl (-O-CH₂-) group is inserted as the linker between the antibiotic and the carrier group. Structure Property Correlations and multivariate methods such as regression analysis, cluster analysis, principal component analysis, discriminate analysis, self-organizing tree algorithm, and factor analysis clearly showed that nicotinic acid performs as an effective carrier drug and is comparable to dihydropyridine. The skin penetration constant K_p was calculated for all 10 antibiotics having either dihydropyridine or nicotinic acid as carrier, and was found to have a mean of 5.13E-05 cm/hour and 1.83E-05 cm/hour, respectively. The standard deviation for each group showed the numerical values overlap as did the 90% confidence interval for each group. A hierarchical tree organization of skin shows the overlapped dermal layers as they exist in normal skin and for the model utilized in this work. A Deming-Regression analysis also shows the nicotinic acid and dihydropyridine structures to have similar and correlated water solubility. Plotting K_p of the dihydropyridine structures as independent variable versus K_p of the nicotinic acid structures show good correlation (Pearson correlation $r = 0.6606$) and no significant departure from linearity. Connected box plots showed the majority of K_p values for each group of modified antibiotics to exist in a tight cluster. Polar graph of the Log Kow values showed the two groups of modified antibiotics to be correlated and numerically adjacent in trend. ChemSketch property calculations and modeling demonstrates the affects of structural oxygens, nitrogens, carbonyl groups, amide groups, and aromatic rings that are important in understanding the pervasiveness through dermal layers. Continuous model analysis by acsIXtreme is utilized and demonstrates three models of the dispersion of drugs through dermal layers based on diffusivity constant (D), Log K_p from Log Kow and formula weight, and K_p as a function of time.

PENICILLIN ANTIBIOTICS are bactericidal and interfere with the formation of the bacterial cell wall. Penicillins diffuse well into the body tissues and fluids. Penicillins are also referred to as the β -lactam antibiotics, a term which indicates the active amide ring that nullifies the membrane closing activity of transpeptidase enzyme. Ampicillin, one of the most widely used of the β -lactam antibiotics, is utilized as a topical drug but limited by resistant *Staphylococcus aureus*. Important classes of the β -lactam group are the penicillins, cephalosporins, monobactams, and carbapenems.

Bacteria which are important for skin and soft tissue considerations are the *Staphylococcus (S.) aureus*, *S. pyogenes*, *S. epidermidis*, and *Pasteurella*. Strains of the genus *Pasteurella* (gram-negative, coccobacilli) are susceptible to penicillin as well as tetracycline. Staphylococci are gram positive spherical bacteria that are found primarily on the skin or the mucous membranes for which methicillin or vancomycin are effective treatments. Isolates of *Staphylococcus aureus* can still be inhibited by penicillin, however resistance to this antibiotic is a significant problem in health facilities. Staphylococcus are opportunistic pathogens, not significantly invasive unless given the opportunity by skin trauma, lacerations, macerations, etc. *S. aureus* causes localized skin infections. *S. epidermidis* resides primarily in the skin and can cause blood infections if an invasive trauma provides the opportunity. The Staphylococci can adhere to epithelial cells causing problems of multiplication and spread.

To treat the infection threats described above steps have been taken to improve the delivery of antibiotics into skin tissue. Particularly the application of dihydropyridine attached β -lactam antibiotics to improve delivery through biological membranes (1, 2, 3). Induction of skin blisters have been utilized to understand the process of skin absorption of antibiotics (4). The penetration of skin by antibiotics has been shown to be inhibited by other medicinal agents such as hydrocortisone (5). Utilizing tissue cages has shown useful in determining the extent of antibiotic skin penetration (6).

The β -lactam antibiotics are highly effective against most bacteria that cause skin and soft tissue infections (7) and are considered to have good tissue penetration and long duration of activity (7) (with the low molecular weight members being optimal). Previous studies have shown that electrophoresis and phonophoresis can improve tissue penetration of penicillin and streptomycin (8, 9). Use of 6-ketocholestanol has been shown to enhance transdermal delivery of antibiotic (10).

This work shows that nicotinic acid is an effective carrier vehicle which is comparable to dihydropyridine for enhancing skin penetration by β -lactam antibiotics. Ten antibiotics that are currently used in clinical applications were selected for evaluating this mode of enhanced penetration. Each having an attached dihydropyridine or nicotinic acid molecule at the carboxyl group of the antibiotic (total of 20). Use of nicotinic acid as a carrier vehicle will benefit the clinical treatment of skin infections.

Materials and Methods

Numerical Analysis Methods

Multivariate methods such as regression analysis, cluster analysis, principal component analysis, discriminate analysis, self-organizing tree algorithm, and factor analysis were applied to molecular properties of the antibiotic structures having nicotinic acid or dihy-

dropyridine substituents. Dendrograms were utilized to portray distances obtained from cluster analysis. Descriptive statistics were applied to demonstrate numerical relationships of molecular properties for all compounds.

Software and Algorithms

Molecular properties were calculated by utilizing ChemSketch (Advanced Chemistry Development, Toronto, Canada M5H 3V9), Molinspiration Cheminformatics (SK-84104 Bratislava, Slovak Republic), and Syracuse Research Corp. (North Syracuse, New York 13212). Values of Log Kow, rate of ester hydrolysis, water solubility, and dermal penetration rate were evaluated by EPISUITE (US Environmental Protection Agency, Washington, DC USA). Self organizing tree algorithm (SOTA) was accomplished by GEPAS Bioinformatics (<http://gepas.bioinfo.cnio.es/cgi-bin/sotarray>). Hierarchical tree organization of skin structure was accomplished by Treepad (Freebyte, Interland Copyright © 1995–2003) and FLOW (Version 4.00.074 IMSI and COREL Corp. Copyright © 1996–1998).

Continuous Model System

The acsIXtreme software was utilized to evaluate dermal penetration by a continuous model system and determine skin absorption parameters (Aegis Technologies Group, 631 Discovery Drive, Huntsville, AL 35806).

Descriptors of Dermal Absorption

Skin Permeability Coefficient, Kp (cm/hour):

$$\text{Log Kp} = -2.72 + 0.71\text{LogKow} - 0.0061(\text{Formula Weight})$$

Skin Diffusivity Constant, D (cm²/hour):

$$\text{Log D} = -2.72 - 0.0061(\text{Formula Weight}) + \text{Log(L)},$$

where, L = length of stratum corneum (0.004 cm)

Lag Time, τ (hour):

$$\tau = (L)^2/6(D), \text{ see L and D above.}$$

Drug penetration (cm) as function of Time (hours) and Kp (see above):

$$\text{Penetration depth} = \text{Kp}(\text{Time})$$

Permeation Coefficient of Protein Layer, Kpol

$$\text{Kpol} = 0.0002976/(\text{Formula Weight})^{0.7}$$

Permeation Coefficient of Aqueous Layer, Kaq

$$\text{Kaq} = 4.209/(\text{Formula Weight})^{0.7}$$

Results and Discussion

The skin is a highly organized, multilayered, and heterogeneous organ. The skin produces factors that regulate growth, differentiation, and mediators of inflammation and immune response. The skin is made up of three distinct layers: 1) Epidermis (keratinized surface

layers), 2) Dermis (fibro-elastic connective tissue), and 3) Hypodermis (loose connective tissue). The dermis contains blood vessels which serve as an entrance portal to the body for drugs administered as topical agents. General functions of the skin can be described as: 1) Protective, 2) Inhibitory of microbial activity, 3) Regulation of temperature, and 4) Repressing of U.V. light damage. For considerations of skin modeling and skin permeation, it is taken to consist of three compartments: 1) Protein layer of the stratum corneum, 2) Lipid layer of the stratum corneum, and 3) Aqueous layer below the stratum corneum (drugs applied topically must permeate the aqueous layer to enter the bloodstream). These factors of skin constitution and activity are considered here in the comparison of antibiotics having either a dihydropyridine or nicotinic acid substituent. The stratum corneum is the rate-limiting diffusion barrier for most compounds and will be considered in this study.

Dihydropyridine has been used as a substituent of different classes of drugs to facilitate the penetration of membrane tissue such as the blood-brain-barrier. It has been utilized previously to enhance the membrane penetration of β -lactam antibiotics for targeting the central nervous system (11, 12, 3). The synthesis of the dihydropyridine variants of these antibiotics is straight forward and would be accomplished in the same manner for all antibiotic nicotinic acid variants. Briefly, all of the β -lactam antibiotics studied have a carboxylic acid group which is converted to a potassium salt by mild base. Then chloromethanechlorosulfate is introduced which produces a chloromethyl ester group (ie., $-\text{C}(\text{O})\text{OCH}_2\text{Cl}$). Upon introduction of nicotinic acid or dihydropyridine, the formation of the final daughter compound having the desired substituent is energetically favored and is readily obtained (see Figure 1 for example final structures). It has been shown in previous studies that nicotinic acid functioning as a carrier drug will enhance the penetration of antineoplastic alkylating nitrogen mustard groups through the blood-brain-barrier (13).

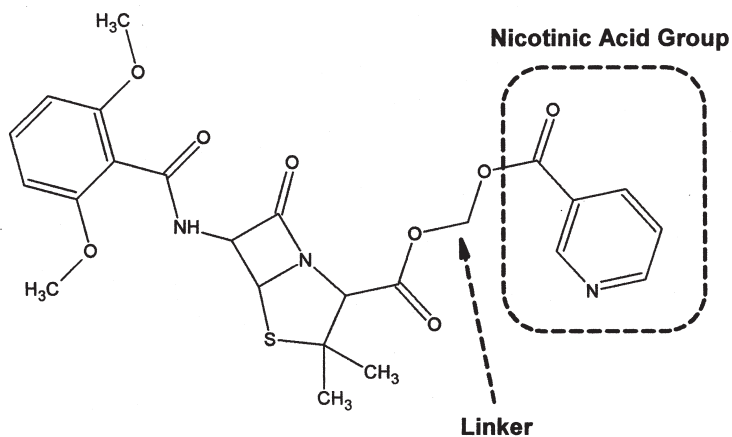
Figure 1 shows a methicillin nicotinic acid and methicillin dihydropyridine products of the reaction of chloromethanechlorosulfate with a β -lactam antibiotic, followed by the desired substituent. Notice the β -lactam ring is intact and a methoxy ($-\text{O}-\text{CH}_2-$) linker is in place between the antibiotic proper and the substituent (see dotted rectangle). The SMILES notation (www.daylight.com) for each compound is given. The nicotinic acid and dihydropyridine constitute the "carrier" portion of these antibiotic variants which enhances their penetration through body membranes.

Organization of dermal layers comprising the skin is presented in Figure 2 as a hierarchical tree organization. The layers which are significant in their influence on drugs applied topically are shown. On the left is the tree organization with the important layers designated as nodes of that tree. To the top of the left-hand tree is the initial administered drug, followed by the epidermis which is in turn comprised by the protein layer, lipid layer, and aqueous layer in sequence as the drug penetrates the skin in depth. The drug must pass the aqueous layer prior to reaching the dermis, which has the blood capillaries which provide passage of the drug to other parts of the body. The hypodermis being a major layer also. The right-hand tree shows the important layers of the epidermis more clearly distinct from the underlying dermis and hypodermis.

Molecular properties for both the nicotinic acid antibiotic variants and the dihydropyridine antibiotic variants are presented in Table I. Note that the antibiotic forms and their properties are designated by columns and placed in the same vertical columns to facilitate comparisons of values. The molecular properties considered are as follows from left to

Methicillin-Nicotinic Acid

O=C(OCOC(C3C(SC2C(NC(c1c(cccc1OC)OC)=O)C(N23)=O)(C)C)=O)c4cccnc4

**Methicillin-Dihydropyridine**

CN1/C=C(/C(=O)OCOC(C3C(SC2C(NC(c1c(cccc1OC)OC)=O)C(N23)=O)(C)C)=O)C\C=C\14

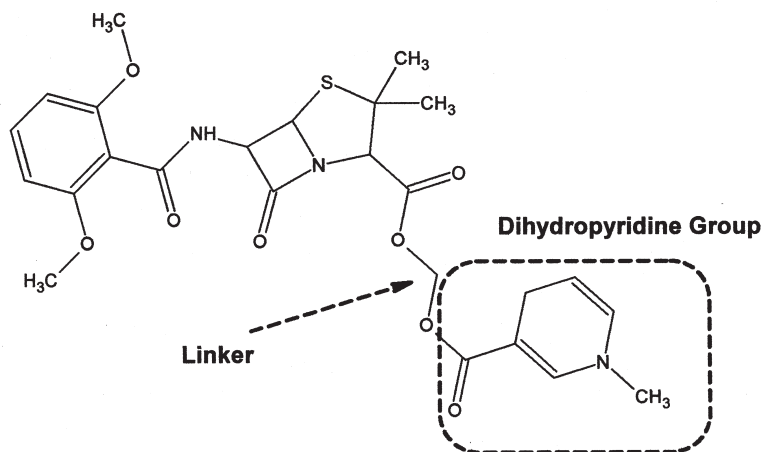


FIGURE 1. Examples of the molecular structures for each group of antibiotic derivatives of nicotinic acid or dihydropyridine utilizing methicillin as the parent compound. SMILES notation is given for each structure. Note the (-O-CH₂-) linker connecting the antibiotic to the carrier group.

- ☐ Drug on Skin
 - ☐ Epidermis
 - Protein Layer
 - Lipid Layer
 - Aqueous Layer
 - Dermis (blood capillaries)
 - Hypodermis

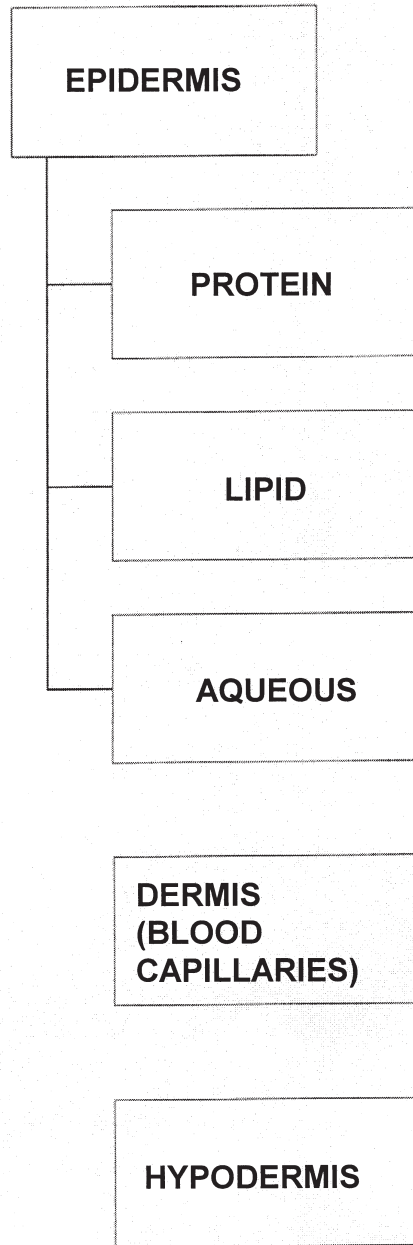


FIGURE 2. Showing the hierarchical tree organization of normal skin, any topically applied drug will pass through the protein, lipid, and aqueous layers of the epidermis prior to reaching the blood capillaries of the dermis layer.

TABLE I

	FW	Molar Refractivity	Molar Volume	Parachor	Index of Refraction	Polarizability	nOnN	nNHOH	miLogP	TPSA
Nicotinic Acid Structures of Antibiotics										
Methicillin	515.54	128.28	357.7	1030.5	1.636	50.85	11	1	2.563	133.28
oxacillin	538.57	138.11	358.7	999.6	1.696	54.75	11	1	3.232	136.51
benzylpenicillin	469.51	120.18	330.6	953.4	1.647	47.64	9	1	2.801	114.91
Penicillin F	447.51	113.9	329.9	927.4	1.606	45.15	9	1	2.88	114.91
Dihydro F	449.52	113.99	336.6	939.8	1.592	45.19	9	1	3.12	114.91
Propicillin	513.56	131.16	389.4	1051.8	1.628	51.89	10	1	3.629	124.143
Carbencicillin	513.52	126.44	341.3	1013.6	1.662	50.12	11	2	1.734	152.21
Penicillin K	477.58	123.25	368.8	1019.9	1.582	48.86	9	1	3.988	114.91
Penicillin X	485.51	121.71	327.4	968.8	1.665	48.25	10	2	2.417	135.137
Ampicillin	484.53	123.78	334.7	981.1	1.661	49.07	10	3	1.12	140.93
Dihydropyridine Structures of Antibiotics										
Methicillin	531.58	134.98	377	1069.9	1.634	53.51	11	1	2.339	123.723
oxacillin	554.62	143.43	379.9	1045.1	1.679	56.86	11	1	3.008	126.853
benzylpenicillin	485.55	126.88	349.9	992.7	1.645	50.3	9	1	2.577	105.26
Penicillin F	463.55	120.6	349.2	966.8	1.607	47.81	9	1	2.436	105.26
Dihydro F	465.56	120.69	355.9	979.2	1.593	47.84	9	1	2.676	105.28
Propicillin	529.61	137.86	388.8	1091.2	1.627	54.65	10	1	3.405	114.49
Carbencicillin	529.56	133.14	360.6	1052.9	1.66	52.78	11	2	1.51	142.55
Penicillin K	493.62	129.96	388.1	1059.3	1.584	51.52	9	1	3.544	105.28
Penicillin X	501.55	128.41	346.7	1007.9	1.662	50.9	10	2	2.194	125.48
Ampicillin	500.57	130.49	354	1020.4	1.658	51.73	9	3	0.896	131.28

right in Table I: formula weight, molar refractivity, molar volume, parachor, index of refraction, polarizability, n_{OnN} (number of oxygens and number of nitrogens), n_{NHnOH} (number of -NH and number of -OH), Log P by Molinspiration (miLog P), and polar surface area by Molinspiration (TPSA). Polar surface area has been shown to be an accurate indicator of absorption of a drug through the intestinal tract (14). All of the antibiotic variants shown in Table I (all of dihydropyridine and nicotinic acid forms) have TPSA values ranging from about 105 \AA^2 to about 142 \AA^2 , which indicate levels of intestinal absorption of 10% to 30%, respectively (14).

The skin permeability coefficient K_p is an important property and can be utilized to approximate the distance into the skin a drug will travel as a function of time. The values of K_p for all antibiotics with nicotinic acid or dihydropyridine as carrier is given in Table II as calculated by EPISUITE. The average value of K_p for each group are comparable, being $5.13\text{E-}05 \text{ cm/hr}$ and $1.83\text{E-}05 \text{ cm/hr}$ for dihydropyridine and nicotinic acid structures, respectively. Frequency analysis of the K_p values for the dihydropyridine structures reveal 90% confidence interval of $1.47\text{E-}05 \text{ cm/hr}$ to $8.79\text{E-}05 \text{ cm/hr}$ (outliers will be >0.0000795 from the median of $2.46\text{E-}05 \text{ cm/hr}$), skewness of 1.794, and kurtoses of 2.388. Frequency analysis of the K_p values for the nicotinic acid structures reveal 90% confidence interval of $5.70\text{E-}06 \text{ cm/hr}$ to $3.09\text{E-}05 \text{ cm/hr}$ (an overlap of the same range for the dihydropyridine structures), having skewness of 2.430, and kurtoses of 6.454 (outliers will be >0.0000301 from the median of $1.09\text{E-}05 \text{ cm/hr}$). Water solubilities for all antibiotics of nicotinic acid and dihydropyridine structure is shown in Table II in mg/mL. Although values vary widely within each group of compounds the numerical values themselves are comparable as a group. Note that each group has only a single outlier as a function of water solubility, that compound being benzylpenicillin for each group. The Grubb's Test for detecting outliers is also called the ESD method or extreme studentized deviate, and indicates that a value is unlikely to come from the same Gaussian population. Z values are calculated and a high Z value indicates that data is far from the other members of the group. Consequently, in terms of the two important properties K_p and water solubility the nicotinic acid group of structures are clearly similar to the dihydropyridine structures of antibiotics.

Analysis of molecular properties for these two groups of compounds by self organizing tree algorithm (SOTA) clearly showed mutual similarities and interrelationships. The results of SOTA analysis is in the form of cluster output which can also be defined in terms of proximity and distance associations (ie., single linkage and euclidean distance). SOTA (15) analysis was applied to seven molecular properties of these two groups in the following order: formula weight, molar refractivity, molar volume, parachor, index of refraction, polarizability, and number of oxygens and nitrogens. For ten compounds in each group that gives a total of 140 data points analyzed by SOTA. Parameters of the SOTA analysis were single linkage and standard euclidean distances. The results consisted of two clusters having members of both groups interwoven as follows: CLUSTER 1: Nicotinic acid structures of methicillin, propicillin, penicillin K with dihydropyridine structures of methicillin, oxacillin, propicillin, carbenicillin, penicillin K, and ampicillin. CLUSTER 2: Nicotinic acid structures of oxacillin, benzylpenicillin, penicillin F, dihydropenicillin F, carbenicillin, penicillin X, ampicillin with dihydropyridine structures of benzylpenicillin, penicillin F, dihydropenicillin F, and penicillin X. Interrelationships and similarities are clearly shown when members of either the nicotinic acid structures or dihydropyridine structures are placed in identical clusters.

TABLE II

Kp (cm/hour)

Kp (cm/hour)

Nicotinic Acid Structures	Parent Antibiotic	Dihydropyridine Structures
1.05E-05	Methicillin,	1.87E-05
4.88E-06	Oxacillin	0.000195
1.12E-05	Benzyloxacillin	2E-05
1.63E-05	Penicillin F	2.92E-05
2.25E-05	Dihydro F	4.03E-05
2.76E-05	Propicillin	4.92E-05
5.38E-06	Carbencillin	9.63E-06
7.57E-05	Penicillin K	0.000135
4.08E-06	Penicillin X	7.29E-06
4.75E-06	Ampicillin	8.5E-06

Analysis of Water Solubility (mg/mL) Values by Grubb's Test

Dihydropyridine Structures		
Row Value	Value Z	Significant Outlier
1	0.0347900	0.329043437
0.11640	0.3457398	
2	0.0048770	0.551575770
0.01632	0.5703164	
3	0.449600	2.756860260
1.50200	2.7635062	Significant outlier. P < 0.05
4	0.0045250	0.554194410
0.01511	0.5730316	
5	0.0471200	0.237316640
0.15700	0.2546346	
6	0.0745700	0.033107348
0.25670	0.0309107	
7	0.0004212	0.584723886
0.05918	0.4741398	
8	0.0582200	0.154740205
0.19430	0.1709345	
9	0.0146800	0.478648131
0.04914	0.4966693	

Further evidence of similarity between nicotinic acid and dihydropyridine structures is elucidated in Figure 3. The skin permeability coefficient K_p values (see Table II) for dihydropyridine compounds is plotted (x-axis) versus the corresponding K_p values of their counter part nicotinic acid structures (y-axis) with the 95% confidence interval (see inset arrows) in the top plot (see Figure 3). All values fall clearly within the 95% confidence interval except for penicillin K (see oval indicating this data point). However, a line drawn from the linear data values near the origin clearly includes the penicillin K data point (see broken line crossing the oval point value) and leaves out the data point encased in the inset rectangle (oxacillin).

A Deming Regression Plot shows linear relationships of data values with the assumptions that the values of the independent variable (x-axis) have error. A Deming regression analysis for the water solubility values (these being important because the drug must cross the aqueous layer of the epidermis) shown in Table II is presented as the middle plot in Figure 3. The formula weight of all nicotinic acid and dihydropyridine structures are plotted as the independent variable (x-axis) versus the water solubility (mg/mL) as the dependent variable (y-axis). Note that all 20 compounds do fall within a linear fashion according to the least squares line (see Figure 3) and only one compound (the benzylpenicillin nicotinic acid, see inset arrow) is radically an outlier from the otherwise linear body of the data. Therefore, the Deming regression analysis clearly demonstrates the similarity of all water solubility values for all nicotinic acid and dihydropyridine structures (high correlation of water solubility to formula weight).

A polar graph is utilized to demonstrate similarities between data values or groups of data values. A polar graph is shown (lower left, Figure 3) having Log Kow values for the dihydropyridine structures indicated by (X) and nicotinic acid structures indicated by triangles (Δ). Log Kow values indicate the dispersion of the drug between an organic solvent layer and an aqueous layer while assuming no charge species of the drug exist. Log Kow is an indicator of the ability of a drug to penetrate lipid by-layers and hence cellular membranes. Values of Log Kow are an important influence on the pharmacokinetic and pharmacodynamic aspect of the drug. The polar graph shows the Log Kow values of the dihydropyridine structures are generally larger than those of the nicotinic acid structures but corresponding values are clearly in close proximity.

In the lower right hand corner of Figure 3, a connected box plot for K_p values of dihydropyridine structures (var 2) are shown compared to K_p values of the nicotinic acid structures (var 3). In the connected box plot the individual data points are plotted normalized to the average value for that specific group of K_p values. Values for var 2 (dihydropyridine structures) have no outliers and the majority of K_p values are tightly clustered around the mean value (see Connected Box Plot Figure 3, var 2). Values for var 3 (nicotinic acid structures) show one outlier (see var 3 furthest point from origin) which is penicillin K while the remaining members of the group are tightly clustered around the mean value (see Figure 3 Connected Box Plot, var 3).

The operation referred to as factor analysis encompasses both component analysis and common factor analysis. Principal component analysis (PCA) is considered simpler. The central concept behind PCA is representation and summarization. The action of PCA is to replace a large set of variables by a smaller set which best summarizes the larger set. The results of PCA on the K_p values of all dihydropyridine and nicotinic acid structures, which form PCA 1 (dihydropyridine structures) and PCA 2 (nicotinic acid structures) are

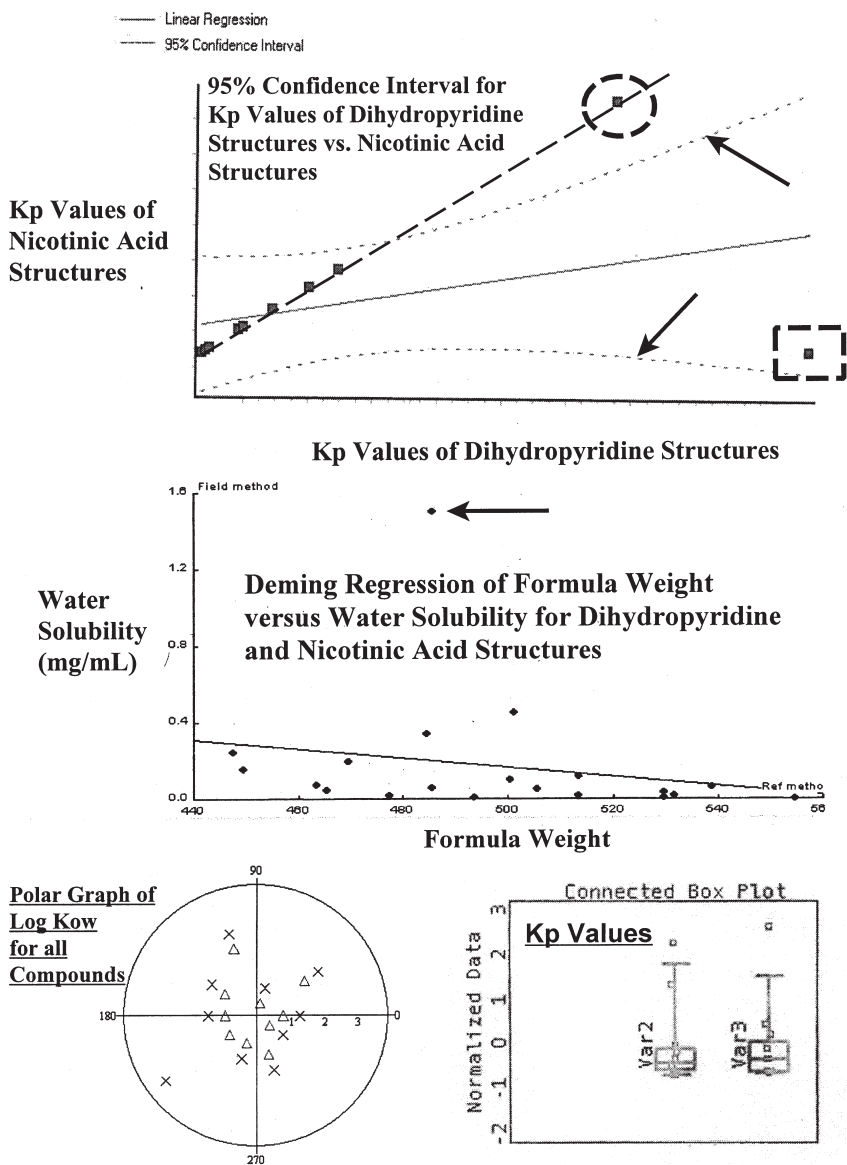


FIGURE 3. Comparison of important properties of the nicotinic acid group of antibiotics to the dihydropyridine group show similarities that support the potential for clinical application of the nicotinic acid derivatives. Top Graph: Linear regression plot of Kp values of all compounds show the majority of derivatives fall together within a 95% confidence interval (indicated by inset arrows) with only one outlier (inset circle). If a line is formed for linear members only, then again most compounds are inclusive with only one outlier (see rectangle). Middle Graph: Deming regression analysis of FW versus water solubility shows clearly the tight linearity of 19 derivatives with only one outlier (see inset arrow). Polar graph shows consistency and similar trend of Log Kow values for all 20 compounds (X= dihydropyridine structures, triangles (Δ)= nicotinic acid structures). Connected box plots show tight clustering of Kp values about the mean value for each group (var2= dihydropyridines, var3= nicotinic acids).

seen in Figure 4. A PCA 1 versus PCA 2 plot indicates that 80% of all 20 compounds are similar and fall within a tight cluster at about the origin of the graph (see inset oval). This cluster includes the nicotinic acid and dihydropyridine structures of methicillin, benzylpenicillin, penicillin F, dihydropenicillin F, propicillin, carbenicillin, penicillin X, and ampicillin. The outliers are oxacillin (see inset arrow) and penicillin K (see inset rectangle). Therefore, PCA shows that 80% of all 20 structures are similar.

Cluster analysis (CA) is a multivariate method that acts to organize data about variables in which homogeneous groups or clusters are formed. The clusters which are formed should have high internal homogeneity (members similar to each other) and highly external heterogeneity (members dissimilar to each other). CA can be applied to a wide variety of input data. The primary result of CA is the dendrogram or tree diagram. In Figure 4 is seen a dendrogram of CA on Kp values for all 20 agents. Note that in each case of the compound name found in the inset key it represents both the nicotinic acid and dihydropyridine structures (i.e., for 1) Methicillin, it means both the nicotinic acid and dihydropyridine form of methicillin). Using single linkage and standard euclidean the following clusters are formed (see dendrogram of Figure 4): Cluster 1 and 3 (methicillin and benzylpenicillin); Cluster 4 (penicillin F); Cluster 7, 10, and 9 (carbenicillin, ampicillin, and penicillin K); Cluster 5 and 6 (dihydropenicillin F and propicillin); Cluster 2 (oxacillin); Cluster 8 (penicillin K). Therefore, CA indicates that 70% of all 20 structures will have similarities with other members of this group.

Factor analysis is utilized to study patterns of relationships among many dependent variables with the actual goal of discerning characteristics of the independent variables that affect them (the independent variables are not measured directly). Figure 5 shows the plot of FA 1 versus FA 2 after factor analysis of Kp values for all nicotinic acid and dihydropyridine structures. Parameters of factor analysis were maximum likelihood and Joreskog's Formula. Note that the majority (80%) of all 20 antibiotic structures examined here fall within an individual clustering and close proximity (thus indicating similarity). Similar compounds that fall within a super cluster include methicillin, benzylpenicillin, penicillin F, dihydropenicillin F, propicillin, carbenicillin, penicillin X, and ampicillin (this includes both the nicotinic acid and dihydropyridine structures of these antibiotics). Outliers not demonstrating similarity with the super cluster are oxacillin (see inset rectangle) and penicillin K (see inset arrow). Therefore it is found that factor analysis also shows that 80% of both forms of the ten types of antibiotics are similar.

Discriminant analysis (DA) is utilized to determine which variables can be shown to discriminate between two or more occurring groups. Computationally, DA is very similar to analysis of variance. DA can be used to determine which variables (descriptors) can best predict the differing attributes of a particular group. This may also be stated as an analysis to assess the relative importance of the independent variables in classifying the dependent variable and to infer meaning of any dimensions that distinguish groups. To accomplish DA on the antibiotic structures that are the focus of this study, three molecular properties of the compounds were selected (formula weight, molar refractivity, and molar volume) and their numerical values for the dihydropyridine structures placed in Group 1 with those for the nicotinic acid structures placed into Group 2. Discriminant analysis of Group 1 versus Group 2 produces output referred to as DA 1 and DA 2, respectively. The plot of DA 1 versus DA 2 is presented in Figure 5 in which both the DA 1 score (x-axis) and DA 2 score (y-axis) can differentiate three super clusters of these compounds. The

Principal Components Analysis (PCA)

PCA 1= Kp Values of Dihydropyridine Structures
 PCA 2= Kp Values of Nicotinic Acid Structures

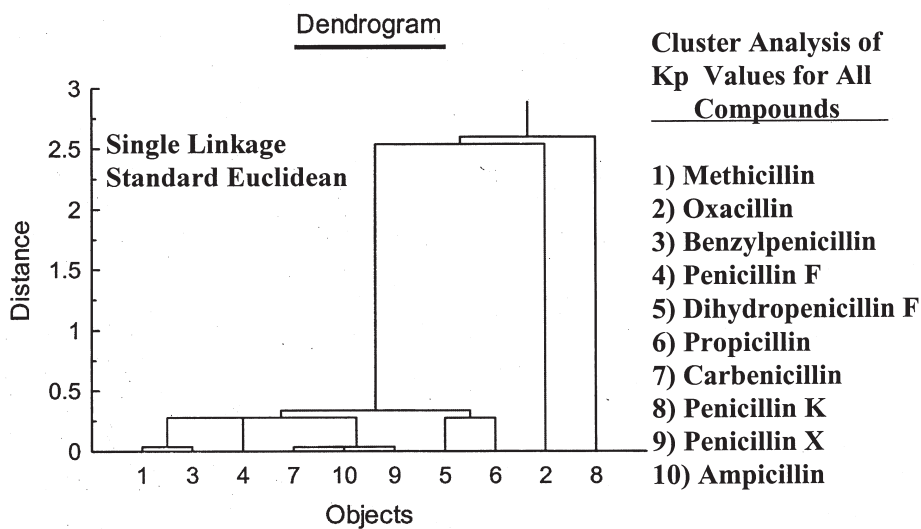
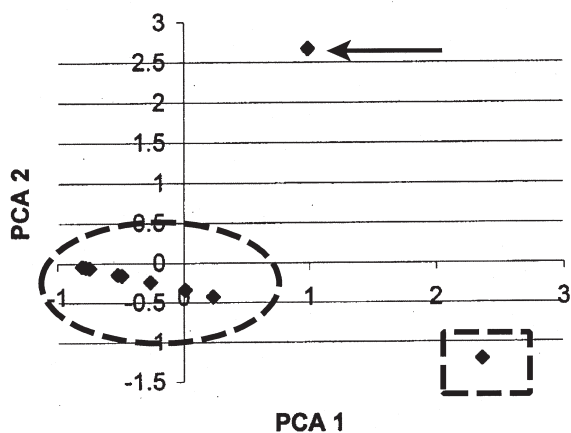
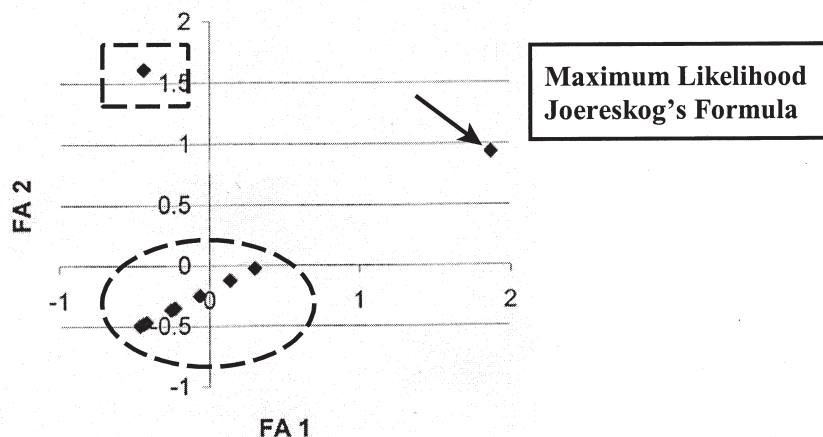


FIGURE 4. Principal component analysis of Kp values show tight clustering of 80% of all 20 compounds about the origin (see inset oval). Cluster analysis by single linkage and standard euclidean shows clusters of similar compounds: Cluster 1 and 3 (methicillin and benzylpenicillin); Cluster 4 (penicillin F); Cluster 7, 10, 9 (carbenicillin, ampicillin, and penicillin X); Cluster 5 and 6 (dihydropenicillin F and propicillin); Cluster 2 (oxacillin); Cluster 8 (penicillin K).

Factor Analysis of Kp Values

FA 1= Kp Values of Dihydropyridine Structures

FA 2= Kp Values of Nicotinic Acid Structures



Discriminant Analysis of Kp Values

DA 1= Dihydropyridine Structures (Formula Weight, Molar Refractivity, And Molar Volume)

DA 2= Nicotinic Acid Structures (Formula Weight, Molar Refractivity, And Molar Volume)

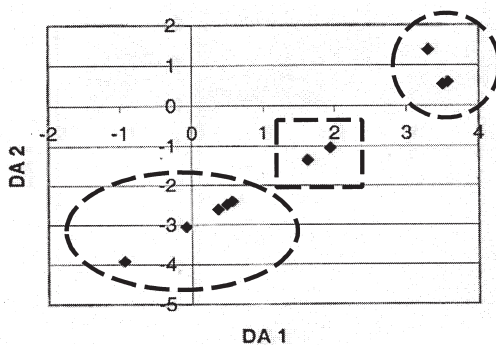


FIGURE 5. Factor analysis shows the strong similarities of nicotinic acid structures with dihydropyridine structures. 80% of all 20 compounds are included within the super cluster about the origin (see inset oval). Discriminant analysis shows that three properties (formula weight, molar refractivity, and molar volume) may be used to show similarities and distinctions of dihydropyridine and nicotinic acid derivatives of antibiotics. Distinctions obtained by DA 1 are analogous to those obtained from DA 2 (both utilizing formula weight, molar refractivity, and molar volume).

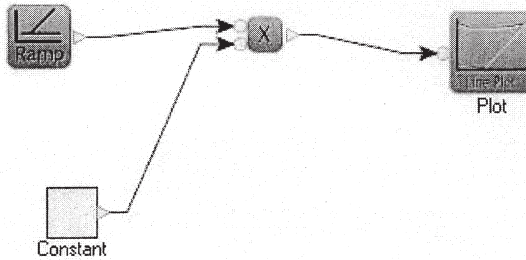
super cluster encased within the inset circle includes oxacillin, penicillin K, and propicillin (i.e., these three compounds are similar). Super cluster encased within the inset square encompasses ampicillin and benzylpenicillin (i.e., these two compounds are similar). The super cluster encased within the inset oval contains the compounds methicillin, penicillin F, dihydropenicillin F, penicillin X, and carbenicillin (i.e., these five compounds are similar). Remember that each data point in the DA graph designates the effects from both the dihydropyridine and the nicotinic acid forms of the same compound. Therefore, it is shown that DA will incorporate all 20 compounds studied here within three super clusters that have distinction from each other. However, members within each group are thereby similar to each other.

AcsIXtreme is program software which generates continuous numerical results from system models that incorporate mathematical algorithms designed within a continuous non-discrete framework. The operator designs a model with mathematical functions that can represent a real world paradigm. The output of such a model is a continuous numerical representation of the functions comprising the model. Three such models are presented in Figure 6, each representing some aspect of the application of the antibiotics studied in this work as topical agents. The first model represents the penetration of a drug in centimeters as a function of its Kp (skin permeability coefficient) and time in hours. The output is a 2-dimensional plot of hours (independent variable) versus distance (dependent variable) having equation of line as: $y = (2.597E-04\text{cm}/\text{hour})x - (2.60E-4\text{cm})$, where slope = $2.597E-04\text{cm}/\text{hour}$. The second model variance of Kp as a function of Log Kow and formula weight (see Materials and Methods). The output of such a model is linear having formula weight as the independent variable and Log Kow as the dependent variable. The equation of the line is: $y = (-0.7071 \text{amu}^{-1})x - 2.0361$, where the slope = -0.7071amu^{-1} . The third model represents the evaluation of diffusivity constant D as a function of formula weight of the drug and depth of stratum corneum (taken here to be 0.004 cm of normal skin). The output is a 2-dimensional plot having formula weight as the independent variable and values of Log D as the dependent variable. The equation of the line that formed is (x axis in hour, y axis in cm^2/hour): $y = (-0.00607 \text{cm}^2/\text{hour}^2)x - 5.112 \text{cm}^2/\text{hour}$, where slope = $-0.00607 \text{cm}^2/\text{hour}^2$. These equations and the output of continuous modeling can be utilized to predict important parameters of the topical application of drugs. These models present the continuous mathematical expression of the parameters, however discrete values may be calculated from the equations for each of diffusivity constant D, Log D, Kaq, and Kpol from values of formula weight and stratum corneum depth in centimeters.

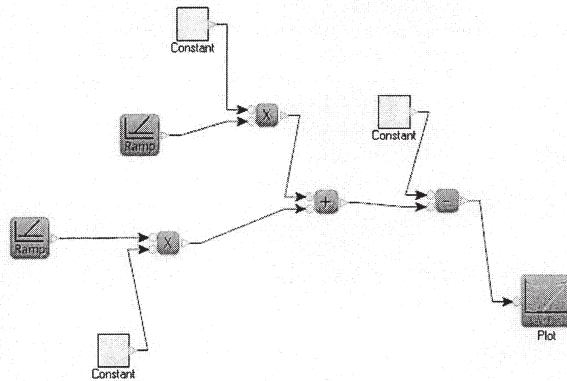
The "lag time" of a drug is time required for a topically applied drug to reach the state in which permeation can be described by Kp, Kpol, Fick's Law, and other functions of the drugs activity. Lag time is a function of skin diffusivity constant D, and length of stratum corneum (see Materials and Methods). Other important parameters for drug dispersion in skin are the Permeation Coefficient of Protein Layer, Kpol; and Permeation Coefficient of Aqueous Layer, Kaq. These relationships describe the movement of a drug through the protein layer and aqueous layer of the epidermis (see Figure 2). Numerical values of both are a function of formula weight of the drug. Therefore, as formula weight increases the value of Kpol decreases, as does the value of Kaq. The relationship with formula weight can be expressed as an equation of a line for Kpol as follows: $y = (-3.175E-08)x + 1.455E-05$, $r = -0.9701$ and $r^2 = 0.9412$. Similarly, the line formed for Kaq becomes:

ACSLXTREME CONTINUOUS SYSTEM ANALYSIS FOR SKIN PENETRATION PARAMETERS

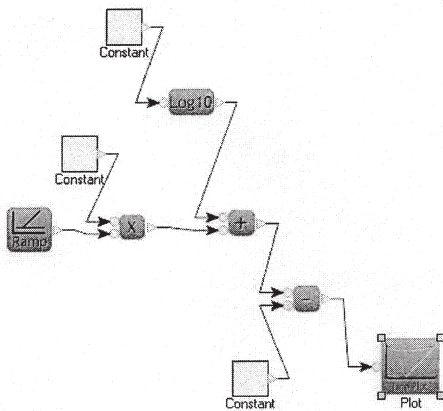
Penetration of Drug (cm) From $K_p \times \text{Time}(\text{hours})$



Variance of K_p Values as a Function of $\text{Log } K_{ow}$ and Formula Weight



Variance of $\text{Log } D$ Values as a Function of Formula Weight and $\text{Log}(\text{depth of stratum corneum})$



Depth of stratum corneum assigned a value of 0.004 cm of normal skin.

FIGURE 6. Continuous system analysis by acslExtreme can be utilized to obtain these three models of drug penetration, variance of K_p , and variance of $\text{Log } D$ values as a function of time, K_p , $\text{Log } K_{ow}$, formula weight, and depth of stratum corneum.

$y = (-4.495E-04)x + 0.2060$, $r = -0.9699$ and $r^2 = 0.9407$. Therefore, as these β -lactam antibiotics are converted to their respective nicotinic acid or dihydropyridine derivatives, the formula weight increases but the values of K_{pol} and K_{aq} decrease (i.e., movement of drug decreases).

In summation, it is shown that normal skin can be represented by a hierarchical tree diagram showing epidermis, dermis, and hypodermis. The carrier groups nicotinic acid and dihydropyridine are attached to the β -lactam antibiotic by a (-O-CH₂-) linker and affect Log P, water solubility, and other properties of these antibiotics. The K_p values for the nicotinic acid derivatives of antibiotics are competitive with those of the currently utilized dihydropyridine derivatives. The nicotinic acid derivatives can be synthesized in the same manner as the dihydropyridine derivatives, thus posing no obstacle for their manufacture and testing. Analysis of molecular properties by cluster analysis, principal component analysis, factor analysis, and discriminant analysis shows clearly that the antibiotic derivatives which have a nicotinic acid or dihydropyridine carrier group attached are similar to each other. Properties, such as formula weight, molar volume, molar refractivity, water solubility, for nicotinic acid derivatives are similar and overlap numerically (by standard deviation) with those of the dihydropyridine derivatives. Therefore, the nicotinic acid derivatives of β -lactam antibiotics are comparable and analogous to the current clinically applied dihydropyridine derivatives and have a high probability of effective and beneficial usage in similar clinical applications.

This work was funded by the Medicinal Chemistry Laboratory, Chemistry Department of the University of Nebraska, Omaha USA.

References

1. Wu, W., Pop, E., Shek, E., Bodor, N. (1990) *J. Med. Chem.* (33)2: 880.
2. Wu, W., Pop, E., Shek, E., Clemmons, R., Bodor, N. (1990) *Drug Des. Deliv.* 7(1): 33–43.
3. Wu, W., Pop, E., Shek, E., Bodor, N. (1989) *Med. Chem.* 32(8): 1782–1788.
4. Hellum, K., Schreiner, A., Digranes, A., Bergman, I. (1978) *Proc. Int. Congr. Chemother. 10th meeting I*: 620–622.
5. Simon, N., Dobozy, A. (1976) *Dermatologica (Suppl 152)*: 215–219.
6. Sabath, L. (1978) *Scand. J. Infect. Dis.* 14: 313–315.
7. Hedstrom, S. (1984) *Scand. J. Infect. Dis.* 42: 135–142.
8. Fagelis, S. (1982) *Azerbaldzhanski Meditsinski Zhurnal* 59(1): 53–60.
9. Ragelis, S. (1982) *Zh. Eksp. Klin. Med.* 22(2): 117–122.
10. Cladera, J., O'Shea, P., Hadgraft, J., Valenta, C. (2003) *J. Pharm. Sci.* 92(5): 1018–1027.
11. Pop, E., Wu, W., Bodor, N. (1989) *J. Med. Chem.* 32: 1789–1796.
12. Pop, E., Wu, W., Shek, E., Bodor, N. (1989) *J. Med. Chem.* 32: 1774–1781.
13. Bartzatt, R. (2004) *Drug Delivery 11*: 1–8.
14. Ertl, P., Rohde, B., Selzer, P. (2000) *J. Med. Chem.* 43: 3714–3717.
15. Herrero, J., Valencia, A., Dopazzo, J. (2001) *Bioinformatics* 17: 126–136.

Received November 19, 2004;

accepted April 27, 2004.

The Thermoelectric Properties of Hornet Cuticle: Correlation With Measuring Body Sites and Activity Status

Vitaly Pertsis*, Anna Sverdlov, Ksenia Riabinin,
Marija Kozhevnikov and Jacob S. Ishay**

*Department of Physiology and Pharmacology, Sackler Faculty of Medicine,
Tel Aviv University, Ramat Aviv, 69978, Israel.*

**Part of a Ph. D. Thesis of V. P.*

*** Address for correspondence*

Abstract: Our study focused on the thermoelectric properties of hornet cuticle at different body compartments and under varying states of awokeness. We also measured the temperature alteration patterns in various body parts of the hornet. Electric voltage and current were dependent on: a) the state of wakefulness; b) the part of the body. The current was lowest in dead hornet cuticle, somewhat higher in narcotized hornet cuticle, considerably higher in the cuticle of hornets awakening from anesthesia and highest in fully awake hornets. Voltage values were of the same order for dead and narcotized hornets, but considerably higher in unanesthetized awake hornets and highest in the cuticle of hornets awakening from anesthesia.

At optimal temperature (29°C) the hornet body temperature was higher on the abdominal cuticle than on other body parts. At an ambient temperature of 20°C, the highest temperatures were recorded on the head and thorax, and the lowest on the abdomen. Body temperatures of live hornets were higher than the cooler ambient temperature outside the nest at night. The results suggest that the hornets possess an intrinsic biological heat pump mechanism, which can be used to achieve active thermoregulation.

OUR LABORATORY has long been engaged in measuring physical properties of the Oriental hornet (*Vespa orientalis*) such as are associated with its normal daily activities. The Oriental hornet is an annual, social insect in the Mediterranean basin and surroundings. A hornet queen that has hibernated founds a subterranean nest in the spring whose population steadily increases during the summer. At its peak, the nest population numbers hundreds and various stages of brood, and by the end of the season — also the sexual stages, namely, drones and queens. The latter then mate and subsequently hibernate. They

will start a new generation or colony in the next year (Ishay *et al.*, 1967; Wilson, 1971; Spradbery, 1973). Furthermore, due to the marked stability of conditions within the hornet's nest, most of the observations and measurements are easily relatable. For instance, within the nest the prevailing temperature is 29°C (Ishay, 1972; Heinrich, 1981), the relative humidity is about 99% (Ishay *et al.*, 1967) and it is dark, while foraging workers intermittently emerge from the nest during the day to collect food and building materials (Ishay and Kirshboim, 2000). Any electric measurements on the hornet are subject to the constraints of time (live hornets are available only during the summer), temperature, and relative humidity.

In the light of our previous findings confirming that hornet cuticle is an organic semiconductor-like tissue (Croitoru *et al.*, 1978; Gutmann *et al.*, 1983), we sought to answer two queries: a) is there any connection between the electric activity of the cuticle on various parts of the hornet's body; and b) are the temperatures different in different regions of the cuticle?

The present study focused on the thermoelectric properties of hornet cuticle at various states of awakensness.

Materials and Methods

Thermoelectric measurements were carried out between 20–30°C. Measurements were made in an incubator, at a relative humidity exceeding 90%, all as previously described (Pertsis *et al.*, 2001). We also took measurements from the cuticle of live hornets subjected to ether anesthesia and from untreated live queens. The latter cannot be affixed to the substrate by amorphous silver like dead or anesthetized hornets, but need to be restrained by alligator bonds after first being immobilized and then attached by rubber bands to the substrate and to the measuring device.

Statistical analysis: We resorted to tables of percentages, observed frequencies and expected frequencies, which were then employed in Chi Square (χ^2) test. Connections between the following variables were assessed: sex or caste (worker, queen, drone) and electric current, state of awakensness (i.e., dead, anesthetized, awakening from anesthesia or live hornet) and voltage level, state of awakensness and current level, body parts (head, thorax, and abdomen) and voltage level. The body temperature of hornets in the nest, or of disparate body parts of wakeful and anesthetized hornets, or of hornets acting as sentinels at or outside the nest entrance, was determined by thermography, using a Therma CAM Model 290 PM (Inframetrics, USA) with the zoom level at x1 (Litinetsky *et al.*, 2001). In total 50 hornet specimens were measured (Table I). In all, 22 workers, 13 drones and 15 queens were evaluated. 9 were dead (at measurement), 11 were under ether anesthesia, 24 were awake post ether anesthesia and 6 were awake without any prior anesthesia. Histograms of low and high maximal voltage are presented in Figures 1A, B and of low and high maximal current in Figures 2A, B.

Results

We assessed the correlation between the state of awakensness and the voltage level (see Figures 1A, B).

TABLE I: Details recorded on 50 hornets and their measured results

N	sex or caste	state of awakeness	cuticular area measured	electrode connection	maximal voltage (mV)	maximal current (A)
1	worker	3	abdomen+thorax	tip of abdomen+thorax	305	8.00E-07
2	worker	3	entire body	head+thorax	415	9.10E-07
3	worker	3	entire body	tip of abdomen+head	350	5.00E-07
4	drone	3	abdomen	tip of abdomen+abdomen	290	4.20E-07
5	worker	3	abdomen+thorax	tip of abdomen+thorax	375	6.60E-07
6	worker	3	entire body	tip of abdomen+thorax	269	3.00E-07
7	worker	3	abdomen+thorax	tip of abdomen+thorax	415	4.30E-07
8	worker	3	abdomen	tip of abdomen+abdomen	405	2.00E-07
9	queen	3	abdomen+thorax	tip of abdomen+thorax	360	1.60E-07
10	worker	3	entire body	tip of abdomen+head	280	7.20E-07
11	drone	3	abdomen+thorax	tip of abdomen+thorax	550	8.10E-07
12	worker	3	entire body	tip of abdomen+thorax	225	1.40E-06
13	worker	3	entire body	tip of abdomen+head	365	7.00E-08
14	queen	3	abdomen	tip of abdomen+abdomen	260	1.60E-06
15	worker	3	entire body	tip of abdomen+head	410	7.70E-07
16	worker	3	entire body	tip of abdomen+thorax	570	9.00E-08
17	queen	3	abdomen+thorax	tip of abdomen+thorax	375	9.20E-07
18	queen	3	abdomen+thorax	tip of abdomen+thorax	270	8.00E-07
19	drone	3	entire body	tip of abdomen+head	150	7.90E-07
20	drone	2	abdomen	tip of abdomen+abdomen	116	1.08E-06
21	drone	3	head+thorax	head+thorax	137	7.50E-07
22	drone	3	head+thorax	head+thorax	182	6.00E-08
23	queen	3	abdomen+thorax	tip of abdomen+thorax	93	7.90E-07
24	drone	2	abdomen	tip of abdomen+abdomen	105	1.92E-08
25	queen	2	entire body	head+thorax	182	8.30E-08
26	drone	3	head+thorax	head+thorax	69	8.40E-07
27	drone	2	entire body	tip of abdomen+head	84	4.00E-08
28	queen	3	entire body	between the antennae	109	4.00E-07
29	queen	2	entire body	tip of abdomen+head	112	1.50E-07
30	worker	2	abdomen+thorax	tip of abdomen+thorax	188	1.00E-07
31	drone	2	abdomen	tip of abdomen+abdomen	118	9.60E-08
32	worker	1	entire body	tip of abdomen+head	132	3.00E-08
33	queen	2	entire body	between the antennae	104	7.00E-07
34	drone	2	abdomen	tip of abdomen+abdomen	183	6.10E-07
35	drone	2	abdomen+thorax	tip of abdomen+thorax	107	7.50E-07
36	drone	2	entire body	tip of abdomen+head	117	6.70E-07
37	queen	4	entire body	*tip of abdomen+thorax	100	1.30E-06
38	queen	4	entire body	*tip of abdomen+waist	410	2.40E-06
39	queen	4	entire body	*tip of abdomen+waist	250	1.80E-06
40	queen	4	entire body	*tip of abdomen+waist	400	3.50E-06
41	queen	4	entire body	*tip of abdomen+waist	420	5.00E-06
42	queen	4	entire body	*tip of abdomen+thorax	100	1.06E-06
43	worker	1	entire body	tip of abdomen+thorax	10	1.50E-08
44	worker	1	entire body	tip of abdomen+thorax	40	2.60E-08
45	worker	1	entire body	tip of abdomen+thorax	35	4.10E-09
46	worker	1	entire body	tip of abdomen+thorax	126	1.40E-08
47	worker	1	entire body	tip of abdomen+thorax	115	1.60E-08
48	worker	1	entire body	tip of abdomen+thorax	53	7.30E-08
49	worker	1	entire body	tip of abdomen+thorax	160	3.10E-09
50	worker	1	entire body	tip of abdomen+thorax	145	3.20E-08

Note: state of awakeness: 1 - dead, 2 - anesthetized, 3 - awoken after anesthesia, 4 - alive, *connection by 'alligators'.

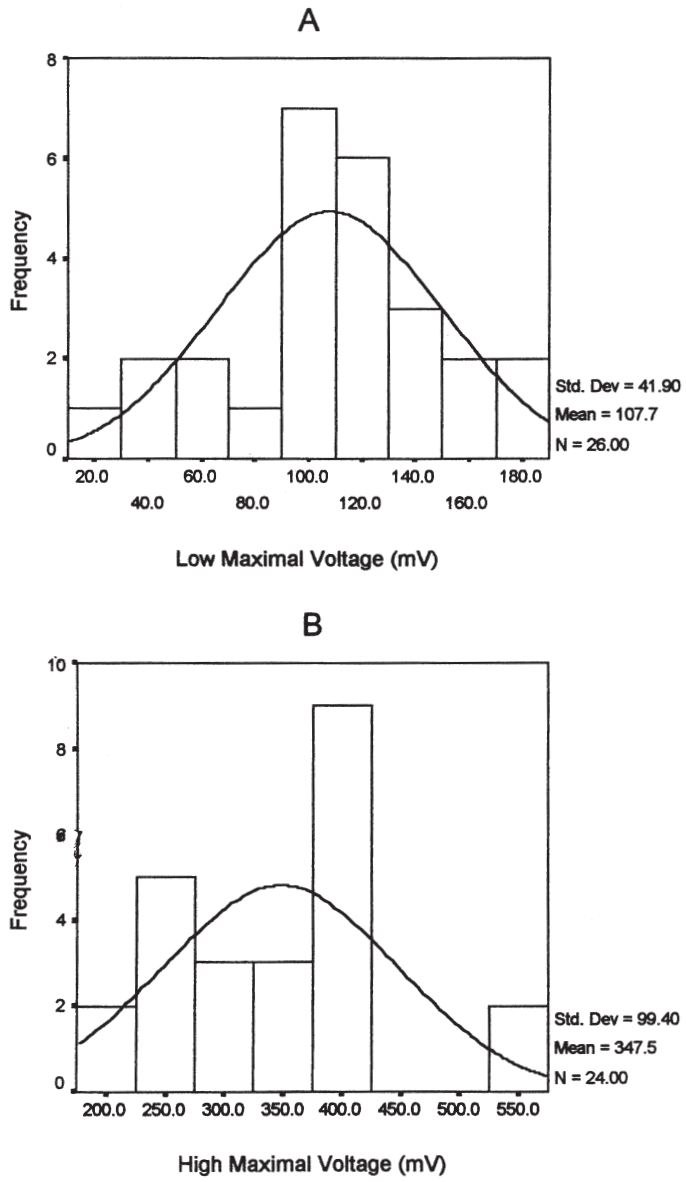


FIGURE 1. Histogram of Low Maximal Voltage (A) and High Maximal Voltage (B).

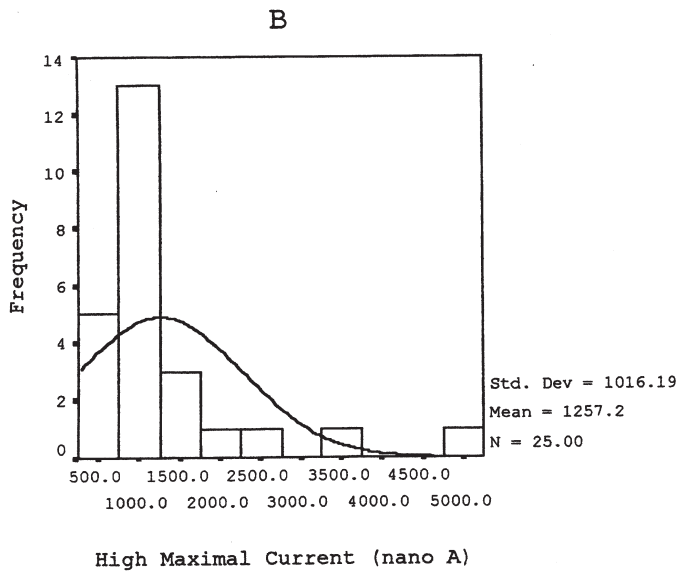
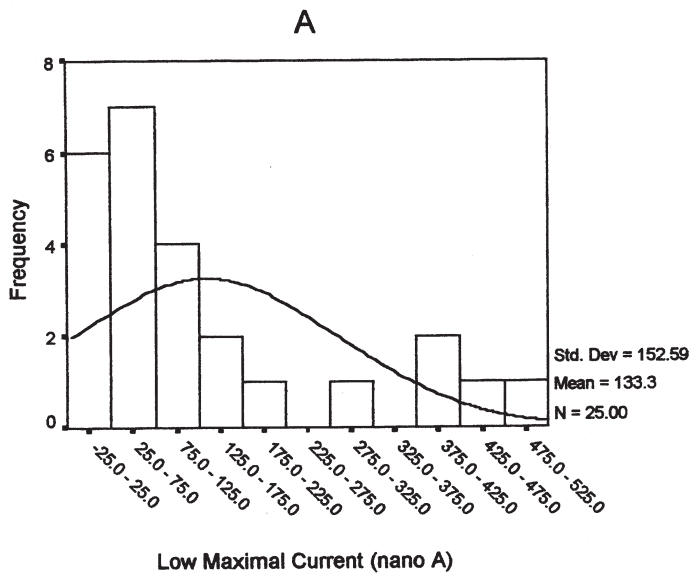


FIGURE 2. Histogram of Low Maximal Current (A) and High Maximal Current (B).

- In the category of low voltage are included 100% of the dead hornets, 81.8% of the anesthetized, 33% of the untreated live and 25% of those awake after anesthesia;
- In the category of high voltage are included all the complement percentage of hornets. Note the total absence of any dead hornets in the category of high voltage, suggesting that dead hornets do not produce high voltage.

Our findings point to the existence of a correlation (at a confidence level of 0.5%) between maximal voltage and the state of awakesness of the hornet.

To elucidate any correlation between the voltage level (see Figures 1A, B) and the cuticular area measured, we tested the following hypothesis: do the measured body parts exert an effect on the voltage level? The conclusions were:

- In the category of low maximal voltage were included 100% of the head and thorax cases *vs.* 60% of the entire body cases, 42.9% of the abdomen cases and 20% of the thorax and abdomen cases.
- In the category of high maximal voltage were included 80% of the thorax and abdomen cases *vs.* 57.1% of the abdomen cases and 40% of the entire body cases.

It appears that low voltage is associated with the head and thorax cases, and high voltage with the thorax and abdomen cases. Our findings point to a correlation between maximal voltage and the cuticular area measured, albeit at a 5% level of confidence.

Next we explored possible correlation between sex or caste and the maximal electric current (see Figures 2A, B). To this end, we assumed that the sex or caste of the hornet exerts an effect on the maximal current. We found that:

- In the category of low maximal current level occurred 72.7% of the worker hornets, 38.5% of the drones and 26.7% of the queens;
- In the category of high maximal current level occurred 73.3% of the queens, 61.5% of drones and 27.3% of workers.

The general conclusion, then, was that a correlation exists between sex or caste of its members and the maximal current output produced by them, with workers producing a low current and queens producing a high current, and this at a confidence level of 2.5%.

Next we investigated possible relationship between the state of awakesness of the hornet and its maximal current level (Figures 2A, B).

- The category of low maximal current incorporated 100% of dead hornets, 54.5% of anesthetized hornets and 41.7% of hornets awaking after anesthesia. The group of live (i.e., untreated) hornets is not represented in the category of low maximal current, since they do not produce a low maximal current.
- The category of high maximal current includes 100% of the live (untreated) hornets, 58.3% of hornets awakened from anesthesia and 45.5% of anesthetized hornets. The category of high maximal current does not include any dead hornets, since they do not produce a high maximal current.

The null hypothesis (no correlation between state of awakesness and maximal current) in this case was rejected at a confidence level of 0.5%.

Using thermographic photography we found that after ether anesthesia, with a nest temperature of 25.5–26.3°C (Figure 3a), the body temperature of the anesthetized hornet was 23.1°C on the dorsal abdomen, 23.0°C on the thorax, and 22.5°C on the head. It is clear, that the body temperature of the hornet is lower than ambient, and that it is not uniform. Rather, the abdomen is warmer than the thorax, which is warmer than the head — this so long as the hornet is situated between the combs of the nest (Figure 3a). All body parts of the hornet are cooler than the nest temperature by about 3°C.

In Figure 3b are shown a number of hornets that had awakened from ether anesthesia and are now emerging from the nest through its exit. At the center of the nest exit, the temperature is above 28°C, while at the periphery of the exit the temperature is lower, close to 26.8°C. The ground temperature around the nest exit on the outside is 23–24.5°C, while the grass on this ground has a temperature of about 22°C. Temperature of the exiting hornets depends on their exact location: those still inside the nest exit show a temperature of 25.5–26.5°C (with abdomen again warmer than head), as compared to the ambient nest temperature of 27.5–28.2°C; those just about to emerge show a temperature of 24.0–25.3°C (and again abdomen warmer than head), and the two hornets already outside — the closer to the nest exit boasting a temperature of 23.3–24.5°C and the one farther away — 22.5–23.7°C.

Figure 3c offers a photograph of awake worker hornet guards at night situated around the nest and also at the nest entrance. At the nest entrance the temperature was 29°C while the hornets located there showed a higher temperature of 30–31.5°C. In those scattered around the nest — comprising 20 individuals at some remove from one another — the thoracic temperature ranged between 29.8–33.4°C and the abdominal temperature between 25.5–28.0°C. In all instances, the body temperature of these hornets outside the nest was invariably higher than the ambient temperature, which was 24–26°C.

A somewhat more magnified picture is given in Figure 3d, which shows a single worker hornet standing guard at the entrance in the field at night. In this hornet the head temperature was 29°C, the thorax temperature was 32–33°C and the abdomen temperature was 27.5°C at an ambient temperature of 24.7°C.

Discussion

There were differences between the various sex and/or caste representatives insofar as electric current. Thus, in queens the highest current value was recorded, and in workers — the lowest current value, while drones were currentwise intermediary between the two. Conceivably the high electric current recorded in the cuticle of queens stems from their greater surface. With regard to possible correlation between the state of awakesness and the voltage, there was indeed significant correlation, with the hornet awaking from anesthesia presenting the highest voltage values and the dead hornets the lowest, and in between the two — hornets that were not placed under anesthesia, or the anesthetized ones. So far as current, live hornets not placed under anesthesia produced the highest values and dead hornets — the lowest.

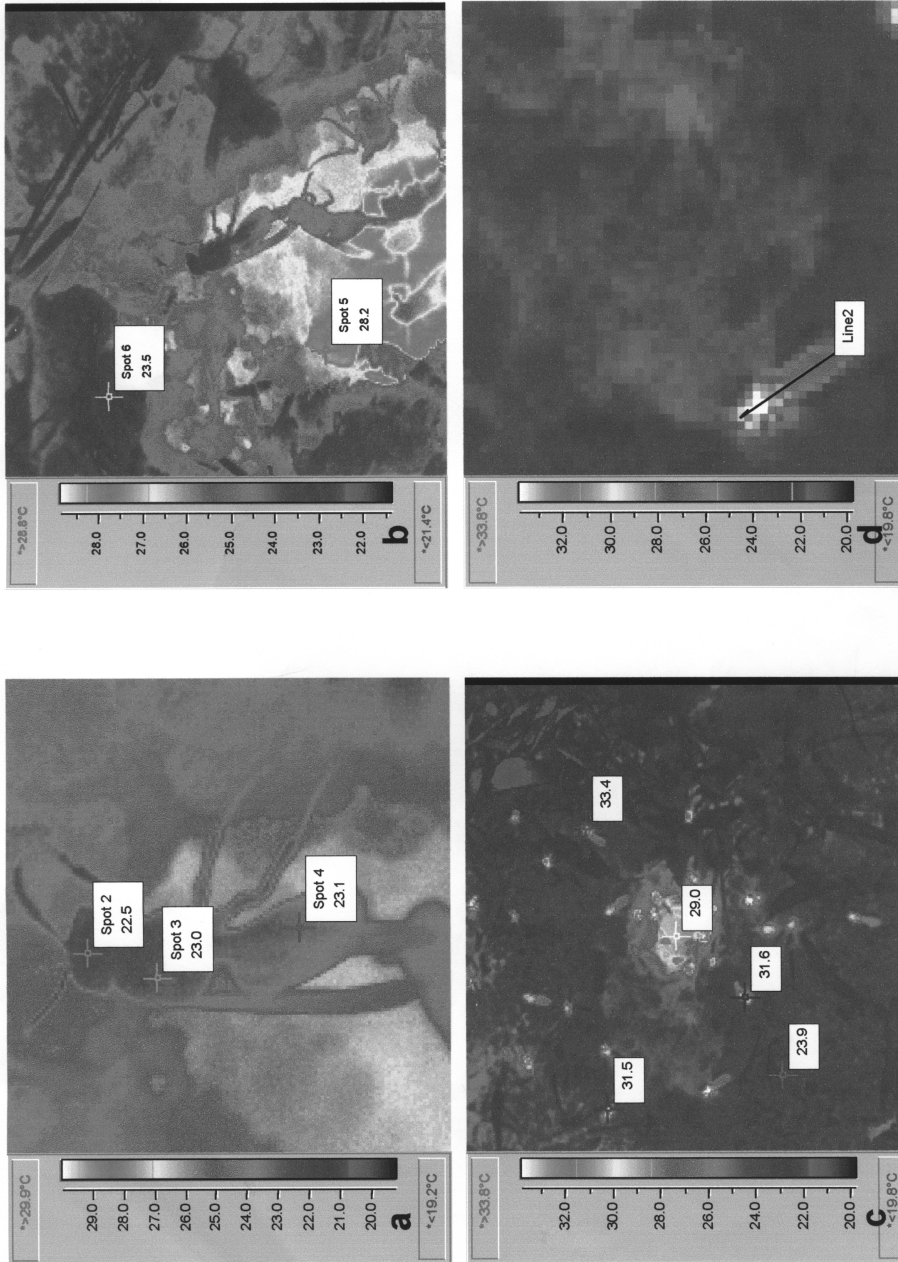


FIGURE 3. Thermographic pictures of adult hornets and their nest. a) adult hornets standing on a comb (bar = x0.3); b) nest temperature and that of hornets walking outside (bar=1cm); c) adult hornets standing guard outside the nest (bar=2cm) and d) one single adult on guard (bar=2cm). For details see Text.

In respect to the region of cuticle measured we found, for the most part, high voltage readings from the thorax and abdomen region and low voltage from the thorax and head region. Regarding possible correlation between the mode of hook-up of the electrodes or their placement on the hornet body and the obtained electric values, it is interesting to note that invariably hookups *via* ‘alligators’ yielded greater current than did ordinary hook-ups (*via* conductive silver and copper wires), and this probably owing to the pressure exerted by the alligators, on their contact points. This result was not statistically significant (we rejected the null hypothesis — no correlation between the electrode insertion points to various cuticular sites and resultant maximal current — at the 10% confidence level), but it is possible that a greater sample may have proved statistical. In brief recap, it is possible to measure the occurrence of electric energy on the cuticle of the Oriental hornet. The level of this energy is dependent on several factors, namely, the nature of the electrodes, their points of contact, the measured cuticular region, the status (e.g., dead, live, etc.) of the hornet and the duration of the measurement. Before proceeding further we need to dwell a moment on the reason why ‘alligator’ connections yield higher electric values than ordinary connections.

As already known (Ishay *et al.*, 1997), hornet cuticle is composed of numerous layers or lamellae, with hemolymph coursing between them. When these layers are pressed forcefully (as in the case of ‘alligators’), they are made to approach one another, and the smaller the distance between them, the greater the electric voltage, with the entire cuticle becoming a sort of electric capacitor (Di Stefano *et al.*, 1981). This capacitor-like cuticle is storing increasing number of electrical charges upon heating, because it is comprised of a material possessing thermoelectric properties (Gutmann *et al.*, 1983; Rowe, 1995; Tritt, 1997). The resultant electric values are positively correlated to the wakefulness of the hornet because they then benefit from the added values of action potential, which are released in the vespan nervous system, apparently in nerve-cuticle connections, like those between the photoreceptors and cuticle in hornets (Ishay *et al.*, 2002).

The photoreceptors and most probably also other types of receptors are prevalent throughout the cuticle, thus promoting high electric readings. In states of wakefulness and regardless of region of the cuticle, as, for instance, when engaging in thermoregulatory activity (Heinrich, 1981), the electric values obtained from the cuticle of live hornets *via* ‘alligator’ connections amount to 100–400 mV and several μ A (see Table 1). Interestingly, these values are close to ones obtained when measuring the electric organs in electric fish (Bennet, 1971). In the latter the electric organ is composed of numerous cells, with each cell (electrocyte) producing electric potentials that are unlike those in the membranes of muscle or nerve cells, but rather modified to maximize external current in series and parallel. Because of this modification, which is the customary explanation given nowadays, in the case of the electric organ of fish, during the state of rest, each side of a cell generates the same resting potential, and since in two neighboring cells the same level of current is generated but in opposite directions, there is no (or hardly any) flow of current outwards (McLaughlin, 1989; Watts, 1990). During activation of the electric organ, the innervated side of the electric cell membrane, namely, the electroplaque, produces an action potential, while the non-innervated side remains unchanged. Consequently, during activation, both sides of the same cell are not equal and opposite, whereupon an emergent current results (Catterall, 1988).

As already mentioned, the cuticle of a hornet is composed of numerous lamellae, amounting to at least 30 and possibly even 70 (Ishay *et al.*, 1998). In hornet cuticle, the

first, outermost layer — the epicuticle — coats the entire outer surface of the cuticle, including an area housing peripheral photoreceptors where the cuticular layers (exo- and endocuticle) are discontinuous (Ishay *et al.*, 2002). Apart from the peripheral photoreceptor area there is an interruption housing a cubicle of interskeleton filling material, which is different than that of the skeleton, which is made up of chitin and consists probably of proteins. Hornet cuticle contains ferroelectric material (Ishay and Shimony (Benshalom), 1983; Xu, 1991; Ishay and Litinetsky, 1996), which shortly, after its exposure to light becomes polarized, i.e., the microscopic electric dipoles become partially oriented and induce an electric voltage. This voltage was measured, and was found to be dependent on the duration of exposure as well as on the light intensity, its wavelength, etc. After prolonged exposure to light irradiation, the cuticular resistance rises to levels of Giga Ohms (G Ω) (Ishay and Litinetsky, 1996), and persists, at that level, as long as irradiated.

In general, one can view the structure of hornet cuticle as resembling that of Mylar (an industrial product for thermal isolation), which is composed of 30–80 layers and outwardly coated with a layer of aluminum (Heaney, 1998). Of course, hornet cuticle lacks an aluminum coating, but it does boast an insulating layer — the epicuticle. In the case of hornet cuticle, the thickness of the layers of exo- and endocuticle progressively diminishes, so that the difference between the outermost and innermost layer amounts to about two orders of magnitude in favor of the former.

In dead hornets all the cuticular layers yield low levels of voltage and current, to wit: 100–140 mV and $4.1 \cdot 10^{-9}$ – $15 \cdot 10^{-9}$ A, whereas in live hornets awaking from anesthesia, and subjected to ‘alligator’ connections, much higher levels were recorded, namely, 280–570 mV and $2 \cdot 10^{-7}$ – $1.4 \cdot 10^{-6}$ A. In other words, in the latter hornets the voltage was about three times higher and the current higher by at least two orders of magnitude (Table 1). This significant increase in current (and somewhat lesser in voltage) may perhaps point to a drop in the resistance as per the equation of Ohm’s Law ($V=IR$) and may stem at least partly from the absence of electrolyte fluid between the cuticular layers of dead hornets, as opposed to the presence of such fluid in live hornet cuticle (whether awaking from anesthesia or otherwise). Yet, for the most part it is probably the result of neural activity such as is associated with awakening (action potential). Although there is no electric voltage or current in dead fish, the cuticle of dead hornets kept under refrigeration for prolonged period still generates significant voltage and a low current, probably due to its structuring of parallel plates with some interposed electrolytic fluid. The awakening of hornets from their first anesthesia usually occurs after 35.055 ± 3.223 minutes and lasts an average of 17.227 ± 1.902 minutes (Ishay *et al.*, 1994; Kristianpoller *et al.*, 1995), following which there is a drop. This drop is probably associated with the fatigue ensuing from the preceding effort of awakening.

Interestingly, in hornets awakening from anesthesia, the electric values, that is, the voltage and the current levels are different from those recorded from wakeful, never (at least not lately) narcotized hornets, in that the voltage is higher in the former than in the latter but the current is lower. The high voltage that is recorded during the wakening from anesthesia (about 35 minutes after the narcotization) resembles in its electric features epileptic seizures. Thus in higher mammals, such as humans, the scalp surface EEG values are 20–100 μ V (Kandel *et al.*, 2000), whereas during an epileptic seizure values of 20–40 mV are recorded (i.e., greater by three orders of magnitude), albeit the latter last merely between 50–200 msec.

In electric fish, different electric values are recorded (Bennet, 1970) but all these fish have in common an electric organ, i.e., an organ specialized for the production of an electric field outside the body. For instance, South African bulldogs (*Marcusenius macrolepidus* Marmyridae) generate brief (less than 1 ms) electric organ discharges, separated by much longer inter-discharge pauses (Werneyer and Kramer, 2002). Be that as it may, what clearly distinguishes the electric organ of electric fish from its equivalent in hornets is the following: 1) only in *live* fish is an electric field encountered whereas in hornets, even in *anesthetized* or fully *dead* specimens, an electric field is detected, albeit weaker than in the active hornets; 2) in the electric fish light does not figure as a stimulant, but in hornets it does, in that they awaken at a certain light wavelength, be it at ultraviolet A (UVA) or UVB (Ishay *et al.*, 1994) and their electric values are enhanced by it; 3) in fish, the electric energy dissipates within milliseconds whereas in hornets it is much more protracted; moreover, the process is repeatable and reproducible when at high level, probably because it is neurogenic and is generated by electrical synapse-like structures (Kandel *et al.*, 2000). In electric fish the electric organ is located in various regions of the body, as a rule in more than one site. Likewise, in the hornet, the equivalent organs, from which one can measure significant levels of voltage and current, are apparently ubiquitous, occurring in every part of the body that bears an outer cuticle. Clearly, then, hornet cuticle displays electric properties throughout, as evident from our statistical analyses pertaining to the sites of measurements, or the site of attachment of the electrodes. We did find that connections and measurements of head and thorax yielded lower electric values than did thorax and abdomen, but even the latter yielded higher values than did total-body measurement.

It is customary for us to measure thermal properties of hornet cuticle primarily at temperatures up to 30°C. The reason for this is that previously (Ishay and Ruttner, 1971) we have ascertained that the temperature prevailing in the hornet's nest between the brood combs is 29°C. This finding, however, took an interesting turn when in subsequent thermoelectric measurements we obtained clear-cut results at temperatures ranging between 20–30°C, with values recorded both in the brood combs as well as on silk removed from the combs (Ishay and Barenholz-Paniry, 1995).

From another examination undertaken by us and pertaining to specific heat (Ishay and Pertsis, 2002), we gleaned that there is a marked difference between the two types of stripes — brown and yellow — such as definitely justifies measuring thermoelectric properties of hornet cuticle in this range of temperatures. Of interest also are the two findings shown in Figure 3a, to wit: a) the temperature of the hornet is lower by about 3°C than the temperature of the brood comb; and b) that in the body of the hornet, the abdomen is warmer than the thorax by 0.1°C, while the thorax, in turn, is warmer than the head by 0.5°C, which means that there is a cascade of temperatures along the body of the hornet. To our mind, we are facing here a phenomenon of a *heat pump*, wherein the body of the hornet is affected by the ambient temperature, yet the hornet somehow succeeds in conserving its own body heat, which is lower than the ambient temperature (Datyner and Cohen, 1991).

Previously we have shown that hornet cuticle displays a Seebeck effect (Shimony and Ishay, 1981) and we deemed it reasonable to assume the presence in the cuticle of elements that induce cooling (Peltier effect) which are responsible for the phenomenon. The large difference in the specific heat between the yellow and brown cuticular stripes substantiates this assumption because according to the Drude model (Aschcroft and Mermin,

1976) the Seebeck coefficient is proportional to the specific heat, i.e., yellow stripe thermo power is much higher than the brown stripe one at the measured temperatures (Ando *et al.*, 1999), with the brown cuticle displaying a specific heat (C_p) of ~ 1.62 J/Kg as compared to that of the yellow stripes with a $C_p=1.82$ J/Kg at 30°C vs. ~ 1.55 for both stripes at 20°C .

We can assume, then, that being equipped with a *heat pump* mechanism, hornets are capable of regulating their body temperature as the need arises. This could explain also our finding of sentinel hornets standing guard around the nest at night, in which the temperature of the muscular thorax is higher than that of the head, which, in turn, is higher than that of the abdomen. In fact, the entire body of such sentinel hornets is warmer by several degrees Celsius than the ambient temperature. That said, we cannot ignore a dissenting opinion voiced by Heinrich (1981), who claimed that the differential temperature in insects is determined by the strength of flow of hemolymph in various bodily parts. According to his view, the stronger the flow the higher the temperature, which would account for the higher temperature in the more highly 'irrigated' thorax than in the hemolymph poor abdomen. Be that as it may, Heinrich's claim cannot hold in cases such as ours, where the entire hornet body is colder than its surroundings, as evinced from Figures 3a and 3b.

The electrical energy produced in the hornet cuticle serves, probably in large part, to activate the *heat pump*, thus producing the differences in temperature between the hornet body and its surrounding, and ending up in a *thermoelectric heat pump* in the various parts of the body which operates according to vespan needs.

References

- Ando, Y., Miyamoto, N., Segawa, K., Kawata, T. and Terasald, J. (1991) Specific heat evidence for strong electron correlations in the thermoelectric material (Na, Ca) CO_2O_4 . *Physical Review B* 60(15): 10580–10583.
- Aschcroft, N.W. and Mermin, N.D. (1976) *Solid State Physics* (Holt Saunders, Philadelphia).
- Bennet, M.V.L. (1970) Comparative physiology: electric organs. *Ann. Rev. Physiol.* 32: 471–528.
- Bennet, M.V.L. (1971) *Fish Physiology. Sensory systems and electric organs*. Volume V. Academic Press. New York.
- Catterall, W.A. (1988) Structure and function of voltage-sensitive ion channels. *Science* 242: 50–61.
- Croitoru, N., Ishay, J., Arcan, L. and Perna, B. (1978) Electrical resistance of the yellow strips of social wasps under illumination. *Photochem. Photob.* 28(2): 256–270.
- Datyner, N.B. and Cohen, I.S. (1991) Cooling-heating module for tissue chambers and solutions. Theoretical considerations and practical design. *J. Neuro. Meth.* 40(1): 49–62.
- Di Stefano, A.V., Franco, J.I., Perissinotti, I. and Walsöe de Reca, N.E. (1981) Behavior of charge transfer complexes for solid state cells. *Solid State Ionics* 5: 693–695.
- Gutmann, F., Keyzer, H., Lyons, L.E., and Somoano, R.B. (1983) *Organic Semiconductors*. Part B. Robert E. Krieger Publishing Company. Malabar, Florida.
- Heaney, J.B. (1998) Efficiency of aluminized mylar insulation at cryogenic temperatures. SPIE-Int. Soc. Opt. Eng. Proc. Spie- The Internation Society for Optical Engineering. 3435: 150–157.
- Heinrich, B. (1981) *Insect Thermoregulation*. Wiley-Interscience, New York.
- Ishay, J. (1972) Thermoregulatory pheromones in wasps. *Experientia* 28(10): 1185–1187.
- Ishay, J.S., and Barenholz-Paniry, V. (1995) Thermoelectric effect in hornet silk and thermoregulation in hornet's nest. *J. Insect. Physiol.* 41(9): 753–759.

- Ishay, J.S., and Kirshboim, S. (2000) Ultraviolet B light stimulates hornet activities — a review. *Semicon. Sci. Tech.* 15: 704–723.
- Ishay, J.S., and Litinetsky, L. (1996) Thermoelectric current in hornet cuticle: Morphological and electrical changes induced by temperature and light. *Physiol. Chem. Phys. & Med. NMR* 28: 55–67.
- Ishay, J.S. and Pertsis, V. (2002) The specific heat of the cuticle and the morphological difference between the brown and yellow cuticle of hornets. *J. Electron Micr.* 51(6): 1–12.
- Ishay, J. and Ruttner, F. (1971) Die thermoregulation im Hornisennest. *Z.v. Physiol.* 72: 423–434.
- Ishay, J.S., and Shimony (Benshalom), T. (1983) Electrical resistivity in cuticle of Oriental hornet queen before, during and after hibernation: Evidence for electronic conductance. *Physiol. Chem. Phys. & Med. NMR* 15(4): 289–310.
- Ishay, J., Bytiniski-Saltz, H. and Shulov, A. (1967) Contributions to the bionomics of the Oriental hornet *Vespa orientalis*. *Israel J. Entomol.* 11: 45–106.
- Ishay, J.S., Pertsis, V. and Levto, E. (1994) Duration of hornet sleep induced by ether anesthesia is curtailed by exposure to sun or UV-irradiation. *Experientia* 50(8): 737–741.
- Ishay, J.S., Goldstein, O., Rozenzweig, E., Kalicharan, D. and Jongebloed, W.L. (1997) Hornet yellow cuticle microstructure: a photovoltaic system. *Phys. Chem. Phys. & Med. NMR* 29(1): 71–93.
- Ishay, J.S., Kirshboim, S., Steinberg, D., Kalicharan, D. and Jongebloed, W.L. (1998) Hornet cuticle: a composite structure comprised of a series of duplex lamellae attenuating towards the interior of the body. *Comp. Biochem. Physiol. A* 120: 661–670.
- Ishay, J.S., Litinetsky, L., Pertsis, V., Barkay, Z. and Ben-Jacob, E. (2002) Sub-micromorphology of the epicuticle of hornets: AFM studies. *J. Electron Micr.* 51(1): 79–86.
- Kandel, E.R., Schwartz, J.H. and Jessell, T.M. (2000) *Principles of Neural Science* (4th Ed.), McGraw-Hill, New York.
- Kristianpoller, N., Goldstein, O., Litinetsky, L. and Ishay, J.S. (1995) Light curtails sleep in anesthetized hornets: extraretinal light perception. *Physiol. Chem. Phys. & Med. NMR* 27(3): 193–201.
- Litinetsky, L., Rosenzweig, E. and Ishay, J.S. (2001) Thermal properties of hornet colonies: a thermoelectric interpretation of thermoregulation of the entire nest and its individual members. *Phys. Chem. Phys. & Med. NMR* 33: 103–118.
- McLaughlin, S. (1989) The electrostatic properties of membranes. *Ann. Rev. Biophys. Chem.* 18: 113–136.
- Pertsis, V., Sverdlov, A., Litinetsky, L., Rozenzweig, E. and Ishay, J.S. (2001) Navigation and thermophotovoltaic activity by hornets at different light conditions: the influence of UVB blockers. *Phys. Chem. Phys. & Med. NMR* 33(2): 187–202.
- Rowe, D.M. (1995) *CRC Handbook of Thermoelectrics*. CRC Press. Boca Raton.
- Shimony, T.B. and Ishay, J.S. (1981) Thermoelectric (Seebeck) effect on the cuticle of social wasps. *J. Theor. Biol.* 22: 497–503.
- Spradbery, J.P. (1973) *Wasps*. Sidgwick and Jackson. London.
- Tritt, T.M. (ed.) (1997) Thermoelectric materials — new directions and approaches. *Mat. Res. Soc. Symp. Proc.* Volume 478.
- Watts, A. (1990) Protein-lipid interactions at membrane surfaces. In: *Biophysics of the Cell Surface* (Glazer, R. and Gingell, D. eds). Springer-Verlag. Berlin, pp. 23–50.
- Werneyer, M. and Kramer, B. (2002) Intraspecific agonistic interactions in freely swimming marmyrid fish, *Marcusenius macrolepidotus* (South African form). *J. Ethol.* 20: 107–121.
- Wilson, E.O. (1971) *The Insect Societies*. The Belknap Press of Harvard University Press. Cambridge, Massachusetts.
- Xu, Y. (1991) *Ferroelectric Materials and Their Application*. North-Holland (Amsterdam).

Received June 10, 2003;
accepted May 14, 2004.

On the Modulation Effect of Pulsing and Static Magnetic Fields and Mechanical Vibrations on Barley Seed Hydration

Armine Amyan and Sinerik Ayrapetyan*

UNESCO Chair-Life Sciences International Postgraduate Educational Center

31 Acharyan St., Yerevan, 375040 Armenia

E-mail: life@arminco.com

**Author for correspondence*

Abstract: The changes of wet and dry weights of barley seed in different periods of swelling were studied in seeds treated with Extremely Low Frequency Electromagnetic Fields (ELF EMF), Static Magnetic Fields (SMF) and Mechanical Vibrations (MV) in cold (4°C) and warm (20°C) distilled water as well as in seeds non-treated (control). The metabolic dependent seed hydration, dry weight loss and water binding in seed were modulated by preliminary EMF, SMF and MV-induced treatment of distilled water. The specific electrical conductivity (SEC) of control and treated distilled water was measured before the seed incubation. Frequency and intensity “windows” (i.e. range of frequency or intensity) for the effect of EMF, MV and SMF (correspondingly) on seed hydration, solubility and water binding in seed were studied. These “windows” were different in various phases of seed swelling. It is suggested that water structure modification is the result of valence angle changes (SMF and EMF) and dipole molecules vibration (EMF and MV) has different effects on the process of hydration, solubility and water binding in seed. These results are important from the point of understanding the mechanisms of the biological effect of EMF, as well as from the point of agriculture.

IT HAS been shown that extremely low frequency electromagnetic fields (ELF EMF), static magnetic fields (SMF) and mechanical vibrations (ELF MV) had a depressing effect on distilled water specific electrical conductivity (SEC) [Ayrapetyan *et al* 1994a; Stepanyan *et al* 1999]. It was established that the inhibitory effect of those factors on SEC depended on their intensity and, in the case of ELF EMF and MV — also, on its

Abbreviations: ELF EMF, extremely low frequency electromagnetic fields; LF EMF, low field electromagnetic fields; MV, mechanical vibrations; SEC, specific electrical conductivity; SMF, static magnetic fields.

frequencies [Stepanyan *et al* 1999]. On the basis of these data it was suggested that LF EMF-induced changes of distilled water SEC could be the result of valence angle changes between protons in water molecules and mechanical vibration of water dipole molecules. According to the quant-mechanical calculations the valence angle in water molecules between O-H bounds must be 90° , however, really this valence angle is nearer 105° , because in water, due to the strong polarity of the H-O bounds, the minimal repulsion of the positively charged hydrogen atoms increases the angle [Pullman & Pullman, 1963]. Therefore, it was suggested that the first pathway of water structure changes could be imitated by distilled water exposure to SMF (Klassen 1982), while the second one- by mechanical vibration of distilled water. However, our incomplete knowledge on the biological significance of each of these two pathways-induced water structure changes is the main barrier for estimating the biological effect of ELF EMF on cells and organisms, which is realized through the water structure changes. From our previous study on the effect of ELF EMF, SMF and ELF MV on SEC of distilled water it is difficult to conclude on specific changes of physico-chemical properties of water from these factors, as all these factors have approximately the same depressing effect on SEC of water. It is suggested that plant seed swelling in distilled water can serve as a very convenient experimental model for such a study. Osmotic properties of seed, dissolving of water soluble components of seed and water binding in them, when metabolic activity of seed is depressed (in cold distilled water), as well as metabolic-dependent cell hydration, root formation and germination were studied.

In the present work, the comparative study of time-dependent changes of wet and dry weights of barley seed in different periods of its swelling in non-treated (control), ELF EMF-, SMF- and ELF MV-treated distilled water in cold medium (4°C) and at room temperature (20°C) was performed.

Materials and Methods

The seeds of spring barley (sort- Nutans 115, forming fibrous root systems, cleistogamous) were used. The seeds were cultivated in the Shirak Valley (Armenia) and were kindly supplied by the Echmiadzin Research Center of Agriculture and Plant Protection (Armenia). The distilled water was obtained using the device- DE-4-2M (Russian production, State Standard 64-1-721-91). Distilled water has initial conductivity at room temperature (20°C) in the range of $1\text{--}10\ \mu\text{s}/\text{cm}$. The latter depended on the "age" of distilled water i.e., time passed after water distillation [Stepanyan *et al*, 1999].

The water was gathered in tightly closed glassware, and then was poured out into three identical glass test tubes. A special setup (Institute of Radiophysics and Electronics (IRPhE) of Armenian NAS, Yerevan, Armenia) was assembled allowing the treatment of distilled water by SMF, ELF EMF and ELF MV. The block scheme of this setup is presented in Figure 1. A glass test tube (1) with 10 mm diameter and 10 ml volume was used. The vibrator was controlled by the sine-wave generator (6) (GZ-118, made in Russian Federation), the signal went to the double pole switch (8): in position I the generator functions as EMF and ELF MV sources, while in position II — as LF MV sources. To obtain MV waves the vibrating device (3) was used generating vertical vibrations by set frequency and intensity. The vibrator was constructed in the Department of Engineering at our center (LSIEC) on the basis of the IVCh-01 device (Russian production). To keep vibration intensity constant (30 dB) at different frequencies, a coil (4) with a feedback am-

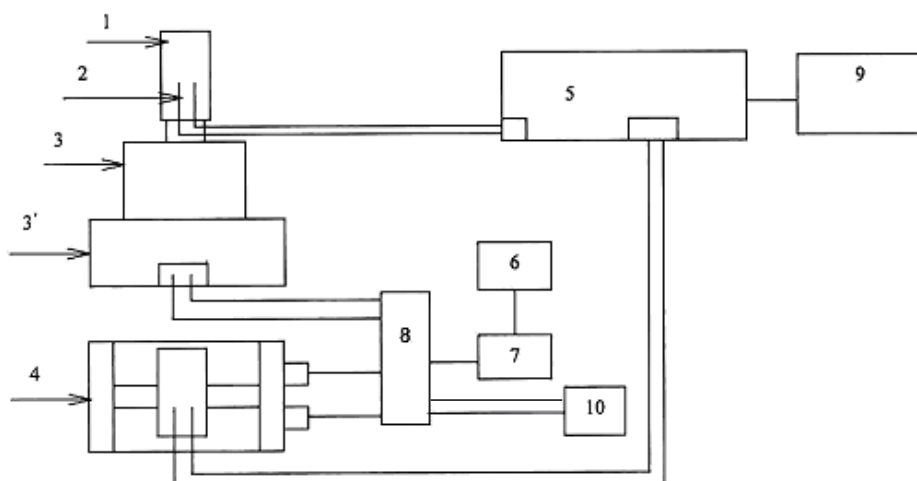


FIGURE 1. The setup for treatment of distilled water by low frequency electromagnetic field (LF EMF), static magnetic field (SMF) and mechanical vibrations (LF MV).

1. Glass test tube with diameter 10 mm and volume 10 ml.
2. Platinum electrodes
3. Mobile part of the vibrator
- 3'. Motionless part of the vibrator
4. The coil
5. The device for the measurement of DW SEC (conductometer)
6. Generator of sinusoid vibration
7. The low-noise amplifier
8. The switch (has 2 positions: I and II, where I- EMF and MV and II- EMF)
9. Personal Computer
10. The generator of a constant field.

plifier system (IRPhE, Yerevan, Armenia) was used. Thus, MV was transmitted to the test tube containing distilled water with insignificant power dissipation. For concordance of high impedance output of generator to low impedance input of vibrator, a special power amplifier (IRPhE, Yerevan, Armenia) was used. MV frequency was controlled by a cyrometer (CZ-47D, production of Russian Federation), while the intensity was measured by a measuring device (IRPhE, Yerevan, Armenia) having a sensor on the vibration table. It was possible to keep the intensity of MV on stable level at all frequencies, including resonance frequency (more than 200Hz for the given setup).

EMF was generated by the controlled generator (6) and low-noise amplifier (7) on the coil (4) (IRPhE, Yerevan, Armenia). The coil had a cylindrical form with 154 mm in diameter and 106 mm in height. The coil consisted of Helmholtz rings generating the homogeneous magnetic field. Rings of Helmholtz were formed by two equal ring coils located coaxially and parallel. The distance between ring coils was equal to their radius (77 mm). The magnetic field created by these rings had high homogeneity. For example, at a distance of 0.25 cm from the center of an axis strength differs from computed by formula only by 0.5% $H = 71.6 \cdot \omega \cdot \frac{I}{R}$ where H is intensity of magnetic field, ω is density, I is amperage and R is resistance. SMF was generated by the generator of a static field (10) and transferred to the coil.

To stabilize the initial structure of seed distilled water for all experiments, the studies were carried out on 24 hours frozen, then melted distilled water. The water was exposed to SMF with intensities of 1.25, 2.5 and 3.75mT, LF EMF and MV –in range of frequencies: 4, 10, 15, 20 and 50 Hz (intensities: 2.5 mT and 30dB, respectively).

Distilled water was treated for 30 min. by one of the afore-mentioned factors, after which 5ml of treated distilled water was added to each Petri dish (vol.~45–50 ml.) containing 20 seeds and this moment was considered as the starting time of seed incubation. To exclude the effect of light the experiments were performed in the dark at 4 or 20°C.

Each experimental sample (version) consisted of 20 seeds. For statistical validity each stage of the experiment was repeated 10 times. In each experiment the initial weight of the seed varied in the range of 40–50 mg. Before the experiments all the seeds were weighed and this weight will be hereafter referred to as “wet weight”. After weighing the experimental groups of seeds were incubated in non-treated and treated distilled water for 2, 24, 48 and 72 hours. Thus, we had the possibility to calculate the quantity of the “free water” and dry substance in the seed in the different periods of its evolution, distinguished by the metabolic activity. In barley seed the growth of the vegetative organs are in close correlation with passing through the stages of organogenesis. As other germinating plants, barley goes through 12 stages of organogenesis [Cuperman, 1982]. According to the “Stron theory” the first stage of organogenesis of germinating plants begins by pre-embryo formation and ends in the phase of seed germination and appearance of shoots [Cuperman, 1982]. At room temperature in distilled water the stage of organogenesis has lasted 72 hours. Usually at room temperature 4 stages of organogenesis of seed growth can be distinguished: 1st stage- 2 hours (water swelling until the critical moisture and active functioning of the ferments), 2nd stage- 24 hours (awakening), 3rd stage- 48 hours (germinal root formation) and 4th stage- 72 hours (germination) [Cuperman, 1982].

Before seed incubation in control and experimental medium, the wet weight and dry weight were determined separately for each seed. It was shown that the decrease of seed wet weight was 4.19 ± 0.004 mg and the level of seed hydration, determined as 1mg water/1mg dry seed, was 0.08 ± 0.004 mg for each seed. The changes of wet and dry weights during seed incubation in control and experimental medium were expressed as percentage of their initial value before incubation.

The effect of factor-treated distilled water on time dependence of seed wet and dry weight changes was studied in different periods of their incubation in cold and warm conditions. The value of seed dry weight was obtained by drying them at a temperature of 104°C during 24 hours in a thermostat [Plotnikova *et al.*, 2001]. Seed hydration (gr.water/gr.dry weight) was calculated as (wet weight-dry weight)/dry weight. The reliability of results was $\alpha = 0.05$. In Figures, where the range of variations is not observed, the values were so small as to be obscured by symbol mark.

The mean value was calculated based upon the average, standard deviations and confidence (Student-t test) with the help of the Excel computer program.

Results

It is obvious, that in order to understand the biological mechanism of the effect of any physical factor (including EMF, SMF and MV) — induced water structure changes on

seed, it is first necessary to study the passive water uptake by seed when their metabolic activity is depressed (in cold condition) compared to the metabolic-dependent seed hydration in warm condition.

As can be seen in Figure 2 the rate of seed hydration was gradually increased during its incubation, which was accompanied by increase of its temperature-sensitivity. The latter was more pronounced in the stage of seed germination during 48–72 hours incubation in warm distilled water.

The time-dependent changes of seed dry weight during 72 hours incubation in distilled water (Figure 3) can be differentiated into three phases: a) first 2 hours- fast decrease, b) 2–24 hours- period of sharp increase and c) 24–72 hours- period of slight increase at cold and slight decrease- at room temperatures. It is obvious, that the sharp decrease of dry weight during the first 2 hours of seed incubation is the result of the loss of their water-soluble components, while the “false increase” of dry weight after the end of 2 hours of incubation can be explained by the increase of water binding in seed, i.e., to obtain a real value of dry weight it is necessary to dry the seed (at 104°C temperature) longer than 24 hours. However, the reason for active decrease of dry weight at 20°C after 24 hours of incubation can be interpreted as the result of decrease of the quantity of binding water in seed. To come to the final conclusion on the latter, it is necessary to carry out more detailed investigations.

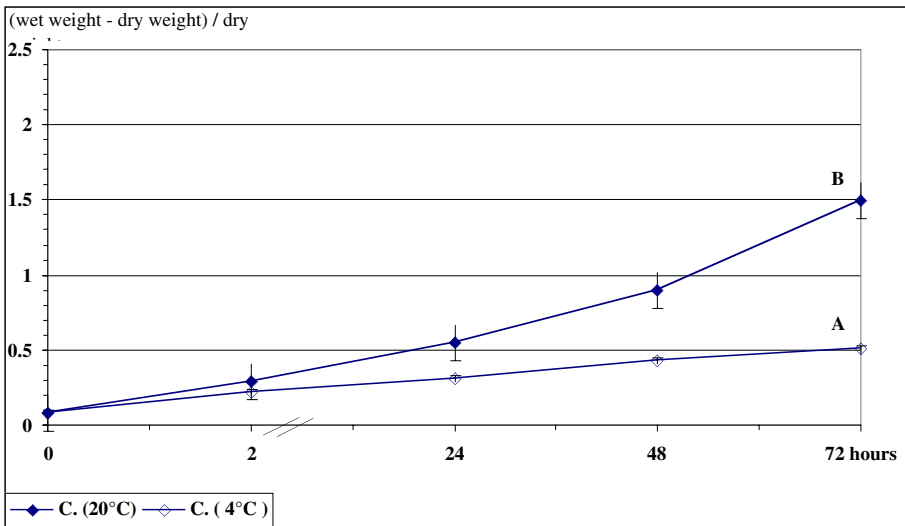


FIGURE 2. The time-dependent seed hydration in non-treated distilled water (Control). Curve A — experimental data obtained in cold medium; curve B — (room temperature) medium. In the present and following Figures “C” means Control. On abscissa — the time (in hours) of seeds incubation and on ordinate- value of seed hydration (mg of H₂O for 1mg of dry weight) are presented.

The confidence limits of computations were in the range of 95%, reliability of results were 0.05%. In Figures where the range of variations is not observed, the values were so small as to be obscured by symbol marks.

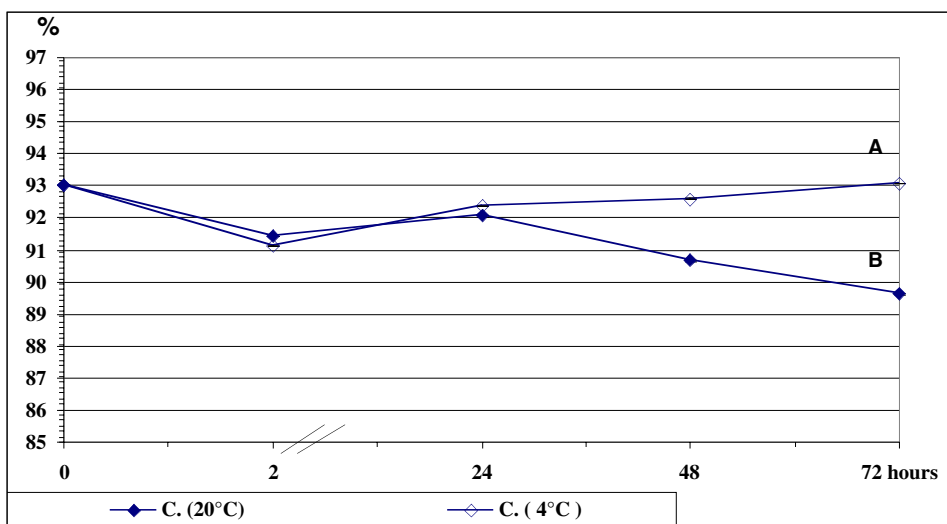


FIGURE 3. The time-dependent changes of seed dry weight in cold (A) and warm (B) non-treated — (Control) distilled water.

On abscissa — the time (in hours) of seed incubation, and on ordinate- percent of seed dry weight change compared to its wet weight₀ are presented.

We studied the effect of the exposure of seeds to LF EMF-, SMF- and MV-treated cold or warm distilled water and control. Our data were based on the time course change of the wet weight and dry weight of seeds and they were interpreted on the basis of altered water structural changes in the following phenomena:

- 1) solubility of seed component;
- 2) water binding in seed;
- 3) passive, non-metabolic dependent seed hydration;
- 4) metabolic dependent seed hydration.

Low frequency electromagnetic field effect

In Figure 4 data are presented on time-dependence of seed hydration in non-treated and in 4, 10, 15, 20, 50 Hz EMF-treated distilled water at cold (A) and room temperatures (B).

As can be seen in Figure 4, pretreatment of distilled water with EMF did not significantly modulate the kinetics of seed hydration in cold condition (A) or during the first 24 hours incubation at room temperature, although, after the first 2 hours incubation, the rate of hydration was comparatively higher than in the cold. The differences between seed hydration in warm and cold distilled water can be considered as a marker for their metabolic activity. The EMF-sensitivity of seed hydration during the first 24 hours incubation was not pronounced, while starting from the period of root formation (48 hours incubation), it became more and more sensitive to water preliminarily treated by EMF. This sensitivity was frequency dependent and became more pronounced at the end of 72 hours incubation, i.e., during the most intensive period of seed germination [Cuperman, 1982]. The seed hy-

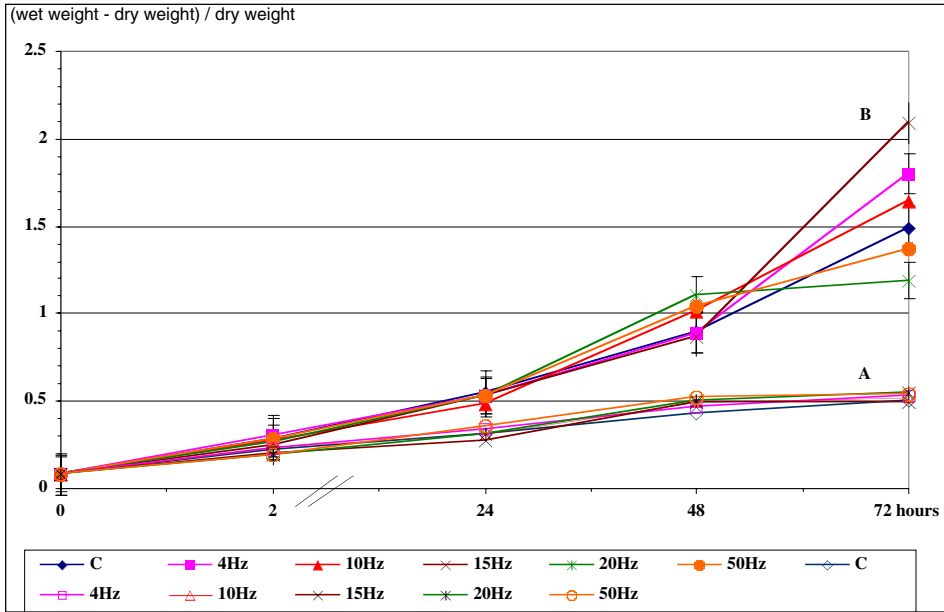


FIGURE 4. The effect of preliminary low frequency electromagnetic field (LF EMF)-treated distilled water on seed hydration during 72 hours incubation. A — seed hydration in cold (4°C) distilled water. B — seeds hydration in distilled water at room temperature (20°C). Abscissa and ordinate as in Figure 2.

dration at the end of 48 hours of incubation in distilled water treated by 4 and 15 Hz EMF was approximately the same as in the control, while 10, 20 and 50Hz EMF-treated distilled water had clear activation effect on it (+13.1±0.05%, +25.2±0.10%, +16.6±0.02%, respectively). It is interesting to note, that at the end of 72 hours of incubation, frequency “windows” for EMF effect on seed hydration were different than at the end of 48 hours incubation. In 20 and 50Hz EMF-treated distilled water seed hydration was depressed compared to the control (−20.2±0.22% and −8.2±0.29%, respectively), while 4, 10 and 15Hz EMF had an activating effect on it (+20.7±0.36%, +9.8±0.36% and +40.1±0.35%, respectively).

These data clearly show that in the metabolic-dependent seed hydration is more sensitive to EMF-induced water structure changes than the metabolic-independent one (in cold distilled water and during the first 2 hours incubation in warm distilled water).

To estimate the effect of LF EMF-treated distilled water on solubility of seed components and water binding in seed, the time-dependent changes of seed dry weight during 72 hours incubation in the control and in the EMF-treated cold and warm distilled water were studied.

As can be seen in Figure 5 (A and B) seed solubility and water binding in seed were significantly different in EMF-treated distilled water, compared to the control. However, the curiously different frequency-dependant character of seed dry weight kinetics in distilled water treated by comparatively high (15, 20 and 50Hz) and low (4 and 10Hz) fre-

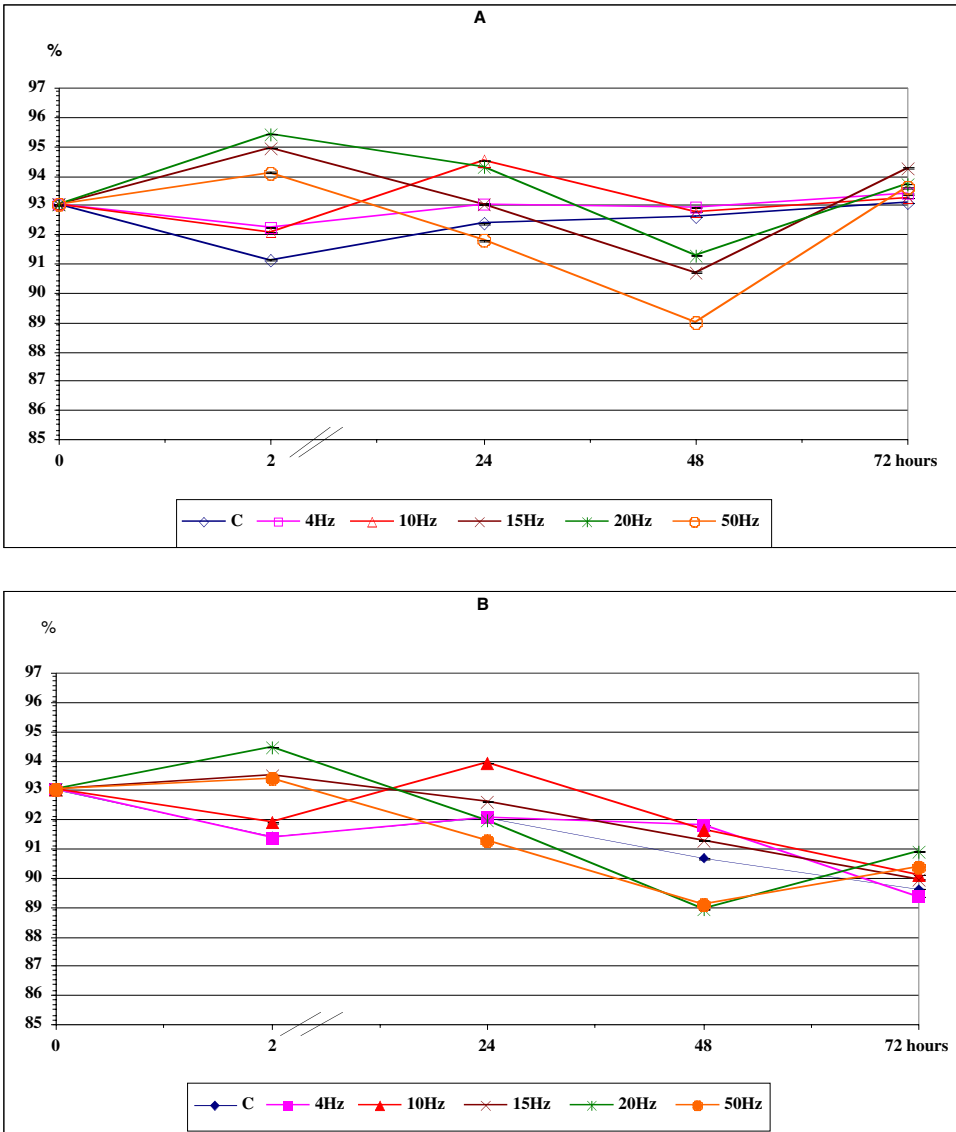


FIGURE 5. The time-dependent changes of seed dry weight during 72 hours of incubation in cold (A) and warm (B) electromagnetic field (LF EMF)-treated distilled water. Abscissa and ordinate as in Figure 3.

quencies seems extremely interesting from the point of theoretical consideration and must be the subject for special detailed investigation. As can be seen in the presented data, in the first two hours 4 and 10Hz EMF had a slightly inhibiting effect on rates of seed dry weight loss, while 15, 20 and 50Hz EMF in the same period had a reversed effect on this process, i.e., dry weight was increased.

It is interesting to note that the differences between the effects of these two groups of EMF frequencies were quite pronounced also at the subsequent phases of seed incubation in cold and warm distilled water. As it was noted above, during 2–24 hours incubation in (control) distilled water, intensive water binding in seed took place. The process was accelerated in 4 and 10Hz EMF-treated distilled water, while 15, 20 and 50Hz EMF had an opposite effect (Figure 5 A, B).

The effect of EMF frequency “windows” on seed dry weight changes was different in cold and warm distilled water. Such complicated EMF frequency “windows” effect on seed solubility and water binding in seed, is very interesting and needs more detailed investigation.

The obtained data clearly show that distilled water treatment by EMF has strong frequency dependent modulation effects on seed hydration and dry weight kinetics and frequency “windows” are different in metabolically active and inactive states.

As mentioned above, EMF-induced water structure changes can be realized by valence angles changes in water molecules and by mechanical vibration of its dipole molecules. Therefore, to estimate the contribution of valence angle-induced water structure changes effect on seed hydration in EMF-treated distilled water, in the next series of experiments the SMF-treated distilled water effect on seed hydration was studied. It is suggested that SMF-induced water structure changes can be the result of valence angle changes [Bistolfi, 1991, Klassen, 1982].

Static magnetic field effect

Seed hydration, their dry weight decrease and water binding in cold and warm distilled water, preliminary treated by SMF with different intensities (1.25, 2.50 and 3.75mT) were studied.

In Figure 6 it can be seen that at room temperature (family of curves B) while the time-dependant seed hydration in the control was linearly increased during the first 48 hours of incubation in SMF-treated distilled water, the rate of seed hydration was inhibited in the period of 24–48 hours incubation. This inhibition was intensity-dependant. The effect of lower intensity (1.25mT:0.67±0.01mg) was more pronounced than the higher one (3.75mT:1.29±0.15mg). It is interesting to note that in the period following (48–72 hours incubation) the rate of seed hydration in 2.50mT SMF-treated distilled water was significantly higher than in the control, while the 1.25 and 3.75mT SMF-treated distilled water were less than in the control.

In the family of curves (A), showing the rates of seed hydration in cold conditions there are no significant differences between the rates of seed hydration in the control and in SMF-treated distilled water. These data allow us to suggest that only the metabolic-dependent hydration (at 20°C) of seed is sensitive to previously SMF-treated distilled water.

In Figure 7 are presented data on time-dependant dry weight changes of seed in control and SMF-treated cold (A) and warm (B) distilled water. This figure shows that time dependant dry weight changes in SMF-treated distilled water had reversed its direction

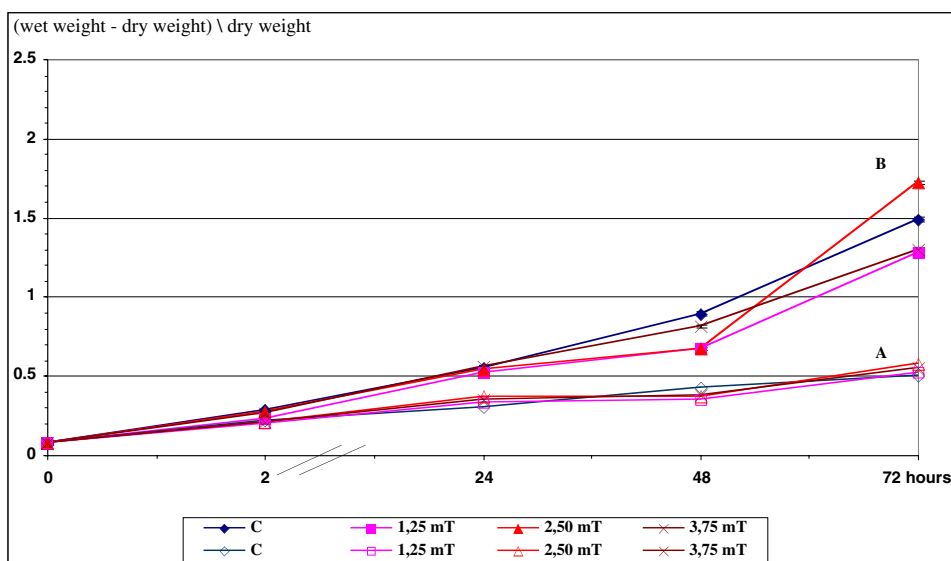


FIGURE 6. The time-dependent seed hydration during 72 hours incubation in static magnetic field (SMF)-treated cold (A) and warm (B) distilled water. Abscissa and ordinate as in Figure 2.

when compared to the control: instead of seed dry weight decrease in the first 2 hours and later increase in 2–24 hours incubation periods as in the control, SMF-treated distilled water seed dry weight was increased and decreased, correspondingly.

This effect was similar to the effect of 15, 20 and 50Hz EMF (Figure 5B), although, during the following phases there are no similarities between kinetics of seed dry weight in SMF and EMF-treated distilled water. The obvious differences between the kinetics of seed dry weight in SMF- and EMF treated distilled water in the period of 48–72 hours incubation could be emphasized. These differences in cold distilled water (Figure 5A, 7A) can be explained from the point of physicochemical properties of water only, because of depression of the metabolic activity of seed. These data seem extremely interesting and can be the subject for special investigations.

It is suggested that the differences between EMF and SMF-treated distilled water effects on time dependent changes of seed hydration and dry weight, could be explained by water molecule vibration-induced water structural changes, in addition to valence angle-induced changes in water molecules.

Mechanical vibrations effects

The study of time-dependent dynamics of seeds hydration and dry weight changes during 72 hours incubation in LF MV-treated cold and warm distilled water has shown that there are significant differences between kinetics of these parameters of seeds, incubated in control and MV-treated distilled water. As can be seen in Figure 8, the effect of MV-treated distilled water has complicated character in the first period of incubation at room temperature, while in the period of 48–72 hours of seed incubation (period of germination), a clear increase of seed hydration rate in MV-treated distilled water was observed.

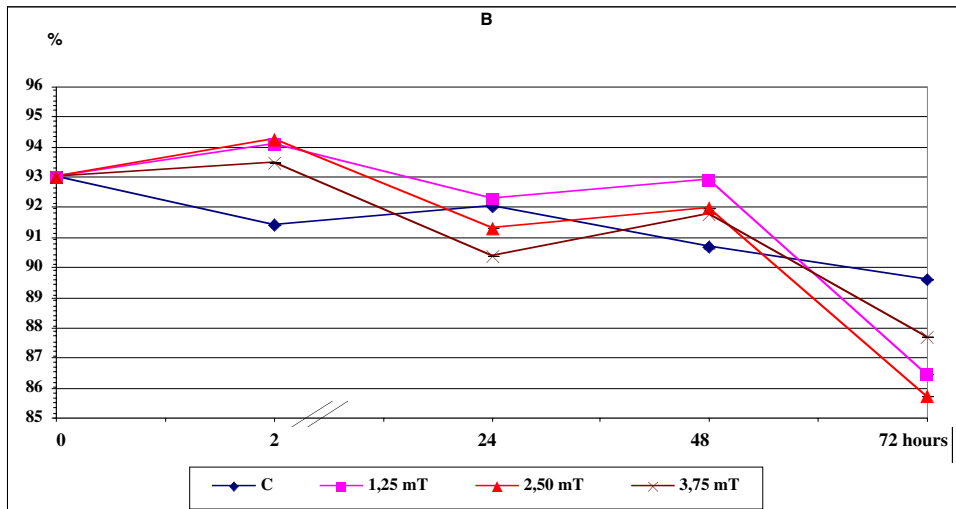
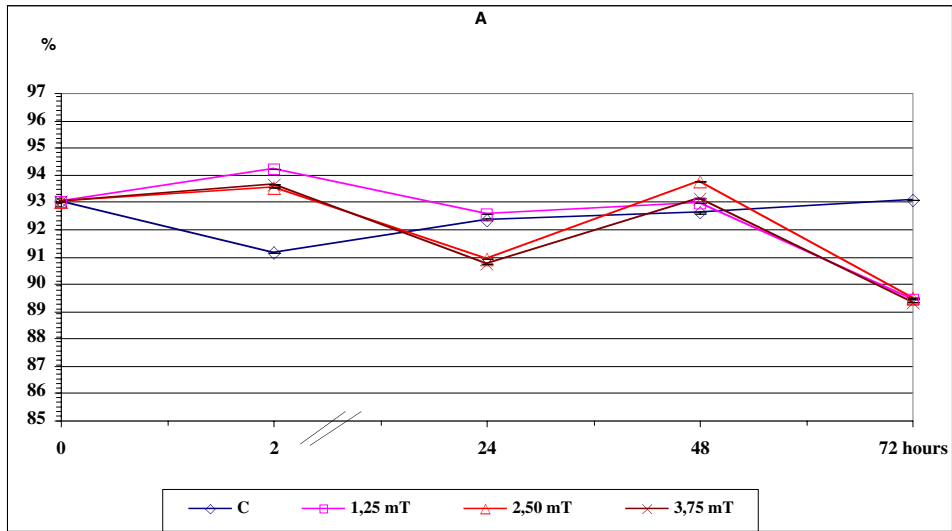


FIGURE 7. The time-dependant changes of seed dry weight during 72 hours incubation in cold (A) and warm (B) distilled water pretreated by static magnetic fields (SMF). Abscissa and ordinate as in Figure 3.

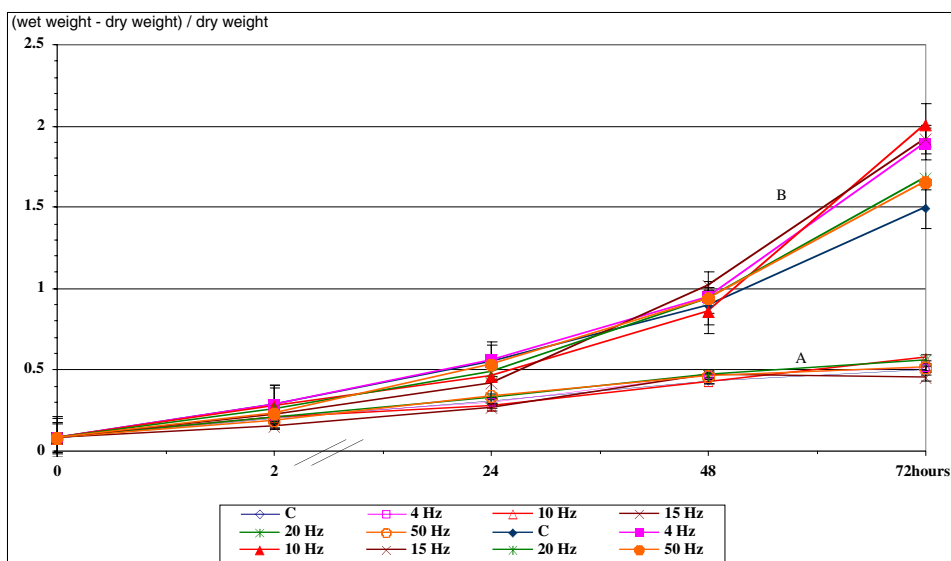


FIGURE 8. The time-dependent seed hydration during 72 hours incubation in cold (A) and warm (B) distilled water pretreated by mechanical vibration (MV). Abscissa and ordinate as in Figure 2.

This effect was MV frequency dependent: a more pronounced effect was observed at frequencies of 4, 10 and 15 Hz. These frequencies have an activation effect on seed hydration in the case of EMF also, however, in this case the effectiveness of these frequencies was different. At 4, 10, 15, 20 and 50 Hz MV wet weight of seeds at the end of 72 hours incubation was increased $+26.9\% \pm 0.28$, $+34.3\% \pm 0.39$, $+28.5\% \pm 0.10$, $+12.5\% \pm 0.21$ and $+10.5\% \pm 0.35$, respectively, compared to the control.

The study of dynamics of seed dry weight in MV-treated distilled water has demonstrated its similarity with dry weight changes in EMF-treated distilled water (Figure 9). During the first 2 hours of seeds incubation 4 and 10 Hz MV had a depressing effect on the rate of dry weight decrease in the control, while the group of comparatively higher frequencies (15, 20 and 50 Hz) had an elevating effect on seed dry weight in the same period. However, the effectiveness of these frequencies in the case of MV and EMF was different. The sharp differences between kinetics of dry weight at 10 and 15 Hz of MV-treated distilled water allow us to suggest that there is a critical frequency “window” between them which could change the interaction between water molecules and seed components.

Thus, the values of dry weight after 2 hours of swelling were $95.4\% \pm 0.01$, $94.1\% \pm 0.01$, $96.2\% \pm 0.01$, $92.6\% \pm 0.01$ and $92.7\% \pm 0.01$ at frequencies 50, 20, 15, 10 and 4 Hz, respectively, while in the control it was $91.1\% \pm 0.01$.

After 72 hours incubation in distilled water preliminary treated by MV the values of dry weight were $90.2\% \pm 0.01$, $90.0\% \pm 0.01$, $90.1\% \pm 0.01$, $88.0\% \pm 0.01$ and $91.1\% \pm 0.01$ at frequencies 50, 20, 15, 10 and 4 Hz, respectively, while in the control it was $89.6\% \pm 0.01$.

The differences between the rates of dry weight dissolving in control (as well as at 4 and 10 Hz MV-treated distilled water) and 15, 20 and 50 Hz-treated distilled water during

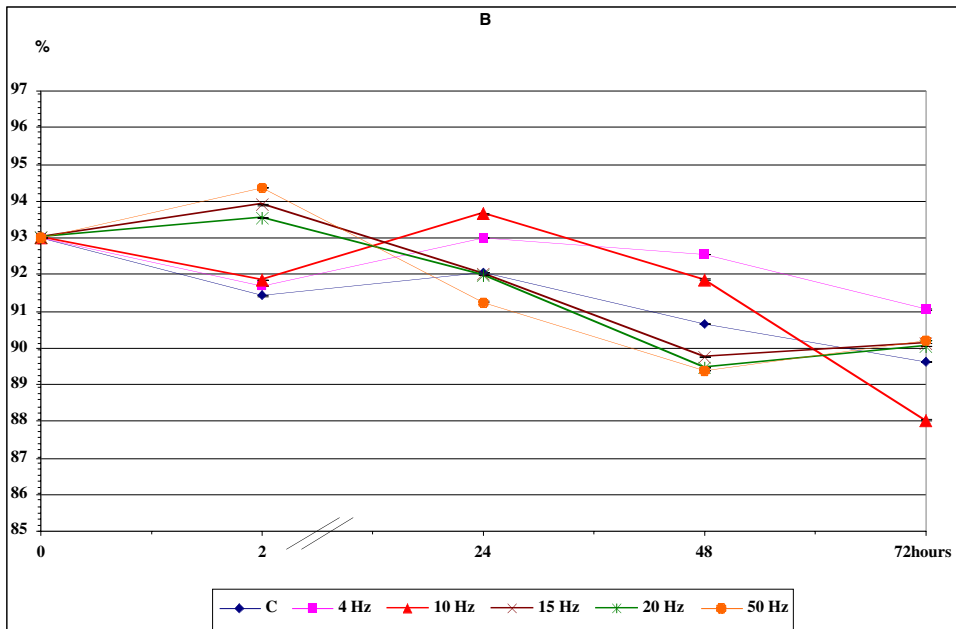
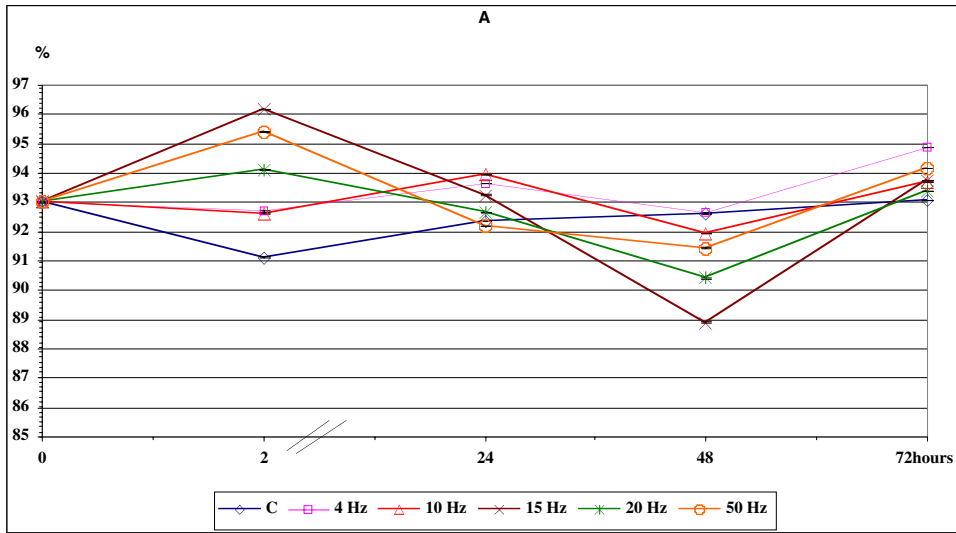


FIGURE 9. The time-dependant changes of seed dry weight during 72 hours incubation in cold (A) and warm (B) distilled water pretreated by mechanical vibration(MV). Abscissa and ordinate as in Figure 3.

the first 2 hours of seed incubation was less at room temperature than in cold distilled water. It is also interesting to note that at the end of incubation (48–72 hours) in MV-treated cold distilled water the seed dry weight was sharply increased, while in SMF-treated cold distilled water the seed dry weight was changed in an opposite direction, i.e., was decreased.

Discussion

Over the last 20 years of study the results have shown that magnetic fields at extremely low frequencies and very low intensities have modulation effect on plant germination and final crop yield in quality and quantity [Smith & Mays 1984, Celestino *et al.* 2000, Leelapriya *et al.* 2003]. Recently a group of scientists from Hungary, UK and USA has demonstrated the increase of seed germination potential by EMF and SMF-induced seed treatment [Vincze *et al.*, 2003 a, b]. The data obtained in the present work clearly show that the bathing aqua solution treated by EMF and SMF also have a modulation effect on seed germination.

It is well known that LF EMF can modulate the physico-chemical properties of water and water solutions [Klassen 1982, Adey 1981] and long ago these effects had different biotechnological [Mohsenin, 1984] and therapeutic [Bistolfi 1991] applications. The effect of LF EMF on water properties is usually explained by LF EMF-induced changes of valence angle in the water molecule without considering its dipole molecules vibration-induced water structure changes [Klassen 1962, Ayrapetyan *et al.* 1994b]. However, the frequency-dependent effect of MV on water conductivity, which was demonstrated in our previous works [Stepanian *et al.* 1999] allow us to suggest that EMF-induced water structure changes could also be the result of water dipole molecules vibration. The aim of the present experiments was to find out the biological meaning of both the valence angle-induced and dipole molecule vibration-induced water structure changes for cells metabolic independent and metabolic dependent hydration processes. It was suggested that any factor-induced water structure changes could predict the adequate changes of water thermodynamic (osmotic) properties, which could modulate cell hydration and intracellular metabolic activity.

In the present work, the barley seed hydration during 72 hours incubation in EMF-treated distilled water could be chosen as a marker for estimation of the contribution of the above mentioned two pathways of water structure change through which the biological effect of EMF could be realized. This period is known in plant physiology as a period of seed germination [Cuperman 1982]. Thus, it is suggested that seed hydration in the period of germination could serve as a very convenient model for studying the effects of physical factors on metabolic independent (in cold) and metabolic dependent (at room temperature) cell hydration. As any changes of water thermodynamic properties predict the changes of free and bound water ratio in cells, the determination of seed dry weight in different periods of incubation could give information on changes of this ratio. In the present experiments, for determination of seed dry weight, they were dried in a thermostat at 104°C for 24 hours. Traditionally it is suggested that in these conditions the free water in seed is evaporated [Plotnikova *et al.*, 2001]. Therefore, in condition, when seed metabolic activity is depressed, their dry weight “false” increase could be interpreted as the result of seed binding water increase.

To imitate the effects of valence angle- and mechanical vibration-induced changes of water structure, caused by LF EMF on seed hydration and the ratio of free and bound water in seed, the effects of SMF and MV on the mentioned parameters of seed were studied. On the basis of the obtained data on time-dependent changes of seed hydration during 72 hours incubation, two phases can be distinguished: a) the phase of slow gradual elevation (first 48 hours incubation) and b) phase of sharp increase (48–72 hours incubation) of seed hydration (Figure 2B). The last phase, which was absent in cold distilled water, and corresponding to seed active (metabolic) germinations phase, was very sensitive to preliminary treatment of bathing aqua solution by EMF (Figure 4), SMF (Figure 6) and MV (Figure 8). These effects were frequency-dependent in the case of EMF and MV and intensity-dependent in case SMF. Previously it was shown that EMF and MV effects on SEC of distilled water had the same frequency windows: 4 and 20 Hz, however, in the case of seed hydration we have different frequency “windows” at different phases of seed incubation. Such differences between the frequency “windows” of EMF and MV effects on SEC of distilled water and seed hydration can be explained by interaction of water and seed components, which could serve as a subject for special investigation .

The obtained data can serve as phenomenological evidence for the suggestion that SMF- (valence angle changes) and MV (dipole vibration)- induced changes of water properties could determine EMF effect on seed hydration. The study of seed dry weight kinetics during incubation in control and preliminary LF EMF-, SMF and MV treated distilled water in cold and warm conditions brought us to the same conclusions.

The obtained data have shown that in control distilled water based on the rate of seed dry weight changes, the period of 72 hours of seed incubation can be separated into three phases: a) fast decrease-first 2 hours of incubation, b) fast increase– 2–24 hours incubation and c) slow increase in cold or decrease in warm distilled water (24–72 hours incubation). The dramatic changes of seed dry weight kinetics in LF EMF-, SMF- and MV-treated distilled water, compared to the control and their frequency and intensity-dependent characters, allow us to suggest that these factors-induced changes of water properties is the result of valence angle changes (SMF) and that vibration of water molecules dipoles (MV) can determine EMF effect on seed hydration, solubility of water components and water binding in seed.

Thus, the obtained data allow us to come to the following conclusions:

1. The metabolic-dependent seed hydration, loss of seed dry weight and water binding in seed can be modulated by distilled water preliminary treated by LF EMF, SMF and MV.
2. SMF- and MV-induced changes of water properties could serve as a messenger for realizing the biological effects of LF EMF on seed germination and different functions of various cells and organism. To finalize these conclusions more detailed investigation on LF EMF, SMF and MV effects on physico-chemical properties of water and water solutions is necessary, which is subject for our current investigation.

References

- Adey, W.R. (1981) *Physiol. Rev.* 61: 435–514.

- Ayrapetyan, S.N., Avanesian, A.S., Avetisian, T., Majinian, S. (1994a) In: *Biological Effects of Electrical and Magnetic Fields* (eds: Carpenter, D. & Ayrapetyan, S.), Vol. 1 Academic Press, pp. 181–192.
- Ayrapetyan, S.N., Grigorian, K.V., Avanesian, A.S., Stamboltsian, K.V. (1994b) *Bioelectromagnetics* 5: 133–142.
- Bistolfi, F. (1990) In: *Biostructures and Radiation Order Disorder*. Edizioni Minerva Medica S.p.A. Torino.
- Carbonel, M.V., Martinez, E., Amaya, J.M. (2000) *Electro-Magnetobiology* 19(1): 121–128.
- Cuperman, F.M. (1982) In: *The Biology of the Development of Gramineous Plants*. Chemistry Publisher, pp. 118–122 (in Russian).
- Klassen, V.I. (1982) In: *Magnetized Water Systems*. Vishaya Shkola Press, p. 296 (in Russian).
- Lednev, W. (1991) *Bioelectromagnetics* 12: 71–76.
- Leelapriya, T., Dhillip, K.S., Sanker, Narayan PV. (2003) *Electromagnetic Biology and Medicine* 2(2&3): 117–125.
- Mohsenin, N.N. (1984) In: *Electromagnetic Radiation Properties of Food and Agricultural Products*. Gordon and Branch Publishers, New York.
- Plotnikova, I.V., Jivukhina, E.A., Mikhalevskaya, O.B. (2001) In: *Practicum on Plant Anatomy and Physiology*. Academia Press, p. 7 (in Russian).
- Pullman, B., Pullman, A. (1963) In: *Quantum Biochemistry*. Interscience Publishers, New York.
- Smith, S.D., Mays, R. (1984) *Bioelectrochem. Bioenerg.* 12: 567–573.
- Stepanyan, R.S., Ayrapetyan, G.S., Arakelyan, A.G., Ayrapetyan, S.N. (1999) *Biophysics* 44(2): 197–202 (in Russian).
- Vincze, G., Szasz, N., Szendro, P., Szasz, O., Szasz, A. (2003a) *Proceedings of the Bioelectromagnetics Society (BEMS) 25th Annual Meeting, Maui, Hawaii, (P-152-B)* p. 332.
- Vincze, G., Szasz, N., Szendro, P., Szasz, O., Szasz, A. (2003b) *Proceedings of the Bioelectromagnetics Society (BEMS) 25th Annual Meeting, Maui, Hawaii, (P-153-C)* p. 333.

Received October 21, 2003;
accepted September 10, 2004.

Erratum to

A Quantitative Theory of Solute Distribution in Cell Water According to Molecular Size

GILBERT N. LING

Damadian Foundation for Basic and Cancer Research
Fonar Corporation, 110 Marcus Drive, Melville, New York 11747

From Volume 25 (1993), Number 3, pages 171 and 172

Please substitute the following two pages for the two pages which appeared in the original publication to correct this paper.

The logarithm of W_{cf} , multiplied by the Boltzmann constant, k , is equal to ΔS_{cf} , the *entropy of mixing* (i.e., the gain of configurational entropy from mixing the solvent and solute). We can simplify equation 3 by using Stirling's approximation ($\ln n! = n \ln n + n$), and obtain the following equation for the entropy of mixing:

$$\Delta S_{cf} = k \ln W_{cf} = -k(n_A \ln x_A + n_B \ln x_B) , \quad (4)$$

where n_A and n_B are the numbers, and x_A and x_B , the mole fractions of water and solute respectively.

Equation 4 is based on the assumption that the solute and water molecules have approximately the same size. Since it is our primary goal to find out how molecules of *different size* distribute themselves between cell water and external medium, as such this equation is not applicable. What we need is a similar equation that does not suffer this molecular-size restriction. Luckily, such an equation is already available, derived not for the purpose we have in mind but for predicting properties of solutions of linear polymers.

In deriving such an equation, a linear polymer molecule was considered as a chain of σ repeating segments; each individual segment equals in size that of one solvent molecule. With this assumption, Flory derived the following equation for the configurational entropy of mixing solvent with linear polymers (see Flory, 1953, pp. 497–503):

$$\Delta S_{cf} = k \ln W_{cf} = -k(n_A \ln v_A + n_B \ln v_B) , \quad (5)$$

where n_A and n_B are the numbers of water and solute molecules respectively and v_A and v_B are their respective *volume fractions*, and

$$v_A = \frac{n_A}{n_A + \sigma n_B} ; \quad v_B = \frac{\sigma n_B}{n_A + \sigma n_B} . \quad (6)$$

We will use this equation for the entropy of mixing of *solute molecules of any size*, assuming that they can all be approximately represented as a flexible chain of σ segments, each segment having roughly the size of a water molecule.

Limiting ourselves to dilute solutions, we write down the total Helmholtz free energy of the system of living cells and its surrounding medium as follows:

$$F = -kT \{ {}^1n_A \ln {}^1(p.f.)_A + {}^1n_B \ln {}^1(p.f.)_B + \ln {}^1W_{cf} + {}^2n_A \ln {}^2(p.f.)_A + {}^2n_B \ln {}^2(p.f.)_B + \ln {}^2W_{cf} \} , \quad (7)$$

where 1n_A and 1n_B represent the number of water and solute molecules in the living cell, while 2n_A , and 2n_B represent the number of water and solute molecules in the surrounding medium. ${}^1(p.f.)_A$, and ${}^1(p.f.)_B$ represent the partition function of the water and solute molecules in the cell water, while ${}^2(p.f.)_A$ and ${}^2(p.f.)_B$ represent the partition functions of water and solute in the external medium. $k \ln {}^1W_{cf}$ and $k \ln {}^2W_{cf}$ are the configurational entropy of the solute in cell water and the surrounding medium respectively.

When dm water molecules are transferred from cell water to the external medium, we have

$$dm = d {}^1n_B = -d {}^2n_B , \quad (8)$$

or

$$\frac{\delta}{\delta m} = \frac{\delta}{\delta {}^1n_B} = -\frac{\delta}{\delta {}^2n_B}$$

From equation 7, we derive

$$\frac{\delta}{\delta^1 n_B} (\ln {}^1 W_{cf}) = (\sigma - 1) {}^1 v_A - \ln {}^1 v_B; \quad -\frac{\delta}{\delta^2 n_B} (\ln {}^2 W_{cf}) = \ln {}^2 v_B - (\sigma - 1) {}^2 v_A. \quad (9)$$

and

$$\frac{\delta F}{\delta^1 n_B} = -kT [\ln {}^1(p.f.)_B - \ln {}^2(p.f.)_B + (\sigma - 1) {}^1 v_A - \ln {}^1 v_B - (\sigma - 1) {}^2 v_A + \ln {}^2 v_B]. \quad (10)$$

The condition for equilibrium in the distribution of the solute between cell water and its surrounding medium is $\delta F / \delta^1 n_B = 0$, or

$$-kT [\ln {}^1(p.f.)_B - \ln {}^2(p.f.)_B + (\sigma - 1) {}^1 v_A - \ln {}^1 v_B - (\sigma - 1) {}^2 v_A + \ln {}^2 v_B] = 0. \quad (11)$$

Since σ is a constant for each solute, and for the (low) v_B range being studied, we may assume

$$(\sigma - 1) {}^1 v_A = (\sigma - 1) {}^2 v_A. \quad (12)$$

We then have

$$\ln \frac{{}^1(p.f.)_B}{{}^2(p.f.)_B} + \ln \frac{{}^2 v_B}{{}^1 v_B} = 0. \quad (13)$$

where the two partition functions, ${}^1(p.f.)_B$ and ${}^2(p.f.)_B$, are referred to the same zero of energy. I now introduce partition functions, ${}^1(\mathbf{p.f.})_B$ and ${}^2(\mathbf{p.f.})_B$, each referred to its own zero energy. Choosing the zero energy of solute B in the external solution as zero of the whole system, the zero energy of B in the cell water ${}^1(\mathbf{p.f.})_B$ now lies below the new zero energy by an amount equal to χ in ergs per molecule. Therefore

$$\frac{{}^1 v_B}{{}^2 v_B} = \frac{{}^1(\mathbf{p.f.})_B}{{}^2(\mathbf{p.f.})_B} \cdot \exp\left(-\frac{\chi}{kT}\right), \quad (14)$$

where k is the Boltzman constant. Now

$${}^1 v_B / {}^2 v_B = {}^1 n_B / {}^2 n_B = {}^1 C_B / {}^2 C_B, \quad (15)$$

where ${}^1 C_B$ and ${}^2 C_B$ are the concentration in moles per liter of the solute B in cell water and in the water of the external medium respectively.

Therefore,

$$\frac{{}^1 C_B}{{}^2 C_B} = \frac{{}^1(\mathbf{p.f.})_B}{{}^2(\mathbf{p.f.})_B} \cdot \exp\left(-\frac{\eta}{RT}\right), \quad (16)$$

where $\eta = \chi L$, $R = kL$ and L is the Avogadro number. Since the equilibrium distribution coefficient of B between cell water and the external solution is represented by the symbol q , or

$${}^1 C_B / {}^2 C_B = q, \quad (17)$$

we then have an equation for the solute distribution in living cells:

$$q = \frac{{}^1(\mathbf{p.f.})_B}{{}^2(\mathbf{p.f.})_B} \cdot \exp\left(-\frac{\eta}{RT}\right). \quad (18)$$